



**KINETIC MODEL
OF A SPACE-BASED,
Br ($4^2P_{1/2} \rightarrow 4^2P_{3/2}$) LASER PUMPED
BY SOLAR PHOTOLYSIS OF IBr**

THESIS

**Barry N. Behnken, Captain, USAF
AFIT/GAP/ENP/99M-01**

**DEPARTMENT OF THE AIR FORCE
AIR UNIVERSITY
AIR FORCE INSTITUTE OF TECHNOLOGY**

Wright-Patterson Air Force Base, Ohio

Approved for public release; distribution unlimited

DTIC QUALITY INSPECTED 2

19990402 033

AFIT/GAP/ENP/99M-01

KINETIC MODEL OF A SPACE-BASED,
Br ($4^2P_{1/2} \rightarrow 4^2P_{3/2}$) LASER PUMPED
BY SOLAR PHOTOLYSIS OF IBr

THESIS

Presented to the Faculty of the Graduate School of Engineering
of the Air Force Institute of Technology
Air University
In Partial Fulfillment of the
Requirements for the Degree of
Master of Science in Engineering Physics

Barry N. Behnken, B.S.

Captain, USAF

March, 1999

Approved for public release, distribution unlimited.

Acknowledgements

In the course of undertaking this project, I have been fortunate to have the guidance and support of several important people. For this I am truly grateful. Firstly, I would like to thank my advisor, Lt Col Glen Perram, for his insight, encouragement, and contributions to this thesis. His direction saved me from undertaking many ill-fated pursuits, and often provided valuable answers to questions I was unable to satisfy elsewhere. I also count myself extremely fortunate to have two esteemed former professors, Dr Won Roh and Lt Col Paul Wolf, as thesis committee members. Their conscientious inputs provided further balance and perspective to this work, and I thank them for their generous commitments of time and energy.

On a personal note, I would like to thank my wife, Yvonne, for her limitless patience and understanding throughout my recent graduate sojourn. I could not have sustained eighteen months of social wasteland without her devoted accompaniment.

Finally—for their eternal support throughout all of my life endeavors—I would like to thank the rest of my family, including especially my father, Lawrence Behnken, who passed away shortly before my arrival at AFIT. My thoughts were often filled with him as I worked on this project. Although it is a somewhat sterile product, I would like to dedicate this thesis to him.

Table of Contents

Acknowledgements	ii
List of Figures	v
List of Tables.....	vi
Abstract	vii
I. Introduction.....	1
1.1. Background	2
1.2. Problem Statement	5
1.3. Research Objectives.....	6
1.4. Assumptions.....	8
1.5. Nomenclature	8
1.6. Sequence of Presentation	9
II. Background.....	11
2.1. Literature Review.....	11
2.1.1. Characteristics of Solar-Pumped Lasers	11
2.1.2. The IBr Photodissociative Laser	13
2.1.3. Space-Based Resonator Design.....	15
2.2. Limitations of Previous Modeling Efforts	17
III. Methodology	20
3.1. Solar Emission & Concentration.....	21
3.2. Absorption Cross Section.....	24
3.3. Molecular Photodissociation.....	27
3.4. ($^2P_{1/2}$) Photolysis Yields.....	29
3.5. Kinetic Interaction of Chemical Species.....	32
3.6. Photon Emission	38
3.7. Lasant Circulation Processes	39
IV. Computer Models of the IBr Photolysis Laser.....	43
4.1. Model Overview	43

4.2. Time-Dependent Kinetic Model	45
4.2.1. Results of Kinetic Simulation	45
4.2.2. Sensitivity Analysis	47
4.2.3. Experimental Validation	48
4.3. Analytic Model: Continuous-Wave IBr Laser	53
4.3.1. Kinetic Assumptions	53
4.3.2. Accuracy and Applicability.....	55
V. Results and Analysis	56
5.1. Attainment of CW Oscillation	56
5.2. Resonator Design	58
5.2.1. Pumping Geometry/Photolysis Path Length	58
5.2.2. Gain Cell Dimensions	60
5.3. Parametric Optimization	60
5.3.1. Precursor Concentration	60
5.3.2. Gain Flow Velocity	62
5.3.3. Bandpass Design	64
5.3.4. Optimum Coupling.....	65
5.3.5. Solar Concentration.....	66
5.4. Temperature Effects.....	68
5.5. Comparisons with Competing Systems	71
5.5.1. Efficiency	71
5.5.2. Output Power.....	78
5.5.3. Design Costs.....	78
VI. Conclusions and Recommendations	80
6.1. Conclusions.....	80
6.2. Recommendations.....	81
6.2.1. Applications	81
6.2.2. Pursuit of a Space-Based, Solar-Pumped IBr Laser.....	81
Appendix A. Modifications to ILSA Kinetic Code.....	84
Appendix B. ILSA: Mathematica [®] Source Code	89
Vita.....	163
Bibliography.....	164

List of Figures

Figure 1-1. Spectral comparison of IBr and <i>t</i> -C ₄ F ₉ I absorption coefficients with solar photon flux.....	4
Figure 2-1. Geometrical design of a frustum-oriented solar concentrator.....	17
Figure 3-1. Energy level diagram reflecting chemistry of interaction of an IBr laser system.....	21
Figure 3-2. Absorption cross sections for IBr, Br ₂ , and I ₂ as a function of wavelength.....	27
Figure 3-3. (² P _{1/2}) quantum yields from IBr, Br ₂ , and I ₂ photodissociation.....	31
Figure 4-1. Typical ILSA-modeled output pulse.	46
Figure 4-2. IBr-pressure dependence of an instantaneously-pumped laser	50
Figure 5-1. Output power as a function of gain cell length.....	60
Figure 5-2. Laser performance as a function of initial IBr partial pressure.	62
Figure 5-3. Output power as a function of transverse flow velocity.	63
Figure 5-4. Total laser efficiency as a function of solar concentration and IBr partial pressure.	67
Figure 5-5. Relative output power from IBr laser systems under simulated temperature conditions	70
Figure 5-6. Absorbed efficiency of the IBr laser as a function of bandpass width.	78
Figure A-1. Br (² P _{1/2}) and I (² P _{1/2}) production from Br ₂ and I ₂ photolysis.....	87

List of Tables

Table 3-1. Experimental and Modeled Extinction Coefficients for I ₂ (liters/mol-cm)	26
Table 3-2. Gaussian Modeling Parameters for IBr, Br ₂ , and I ₂ Extinction Coefficients	26
Table 3-3. Rate Coefficients Used in Numerical Model of IBr Laser.....	38
Table 5-1. Operating Efficiencies of IBr and <i>t</i> -C ₄ F ₉ I Laser Systems.....	74
Table A-1. Steady-State Comparisons of ILSA-Modeled Parameters.....	88

Abstract

A kinetic model of the directly solar-pumped, atomic bromine laser—operating on the Br ($4\ ^2P_{1/2} \rightarrow\ ^2P_{3/2}$) transition under IBr photolysis—was developed, executed, and interpreted. In recognition of an evolving national interest in space-based laser development, the model presumed operation on a space station platform. Mathematical representations for such processes as incident solar flux, molecular photolysis, and quantum yield were combined with those for chemical reactions and lasant flow in a set of nonlinear differential equations designed to model temporal behavior of chemical and photon populations within the gain cell. Numerical solutions to these equations indicate that a well-engineered IBr laser is capable of generating 1.2 kilowatts of continuous-wave (CW) power under a pumping concentration of 20,000 solar units. Such performance translates to an efficiency of roughly 0.29%, appreciably better than the 0.1% ascribed to the heretofore leading solar-pumped competitor. An extensive analysis of kinetic results suggests the unanticipated conclusion that, under proper parameter selection, sustained CW oscillation can be achieved absent any flow mechanism whatsoever. This result seems most strongly predicated upon proper bandpass discrimination: a 457-545 nm range of incidence produced optimal results. Sensitivity analysis revealed a strong degree of competition among the laser's constituent processes; two-body quenching and exchange reactions were predominant. With the significant exception of iodine recombination, three-body processes were negligible. Thermal increases, as well as rapid growth of atomic iodine, appear to pose the greatest kinetic threat to CW lasing.

KINETIC MODEL OF A SPACE-BASED,
Br ($4^2P_{1/2} \rightarrow 4^2P_{3/2}$) LASER PUMPED
BY SOLAR PHOTOLYSIS OF IBr

I. Introduction

In 1980, amid increasing national interest in the development and use of high-power laser systems, the National Aeronautics and Space Administration (NASA) chartered a working group to investigate the viability of deploying laser devices on a space-based platform [1]. Such a capability would be enormously helpful for carrying out an array of functions, including communications, power beaming, or elimination of orbital debris. However, the question of *which* specific laser system would best be suited for such a platform has remained an elusive one. Due to costs associated with space transport, for instance, any system with conventional (i.e., chemical) fueling requirements would be extremely expensive to sustain in orbit.

In the ultimate analysis, a solar-pumped laser system proves perhaps the most compelling option for a space-based device. With proper engineering and design, such a system could be self-contained, self-sufficient, and minimally expensive to operate after initial deployment. However, the solar-pumped laser scenario introduces a number of technical concerns and liabilities that make proper laser selection an even more difficult task. Working within the inflexible constraints imposed by the sun (radiative spectrum, intensity, etc), one can combine computer modeling and parametric selection to accurately assess the viability of a potential system.

Due to favorable pumping characteristics, the iodine monobromide (IBr) photodissociative laser is a promising candidate for this undertaking. Although there are technical issues that must be remedied before IBr may be considered a competitive alternative for the solar-pumped laser, this process can be greatly accelerated by the use of computational methods. Alternatively, computer analysis can effectively determine whether the proposed process is inherently *unfeasible*. In either event, merits of the IBr laser should be duly considered and compared to other potential candidates for this important role in technological development.

1.1. Background

To effectively meet its proposed mission demands, a space-based laser system must satisfy several technical criteria, including continuous wave (CW) oscillation, self-sustainability (to include, at a minimum, effective recycling of laser gain material), and efficient pumping. For the directly solar-pumped laser, an “efficient” pumping process is one that is spectroscopically well-matched to the solar spectrum.

Molecular photodissociation is a process that seems to most effectively lend itself to this pumping scenario. Given a photon flux of sufficient energy, a molecular precursor can be disassembled into its atomic and/or molecular constituents [2]. Under proper conditions, the dissociation results in production of spin-orbit excited atoms that can serve as the upper state of a lasing transition. In the case of iodine monobromide, the dissociation processes are:



where Br ($4^2P_{1/2}$) and Br ($4^2P_{3/2}$) are spin-orbit excited and ground bromine atoms, respectively [3, 4]. Stimulated emission is then achieved, at 2.714 μm , on the resulting Br ($^2P_{1/2} \rightarrow ^2P_{3/2}$) transition. A wavelength-dependent quantum yield, ϕ_{IBr} , determines the proportion of bromine atoms that realize an excited state; population inversion is established by exploiting this yield in a laser gain cell. Other molecular precursors, such as those within the presently more “popular” class of perfluoroalkyl iodides, operate on the same principle but with decidedly higher quantum yields—often near unity [5]. The specific precursor *t*-C₄F₉I, which serves as a parent molecule for spin-orbit excited iodine atoms, is one that has been extensively studied, with considerable success, in previous investigations of the solar-pumped laser [5, 6, 7].

Spectral efficiency provides perhaps the most compelling argument for selection of IBr as a photolytic precursor. As depicted in Figure 1-1, the IBr absorption coefficient is much better matched to the sun’s spectral profile than is *t*-C₄F₉I. Under solar illumination, therefore, a much higher percentage of incident photons fall within the absorption range of IBr: a full 23 percent, compared to 2 percent for *t*-C₄F₉I. Moreover, the peak absorption cross section of IBr is nearly twice that of *t*-C₄F₉I. At least in *prima facie* terms, then, this higher “spectral-absorptive” efficiency translates into more modest pumping requirements, and would perhaps relax the size and expense associated with a solar collection/reflection module.

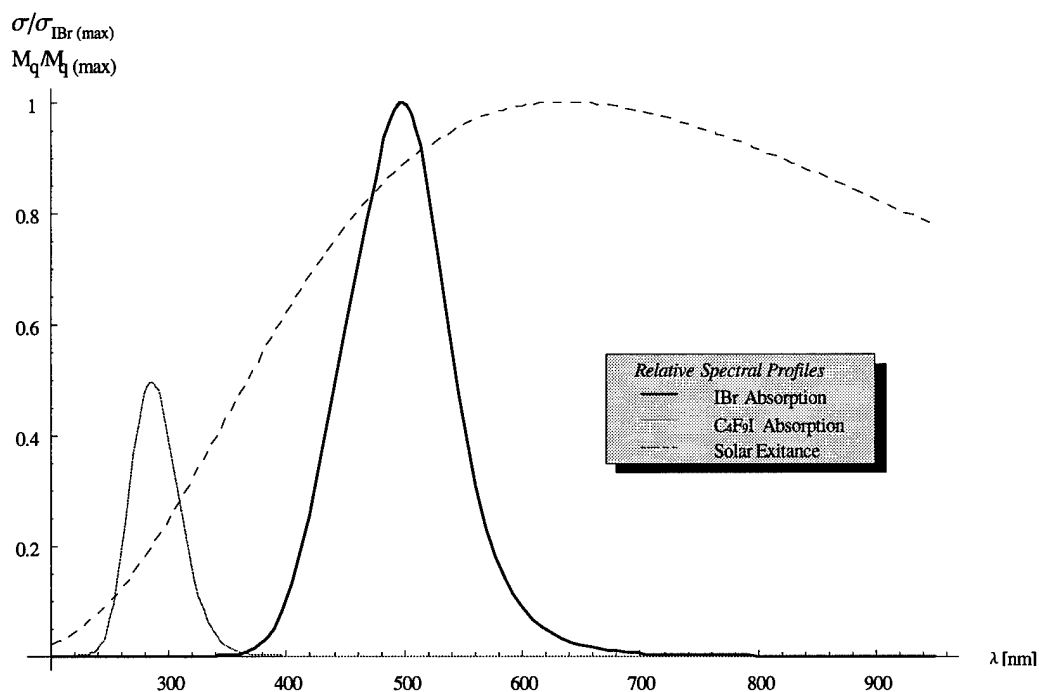


Figure 1-1. Spectral comparison of IBr and *t*-C₄F₉I absorption coefficients (300K) with solar photon flux.

Undesirable factors, such as an inferior quantum yield and kinetic interference, serve as detractions to IBr selection. Indeed, previous studies [8, 9] indicate that the system is hindered by slow depopulation of the lower laser level; as a result, population inversion is difficult to sustain and CW operation is frustrated. Nevertheless, potential advantages of this candidate warrant its further investigation.

Central to the proposed modeling of a solar-pumped laser is the development of an accurate excitation mechanism. The characteristics of a solar pump are implicitly dependent upon such factors as absorption cross section of the precursor, spectral profile of the solar source, and overall concentration of incident radiation. Moreover, great care must be given to selection of the spectral range used in pumping the system. For, although a given precursor may exhibit photodissociation over a broad range of spectral

incidence, the quantum yield of excited atoms via photolysis (ϕ) is generally wavelength-dependent [3, 4]. As such, full-spectrum pumping may actually frustrate population inversion outside of a comparatively narrow range.

The solar pumping rate of excited Br atoms, in molecules/sec-cm³, is given by a modified expression of Beer's Law [7]:

$$R_p = \frac{S_c}{D_p} \int_{\lambda_1}^{\lambda_2} \phi(\lambda) F(\lambda) \left[1 - e^{-\sigma_{abs}(\lambda, T) N_{Br} D_p} \right] d\lambda, \quad (1-3)$$

where $F(\lambda)$ is the incident photon flux; S_c is the effective concentration of incident solar radiation; D_p characterizes the photon path length; λ_1 and λ_2 designate the lower and upper bounds (respectively) of incident wavelength which are allowed to enter the gain cell.

Modifications of the above expression may be used to likewise model the pumping rate of other atoms generated by the photodissociation of IBr, I₂, or Br₂. In addition, appropriate quenching, exchange, and recombination processes must be adequately included. Thus, by addressing all kinetic processes at work in the laser and coupling them with appropriate rate equations, a time evolution of the entire system can be generated and observed. Peripheral engineering topics can then be more specifically assessed.

1.2. Problem Statement

Despite its natural affinity for the solar spectrum, the IBr photodissociative laser demonstrates kinetic behavior that has discouraged its selection as a leading candidate for space-based deployment. Undesirable factors—such as an inferior quantum yield, rapid

lasant quenching, and slow depopulation of the lower laser level—counteract the advantages of using IBr precursor within a sealed gain cell. As a result, population inversion is difficult to sustain and CW oscillation is frustrated.

This difficulty has allowed alternate laser systems—many with starkly lower spectral efficiencies—to shift to the forefront. However, no definitive examination of the solar-pumped, *continuous-wave* IBr laser has been performed to date. The introduction of a nominal flow process, or other minor design changes, may prove sufficient for eliminating this disqualifying factor. Nor has the IBr laser been compared, in absolute performance terms, to the established line of perfluoroalkyl-based iodine competitors. The ongoing, independent efforts by NASA and the Air Force Research Laboratory (the sponsor of this thesis) to construct and deploy a space-based laser would, in the author's opinion, be greatly assisted by such a parameterization and comparison. Whether computer modeling reveals the IBr system to be preferable or not, a refined evaluation of laser candidates will ultimately aid the realization of this provocative objective.

1.3. Research Objectives

The purpose of the present research is to develop and execute a computer code package which accurately simulates all kinetic processes associated with a Br ($4^2P_{1/2} \rightarrow 4^2P_{3/2}$) laser, pumped by photolysis of IBr via concentrated solar radiation. Investigation of the resulting numerical solutions may serve as the basis for critical analysis and design of an IBr laser. End objectives of this thesis are threefold:

1. Confidently assess the severity of those technical issues serving as barriers to development of a continuous-wave, solar-pumped IBr laser system suitable for deployment on a space platform.

2. Characterize the envelope of design parameters that mitigate or circumvent such technical obstacles, allow CW oscillation, and optimize overall laser performance.

3. Compare anticipated performance characteristics to those already demonstrated by established solar-pumped laser candidates (e.g., $t\text{-C}_4\text{F}_9\text{I}$), evaluate relative strengths and weaknesses, and recommend candidate selection.

Successfully accomplished, these undertakings will constitute an important tool in evaluating the technical feasibility of a solar-pumped, space-based IBr laser. Favorable results may provide a reason for reconsidering this laser in future developments of space exploration. Unfavorable results would implicitly reaffirm the attractiveness of currently scrutinized lasers. Either outcome may offer contributions to the ongoing research effort of a space-based laser.

1.4. Assumptions

The kinetic model presented in this thesis is designed to accept a wide range of user-defined parameters. In this manner, one can phenomenologically optimize the operating conditions for the laser. However, there are some general assumptions that are fundamental to the model and therefore not malleable to user preferences. Therefore, to better clarify the effective constraints and limitations of the model, it is important to define these assumptions at the outset.

Aside from its unusual pumping methods, the laser system modeled in this paper is assumed to be of simple, standing-wave variety. A gain cell, positioned within a plano/concave resonator cavity, contains the gain material (IBr precursor, as well as fragment products) and is assumed to have an imperfectly-transmitting window on each of its ends. For cases in which gain flow is simulated, it is assumed that such removal occurs in either transverse or longitudinal directions with respect to the tube axis. No assumptions are immediately advanced with respect to the laser's pumping geometry; this treatment will be undertaken later, in light of computational data.

The effects of temperature on chemical operation of the laser are significant, yet difficult to model. Therefore, such effects have not been explicitly integrated into the computer algorithm. However, a qualitative discussion on the implications of thermal management, performed with an *ad hoc* code modification, is presented in Section V.

1.5. Nomenclature

A brief word is in order to clarify some specific terms, commonly repeated throughout this thesis, associated with the IBr laser system. Consistent with accepted

convention [4], “Br^{*}” and “Br” labels will be liberally used as a convenient substitute for spin-orbit excited (Br (4 ²P_{3/2})) and ground-state (Br (4 ²P_{3/2})) bromine atoms. Spin-orbit states of iodine atoms are similarly defined: I ≡ I (5 ²P_{3/2}); I^{*} ≡ I (5 ²P_{1/2}).

The terms “number density,” “concentration,” and “population” are used interchangeably in this work to describe an important laser metric: the number of atoms or molecules (depending on the species) per unit volume, [cm⁻³]. Owing to the common need for this quantity when performing kinetic analysis, the popular designator [N_i] will be used as an occasional surrogate for “number density of species N_i.”

The generic shortcut designations N_i, N_i^{*}, and [N_i] prove particularly convenient in plots or tables involving kinetic data, wherein brevity is paramount. Therefore, in these venues, they are used almost exclusively over the more complete definitions.

1.6. Sequence of Presentation

In general, this thesis is presented in the same chronological order as it was developed. After providing a survey of relevant laser research, the author will introduce ILSA (IBr Laser Simulation Algorithm), the computer program written to examine kinetic behavior of an IBr photolysis laser. By detailing the mathematical expressions used to simulate key laser processes—as well as the assumptions and simplifications inherent in such expressions—the theoretical foundations of the ILSA kinetic model should be well established.

Derivation of the computer model is followed by its use; accuracy is validated by comparison with independently-published, experimental results. Executing the ILSA model several times, with wide variations in its input parameters, provides a means of

revealing the central processes at work in an IBr photolysis laser. This anchor of understanding has an important function: it facilitates accurate sensitivity analysis, upon which reasonable simplifications to the model can be made.

In an attempt to exploit these kinetic simplifications, a time-independent, analytic solution is then considered. It is the continuous-wave, rather than pulsed, properties of the IBr laser that are of prime interest to a potential user. Therefore, the prospect of a steady-state model, minimally complex in design, is quite attractive. Such a model would be an efficient tool for further refining the laser's parametric envelope.

Data consolidated from each type of IBr laser model are presented, discussed, and analyzed in final form in Section V. Using efficiency as a prime criterion, laser performance is optimized through parameter selection and then compared, in objective terms, to the t -C₄F₉I system.

In a concluding section, the more immediately relevant issue of design viability is addressed. Based upon results culled from ILSA simulations, the author will offer recommendations on whether the IBr photolysis laser is worthy of further study and development.

II. Background

2.1. Literature Review

2.1.1. Characteristics of Solar-Pumped Lasers

Due to the restrictive nature of the space environment, there are few laser systems that could be considered ideally suited to deployment in this setting. Dependability and mission suitability, while important, must be tempered with concerns of self-sustainability and cost efficiency. High-energy chemical lasers are being investigated by NASA as the prime fallback candidate for weapons missions [1]. However, the costs associated with fuel delivery for low-power missions raise acute questions of practicality. It is for this reason that the harnessing of solar radiation is worthy of vigorous investigation. If only on an intuitive level, solar-pumped lasers are ideally suited for space-based deployment.

Solar pumping is a term that has multiple interpretations within the scientific community. In addition to the more forthright method of "direct" pumping (in which solar radiation is instantaneously collected, concentrated, and re-emitted toward the gain cell of a laser by reflective dish), it is possible to fashion solar energy transfer via blackbody cavity or photolytic cell arrays [1]. In its first report on prospective space-based lasers, the NASA High-Power Laser Working Group examined each of these methods in a comprehensive context. Because of its technical simplicity and high

transfer efficiency, direct pumping was deemed the preferable alternative. In deference to this conclusion, the direct method is likewise assumed throughout this thesis.

Although true solar-pumped laser systems have been successfully developed and operated [10], they are not common in the experimental setting. More frequently, scientific investigations of these modules take the form of conceptual design and computer simulation [5, 7, 9, 11]. Typically, experimental treatment is confined to the use of artificial flashlamp simulators [6, 8, 12, 13, 14].

Existing research overwhelmingly suggests that photodissociative lasers—which operate on stimulated emission of excited atoms generated via molecular photolysis—are particularly well conditioned for direct solar pumping [1, 12]. Molecular photodissociation generally occurs within relatively wide bands of the optical spectrum; concentration of solar energy onto a parent molecule therefore provides a convenient mechanism by which to impart electronic excitation to a lasing atom. Broad absorption bands also present the added benefit of eliminating system sensitivity to a particular pump wavelength; this is highly desirable for environments in which ambient effects like vibration are not easily controlled [15]. In NASA's more recently published papers, it has tacitly concluded that perfluoro-*t*-butyl iodide ($t\text{-C}_4\text{F}_9\text{I}$) is the most promising precursor candidate for the solar-pumped arena [6]. As a result, most of NASA's related research projects have come to explicitly assume, construct, or test the $t\text{-C}_4\text{F}_9\text{I}$ model. While the prospect of an IBr system has been briefly mentioned in NASA's earlier papers, further study of this candidate was discouraged due to its propensity for bottlenecking [1].

Given the wide spectral character of solar radiation, total operating efficiencies of solar-pumped lasers are manifestly low. Even the favored $t\text{-C}_4\text{F}_9\text{I}$ precursor offers a practical efficiency of no better than 0.1 percent [6]. While such performance is certainly acceptable in *economic* terms, the immediate aim of any insolation-based system should be to optimize the overall spectral match between source and device. As mentioned previously, it is largely *this* consideration which serves as the strongest argument for IBr selection.

2.1.2. The IBr Photodissociative Laser

In 1969, with the success of other photolytically-driven lasers well established, Giuliano and Hess constructed and operated the first IBr photodissociative laser [16]. In their study, the experimenters obtained Br^*/Br inversion via flash photolysis by a 540 J xenon flashbulb with firing duration of 15 μs . The resulting laser pulse was roughly 5 μs in duration, with a peak output power of 50 W. Aside from establishing the viability of an IBr laser, the Guiliano and Hess study also constituted one of the first kinetic examinations of bromine/iodine interaction under intense photolysis. Many of these observations were encouraging in their implications for future IBr laser devices. Of particular note was a rapid regeneration of photofragments into the initial IBr precursor: a three millisecond lapse time was sufficient for restoring IBr concentrations almost completely to pre-dissociated levels. Predictably, this phenomenon supported excellent reproducibility of performance over relatively modest relaxation intervals. For this reason, Guiliano and Hess asserted, the IBr laser exhibits an engineering advantage rare within the family of chemical lasers: the ability to repetitively lase—several hundred times per second—without assistance from a vacuum flow system.

A significant by-product of the Guilano/Hess paper was experimental resolution of previously conflicting IBr spectroscopy studies. The production of excited bromine (rather than iodine) atoms upon IBr photodissociation was confirmed, and proved itself to be an issue of interest for other researchers in the ensuing years. Indeed, independent investigations of IBr photodissociation, Br ($^2P_{1/2}$) quantum yields, and iodine/bromine kinetic rate coefficients were all soon performed extensively, thus solidifying the theoretical foundations of IBr laser dynamics [3, 4, 17, 18, 19, 20, 21, 22, 23].

A 1983 IBr laser study by Zapata and De Young qualitatively supported the earlier results by Guilano and Hess, but also presented methods for conditionally *improving* laser performance [8]. The insertion of neon buffer gas into the gain cell, for instance, expedited recombination of IBr photofragments after photolysis. As a result, thermal increases were lessened and laser pulse duration was extended to more than fifty microseconds under favorable circumstances. While suspecting that atomic iodine was the dominant Br ($^2P_{1/2}$) quencher, Zapata and De Young attributed the root cause of lasing extinction to temperature increases within the gain cell.

Concurrent with the Zapata/De Young study was one of the first computational modeling efforts of the IBr laser, undertaken by Harries and Meador [9]. Their results served to reinforce the interpretation of atomic iodine as a predominant bromine quencher. The computer model also impressed the significance of the exchange reaction $\text{Br} + \text{IBr} \rightarrow \text{I} + \text{Br}_2$, which enables lasing by continually removing ground state bromine atoms and thus minimizing buildup of the lower laser level. Based on their analysis, Harries and Meador discarded the effects of three-body recombination as kinetically unimportant.

Since the early 1980's, further investigation of the IBr laser as a solar-pumped candidate has been modest at best. The discovery of several iodine-based precursors—each exhibiting excellent I ($^2P_{1/2}$) quantum yields and only modest quenching effects—has driven the bottleneck-prone IBr candidate from high-level consideration. Despite this, the IBr photodissociative laser has recently enjoyed renewed interest under *alternate* excitation scenarios. For instance, because of the high Br ($^2P_{1/2}$) quantum yield from IBr photolysis at 500 nm, frequency-doubled Nd:YAG (532 nm) laser beams are now an attractive method of pumping the IBr laser [21, 24]. The efficiency of Nd:YAG pumping also provides flexibility in application. For instance, inserting small partial pressures of alternate lasants (e.g., nitrous oxide) into the IBr gain cell enables realization of electronic-to-vibrational energy transfer lasers [15, 25]. These advances notwithstanding, consideration of the IBr photodissociation laser as a viable candidate for solar-pumped, space-based operation has all but dissipated. By all indications, this rejection is founded in the perceived difficulty of obtaining continuous-wave oscillation. As a result, contemporary studies of the IBr laser are almost exclusively confined to pulsed operation under laser pumping.

2.1.3. Space-Based Resonator Design

Since NASA's first step towards space-based laser development in 1980, *engineering* contributions to solar-pumped laser research have grown considerably in both number and scope. In a recent attempt to conceptually address the demands of both physics and mechanics in construction of a solar-pumped, space-based laser, NASA researchers Choi *et al* presented a hypothetical module design that could be used as the basis for such a system [7]. In it, the researchers propose an iodine-based

photodissociative laser—directly pumped by a pseudo-parabolic reflecting dish—based upon the master oscillator/power amplifier (MOPA) principle. A diminutive $t\text{-C}_4\text{F}_9\text{I}$ laser, with correspondingly modest pumping demands, constitutes the master oscillator for the system. Spatial filters are used to select a single transverse mode of CW oscillation, with a target output power of 10 watts. A pre-amplifier/power amplifier combination, powered by photolytic cells on the periphery of the reflecting dish, is then used to magnify the beam output by a factor of 5,000. If such a design were successfully implemented, the resulting laser module would be able to serve as a source of power (via beaming) for satellites, surface rovers, or spacecraft. Additional demands for power could be satisfied through the coupling of multiple laser modules into an array.

Current engineering research is applicable to this thesis in a very central manner. Elements of the Choi study, for instance, provide general guidance for selecting realistic parameter ranges (cavity size, geometry, etc.) for computational analysis. Two suggestions in particular warrant mention. Firstly, the desire for a high-power beam in space does not necessitate construction of a high-power master oscillator. With numerous methods available for power amplification (among them, the above-mentioned MOPA principle), the chief objective should be a stable, but energetically-modest output beam. In terms of scale, this would translate to a cavity length on the order of a meter. Adopting this smaller, lower-intensity laser system would mitigate temperature increases within the gain cell, and considerably reduce the requisite size of a solar reflector. Secondly, the Choi study offers novel arrangements for possible pumping *geometries*. A strong case is made for selection of a pseudo-parabolic reflecting dish, positioned at either extreme of the gain tube, such that emitted radiation is contrived to a frustum-like

focal volume matched to the laser tube's geometry. Figure 2-1 reflects the important optical distinction between true and pseudo-parabolic designs. Whereas the shape of a true parabola serves to direct incident radiation on a single focal point, judiciously broadening the curvature of such a dish allows a distribution of radiative power over the entire length of the gain cell (Figure 2-1). This quasi-axial pumping arrangement should be considered a favorable alternative to other (e.g., side-oriented) pumping geometries.

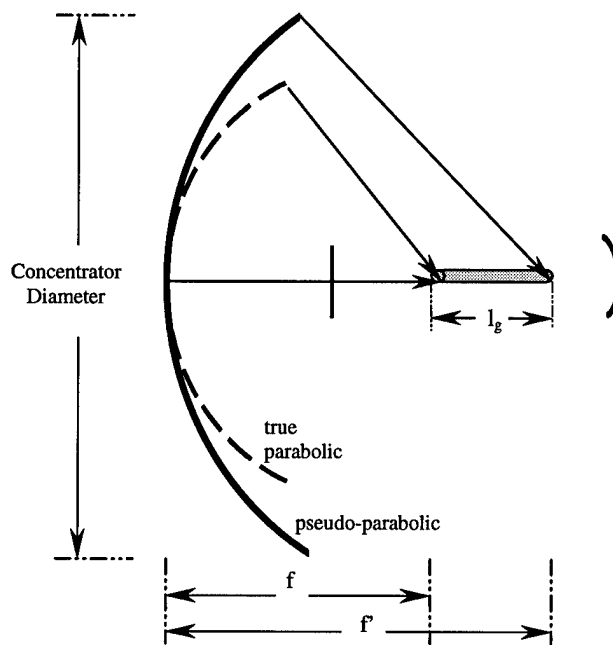


Figure 2-1. Geometrical design of a frustum-oriented solar concentrator.

2.2. Limitations of Previous Modeling Efforts

Although numerous papers have alluded to the prospect of a sustainable, continuous-wave IBr laser [8, 9], to date no published study has resolutely addressed the engineering demands of such a product. Nor have previous modeling efforts considered

the effects of lasant flow within their modeling efforts. Historically, treatment of the continuous-wave scenario has most commonly taken the form of supposition, founded upon observed or modeled results of the pulsed IBr laser. By examining the temporal duration of a sealed-cell laser pulse, one can reasonably estimate the rapidity with which IBr photofragments (and their resulting halogen products) must be flushed from the gain cell to sustain continuous operation. While this approach yields a fair heuristic estimate, it does not constitute solution of the problem. This thesis will propose a straightforward representation of flow that can be used to further develop parameters of the IBr laser.

In addition to developing *new* kinetic processes for the IBr laser model, this thesis will address some of the methodology employed by previous studies. The Harries/Meador work, which constituted the first (and as yet, only) computational model of a solar-pumped IBr laser, was founded upon questionable precepts. It is important that reasons for this departure be documented and explained *a priori*, while avoiding unnecessary indulgence into related technical detail. Full motivation for these alternate approaches will be provided in the following section.

Perceived limitations of the Harries/Meador study are as follows:

1. In modeling of the solar pumping process, no upper or lower wavelength cutoff was defined for IBr, Br₂, or I₂ photodissociation within the gain cell, implying the absence of a bandpass filter in the module. Despite this, a quantum yield of 70.4 percent was used, over the entire photolysis spectrum, to model the rate of Br (²P_{1/2}) generation. In fact, this high a yield is applicable to only a peak incident wavelength of roughly 500 nm [3, 4]. Wavelengths above or below this value induce considerably lower quantum yields, and should be so reflected in the model. Indeed, this paper shall demonstrate that

unrestricted solar excitation produces so weak a Br^*/Br generation ratio, that only short-term (pulsed) lasing is energetically possible under these conditions.

2. Photodissociation rates for each of the three diatomic molecular species (IBr , Br_2 , and I_2) were presented as linearly dependent upon both solar flux and molecular concentration. However, to be precise, a mathematical model for photon absorption should account for attenuation effects along the photolysis path length, as given by the Beer-Lambert Law [26]. Furthermore, the absorption rate of a particular molecular species is affected by competition from other absorbing molecular types. Because IBr , Br_2 , and I_2 all absorb within the optical spectrum [27, 28], accurate pumping expressions for the IBr laser must include a simultaneous functional dependence upon each of these concentrations.

3. In the absence of certain rate coefficients central to kinetic behavior of an IBr laser, Harries and Meador postulated a rate coefficient, based upon the equilibrium condition $\text{I}_2 + \text{Br}_2 \rightleftharpoons 2\text{IBr}$, that would serve to restore molecular balance within the gain cell. Although this approach induces the experimentally-observed restoration of IBr after dissociation, it does so by virtue of an unfounded kinetic mechanism. Additionally, while this proposed four-body exchange reaction may maintain observed balances between molecules, it does not necessarily provide for peripheral effects on atomic bromine or iodine. Such effects could play a substantial role in obtaining population inversion and, consequently, laser output power. It is the author's belief that, even in the absence of established experimental data, fair approximations to important kinetic coefficients can be developed and used to successfully model the IBr photodissociative laser.

III. Methodology

Conclusions drawn from a computer model are only as accurate as the constituent processes upon which that model is founded. For this reason, it is important that each of these processes be explained, documented, and validated if possible. Indeed, ILSA source code draws its architecture from a wide range of applied physics and molecular chemistry literature. This section will endeavor to explain the methods used to integrate such theory into pertinent mathematical representations.

For the proposed laser system, there are four distinct processes needed to describe overall kinetic behavior. The first of these, laser pumping, is driven by the collection, concentration, and absorption of solar radiation, as well as a resulting excitation/dissociation of molecules within the gain cell. Atomic iodine and bromine are thus produced, serving to alter chemical populations and initiate photon emission within the laser cavity. Figure 3-1 reflects the interaction of these processes in the form of a qualitative energy level diagram.

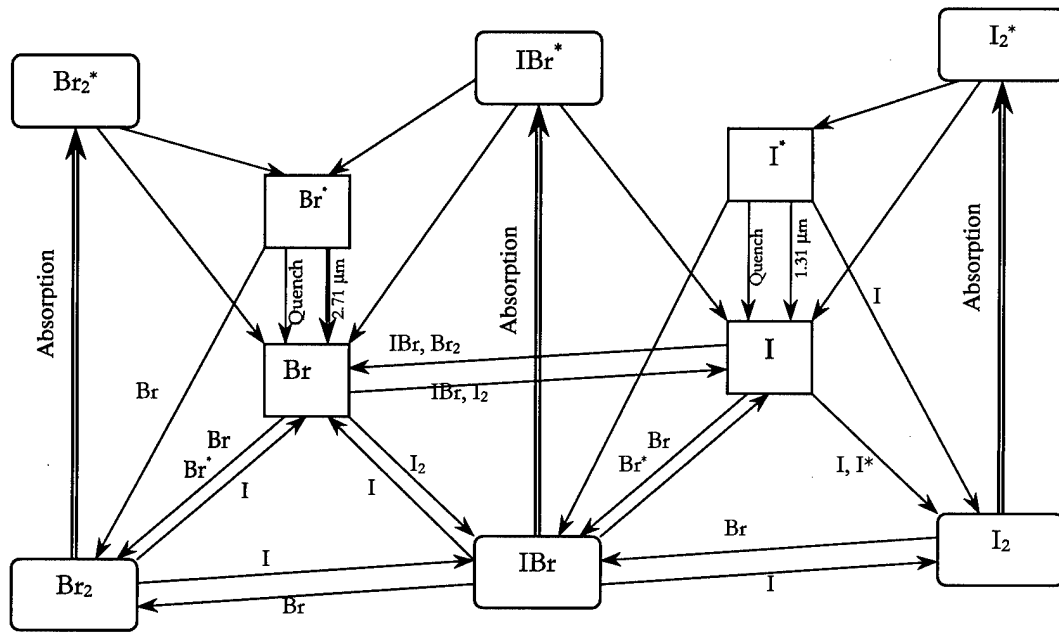


Figure 3-1. Energy level diagram reflecting chemistry of interaction between atoms and molecules of an IBr laser system.

An added consideration is the phenomenon of lasant flow, whereby “spent” gain material is ejected, recombined, then reintroduced to the cell in the form of original precursor. It is instructive to treat each of these processes individually; therefore, each is introduced and derived in the order just described. With such a framework developed, one can then properly combine these processes into a *comprehensive* laser model.

3.1. Solar Emission & Concentration

Using radiometric methods, the sun can be quite accurately modeled as a 5780 Kelvin graybody with emissivity (ϵ) of 99% [29, 30]. A wavelength-dependent variation of Planck’s Law provides the expression for energy exitance (in units of watts/m² per m wavelength) of a generic graybody emitter [31]:

$$M_e(\lambda, T) = \epsilon \frac{2\pi h c^2}{\lambda^5} \frac{1}{e^{hc/\lambda k T} - 1}, \quad (3-1)$$

where h is Planck's constant, c is the speed of light in a vacuum, k is Boltzmann's constant, and T is the applicable blackbody temperature. Dividing by the energy of one photon ($h\nu$) converts exitance from an energetic (M_e) to a photometric (M_q) quantity. Because the phenomenon of photodissociation is driven by absorption of individual photons, it is *this* representation which is central to the IBr laser. Thus, an expression for total solar exitance is:

$$M_q(\lambda)_{\text{SOLAR}} = \epsilon_s \frac{2\pi c}{\lambda^4} \frac{1}{e^{hc/\lambda k T_s} - 1}, \quad \{\epsilon_s = 0.99; T_s = 5900\text{K}\} \quad (3-2)$$

Again using principles of radiometry, one can convert solar exitance into "terrestrial" incidence. The large relative distance between earth and sun allows treatment of the sun as a Lambertian *disk* source [29]. Total incident flux density, $F(\lambda)$, in photons/s·cm² per meter wavelength, is given by:

$$F(\lambda) = 10^{-4} \left(\frac{r_{\text{sun}}}{R_{s,e}} \right)^2 M_q(\lambda)_{\text{SOLAR}} \quad (3-3)$$

where r_{sun} is the radius of the sun, $R_{s,e}$ is the relative distance between sun and earth, and a 10^{-4} conversion factor is used in anticipation of the more conventional units of photons/s·cm² (rather than photons/s·m²). Because the highest practical limit on satellite orbit altitude is roughly 40,000 km (less than 0.03% of the sun-earth separation distance), the expression is virtually identical for both earth- and space-bound scenarios.

Equation (3-3) represents total photon incidence onto a surface positioned normal to the line of sight between source and receiver. Integration of the expression over the

entire solar spectrum (roughly 0.2 - 5 μm) returns a total photon intensity of 6.325×10^{17} photons/sec·cm², a reassuring result that is in agreement with experimental data [29]. If a wavelength-selective bandpass filter were used in the system, wavelength limits of the integral would be changed accordingly.

The feasibility of any solar-pumped laser is predicated upon use of a solar concentration mechanism; only in this manner can sufficient pumping intensity be generated to obtain population inversion of the lasing species. The most promising method of solar concentration—and the one that will be exclusively considered here—is that of a parabolic or elliptical reflection dish, with practical dimensions as large as 8,000 m² [7]. Regardless of the actual geometry or dimension of such a dish, current engineering literature suggests that a concentrator, suitable for installation on a space station, could achieve a magnification factor as high as 20,000. The magnification factor, S_c , is simply defined in geometrical terms: it is the ratio of effective concentrator area (that area exposed to solar incidence) to the cross-sectional area of the gain cell's pumping region. Insofar as a magnification factor is more concise and less mathematically cumbersome than its alternative, this convention shall be used consistently throughout the thesis.

With use of a solar concentrator, then, the total photon intensity (I_v) upon a laser tube is found by augmenting equation (3-3) by the factor S_c , and integrating the expression with respect to λ :

$$I_v = \int_{\lambda_1}^{\lambda_2} S_c F(\lambda) d\lambda = S_c \int_{\lambda_1}^{\lambda_2} F(\lambda) d\lambda \quad (3-4)$$

3.2. Absorption Cross Section

In 1964, Seery and Britton characterized absorption spectra from five iodine- and chlorine-based molecules by spectrophotometer and fit their results to convolved Gaussian distributions [27]. The end product of their study (which included examination of IBr and Br₂, two species central to this thesis) was a temperature-dependent representation of extinction coefficients over each molecule's range of optical absorption. Because of the confirmed accuracy of these measurements, and the ease with which the Gaussian representations can be reproduced in modeling efforts, the Seery/Britton study is still widely cited today [3-4, 8-9, 15-16, 21, 25, 32]. Their results for molecular bromine and iodine have therefore been used as the basis of calculating absorption cross sections in this thesis. Additionally, their methodology has been used here to model a corresponding cross section for molecular iodine, based upon experimental data reported by Tellinghuisen [28]. As IBr, Br₂, and I₂ are each optically-excitable species which exist within the gain cell at all times, accurate models for all three are needed to properly simulate the pumping effects of incident solar radiation.

When plotted as functions of wavelength, molar extinction coefficients for IBr and Br₂ do not conform to a single Gaussian distribution. Although some molecules can be accurately represented by this simple approach (e.g., Cl₂ and I₂), Britton and Seery found it necessary to convolve two or more Gaussian distributions to successfully model IBr and Br₂. Using least-squares computational analysis, they identified those curve parameters that would most closely mirror experimental results. Furthermore, they introduced a scaling factor that effectively accounts for absorption falloff with increasing ambient temperature. In this manner, Gaussian models of molecular absorption were

defined by three parameters: ν_o , frequency of maximum absorption; $\epsilon_m(T)$, peak extinction at $\nu=\nu_o$; and $\Delta\nu(T)$, mean curve variance in frequency space. Each individual curve contributes additively to the total extinction coefficient of a species according to the formula:

$$\epsilon_{\text{Tot}}(\nu, T) = \sum_j \epsilon_j(\nu, T) = \sum_j \epsilon_{m,j}(T) \exp\left\{\left[\nu - \nu_{o,j}\right] / \Delta\nu_j(T)\right\}^2, \quad (3-5)$$

where the temperature-dependent quantities $\epsilon_m(T)$ and $\Delta\nu(T)$ are determined by their peaks values at 0 Kelvin ($\epsilon_m(0)$ and $\Delta\nu(0)$), as well as the applicable molecule's resonant vibrational frequency (ν_v):

$$\epsilon_m(T) = \epsilon_m(0) \sqrt{\tanh\left(\frac{h\nu_v}{2kT}\right)} \quad (3-6)$$

$$\Delta\nu(T) = \Delta\nu(0) \left[\tanh\left(\frac{h\nu_v}{2kT}\right) \right]^{-1/2} \quad (3-7)$$

Since extinction coefficient [ϵ , liters/mole-cm] and absorption cross section [σ , cm²] are related as directly proportional quantities, conversion between the two involves a single multiplicative constant containing Avogadro's number (N_A):

$$\sigma = \frac{\epsilon}{N_A} \left(\frac{1 + \text{Ln}(10/e)}{10^{-3} \text{liters/cm}^3} \right) = \epsilon \left(3.824 \times 10^{-21} \frac{\text{cm}^3 \cdot \text{mol}}{\text{liter}} \right) \quad (3-8)$$

The absorption spectrum of molecular iodine is observed to closely follow a single Gaussian-like distribution about a peak wavelength of 497 nm. Employing Mathematica's[®] *Nonlinear Regression* function, data from the Tellinghuisen study were successfully fit to such a model. Agreement between experimental and modeled results for I₂ absorption is encouraging, especially within the critical wavelength range of 460-

545 nm (Table 3-1). For purposes of completeness and reproducibility, the parameters used in generating all three molecular absorption curves are cataloged in Table 3-2.

Table 3-1. Experimental and Modeled Extinction Coefficients for I₂ (liters/mol-cm)

λ (nm)	Exp.	Model	λ (nm)	Exp.	Model
420	6.9	6.46	540	81	81.4
430	16.9	16.4	550	59	59.0
440	34.5	34.3	560	41	41.3
450	61	61.2	570	27.9	27.7
460	93	94.2	580	18.4	18.0
470	127	127	590	11.8	11.3
480	153	154	600	7.4	6.95
490	168	168	610	4.6	4.17
500	167	167	620	2.8	2.46
510	154	154	630	1.7	1.42
520	131	132	640	0.8	0.811
530	106	107	650	0.4	0.457

Table 3-2. Gaussian Modeling Parameters for IBr, Br₂, and I₂ Extinction Coefficients

Molecule	ν_y (Hz)	ν_0 (Hz)	$\epsilon_m(0)$ (liters/mol-cm)	$\Delta\nu(0)$ (Hz)
IBr	8.02×10^{12}	5.915×10^{14}	169.8	3.40×10^{13}
		6.285×10^{14}	288.0	6.63×10^{13}
		1.119×10^{15}	78.9	1.15×10^{13}
Br ₂	9.69×10^{12}	6.136×10^{14}	90.1	4.75×10^{13}
		7.248×10^{14}	204.2	6.31×10^{13}
I ₂	6.42×10^{12}	6.065×10^{14}	245.3	4.10×10^{14}

Figure 3-2 provides valuable insight into the relative magnitudes and wavelength ranges of IBr, Br₂, and I₂. When multiplied by the population density of each respective species, these absorption cross sections determine the relative probabilities with which molecules absorb incident photons of a particular wavelength.

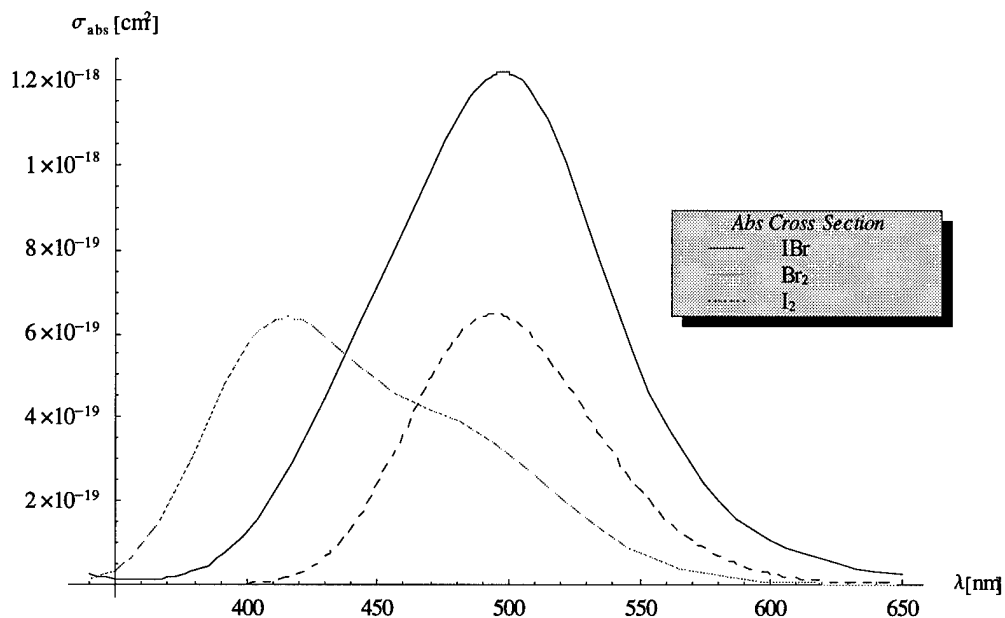


Figure 3-2. Absorption cross sections for IBr, Br₂, and I₂ as a function of wavelength of incident radiation (298 K).

3.3. Molecular Photodissociation

As a photon stream passes through any nonevacuated cell, individual photons have a probability of interaction with the medium that is proportional to both the absorption cross section, σ_{ABS} , and population density, N , of its component species. This results in spatial attenuation of photon intensity along the path of incidence, as expressed by the Beer-Lambert Law [33]:

$$I = I_0 e^{-\sigma N D_p} \quad (3-9)$$

where I_0 is defined here as intensity of the virgin beam (photons/s·cm²), D_p as the optical path length of incident radiation (cm), and N as the population density of the absorbing molecule (cm⁻³).

When the medium is comprised of more than a single molecular species, each species contributes individually to the attenuation of the photon intensity; this contribution is determined by *relative* magnitudes of each product ($N_i \cdot \sigma_i$). It should be noted that species that do not absorb within the spectral range of incident photons are effectively transparent to this radiation, and therefore may be excluded. For the case of the laser currently under examination, only IBr, Br₂ and I₂ exhibit absorption within the (predominantly optical) solar radiation spectrum. A total attenuation factor ξ can thus be defined as:

$$\xi(\lambda) = \sum_i N_i \sigma_i(\lambda) = N_{\text{IBr}} \sigma_{\text{IBr}} + N_{\text{Br}_2} \sigma_{\text{Br}_2} + N_{\text{I}_2} \sigma_{\text{I}_2} \quad (3-10)$$

and the argument of the exponential in equation (3-9) is replaced by $[-\xi D_p]$. For the case of a solar-pumped IBr laser, this expression therefore represents the intensity of penetrating solar radiation at a given depth D_p below the exposed gain cell surface.

At all times, IBr, Br₂, and I₂ molecules “compete” for the absorption of incident photons. The proportion in which each of these species absorbs incident radiation of a given wavelength is determined by the relative magnitudes of the product ($\sigma_i N_i$) at that wavelength. Upon absorption of a sufficiently energetic photon, the molecule photodissociates into its two atomic constituents. Therefore, the spatially-dependent expression for $R_{p(i)}$, the photodissociation of species i , becomes:

$$R_{p(i)}(x) = I \cdot [N_i \sigma_i] = I_0 N_i \sigma_i e^{-\xi x} \quad (3-11)$$

Integration over the entire optical path length of the gain cell yields the total photodissociation rate (molecules/cm³·s) for species i :

$$R_{p(i)T} = \int_0^{D_p} R_{p(i)}(x) dx = \frac{I_0 N_i \sigma_i}{\xi} [1 - e^{-\xi D_p}] \quad (3-12)$$

Finally, drawing from the results of derivations performed in previous sections, this equation can be modified to express the total photodissociation rate of IBr, Br₂, or I₂. Because intensity of incident solar flux (F), absorption cross section (σ), and the attenuation coefficient (ξ) are all wavelength-dependent quantities, this expression must be integrated over the wavelength boundaries defined by an assumed bandpass filter:

$$R_{p(i)T} = \frac{S_c N_i}{D_p} \int_{\lambda_1}^{\lambda_2} \frac{F(\lambda) \sigma_i(\lambda)}{\xi(\lambda)} [1 - e^{-\xi(\lambda) D_p}] d\lambda \quad (3-13)$$

Division by D_p in the above expression serves to spatially average the total photolysis rate over the entire optical path of solar radiation within the cell.

3.4. (²P_{1/2}) Photolysis Yields

Equation (3-13) capably represents the total rate of photodissociation for solar-pumped molecules. For each such photolysis event, the parent molecule temporarily undergoes electronic excitation, then dissociates into its two constituent atoms.

Moreover, because optical photodissociation involves considerable energy transfer, there is a nonzero probability that the process will incite spin-orbit excitation of one of the liberated atoms. This phenomenon is central to the IBr laser considered here, in that it is the Br (²P_{1/2→3/2}) transition that constitutes lasing action.

The interaction potentials that bind iodine and bromine atoms into an IBr, Br₂, or I₂ molecule are comprised of multiple attractive (bound) and repulsive (unbound) electronic states [3-4, 34, 35]. Relative energies of these states are represented, within

potential energy diagrams, as functions of separation distance between the two constituent atoms. At exceptionally large separation distances, such as 5 angstroms or more, the energy of each electronic state converges to one of two distinct asymptotic limits. Every event of molecular photodissociation ultimately results in the realization of one of these energetic limbs, which are characterized by distinct spin-orbit states of the two resulting atoms.* The lower, less energetic limb corresponds to a state in which both halogen atoms dissociate adiabatically into the ground state [36]. The upper, diabatic limb is characterized by dissociation of one atom into each state. As first determined by Guiliano and Hess, IBr photodissociation is energetically incapable of producing excited iodine atoms [16].

Because the dynamics surrounding excited atom production from IBr, Br₂, and I₂ photolysis are determined by the energy of an incident photon, quantum yields for (²P_{1/2}) generation are inherently wavelength-dependent. Peripheral kinetic effects, such as curve-crossing and collisional release [3, 35], can induce electronic transitions that complicate the matter of wavelength characterization. However, numerous experimental studies have been performed on this very concern, and have resulted in successful yield curves for each of the three relevant molecules. In Figure 3-3, quantum yields culled from Haugen *et al* and Brewer & Tellinghuisen are plotted as functions of incident photon wavelength [4, 34].

* Upon absorption of a sufficiently energetic photon, a given parent molecule will undergo immediate excitation to a distinct electronic state and dissociate into its constituents along one of the two electronic limbs.

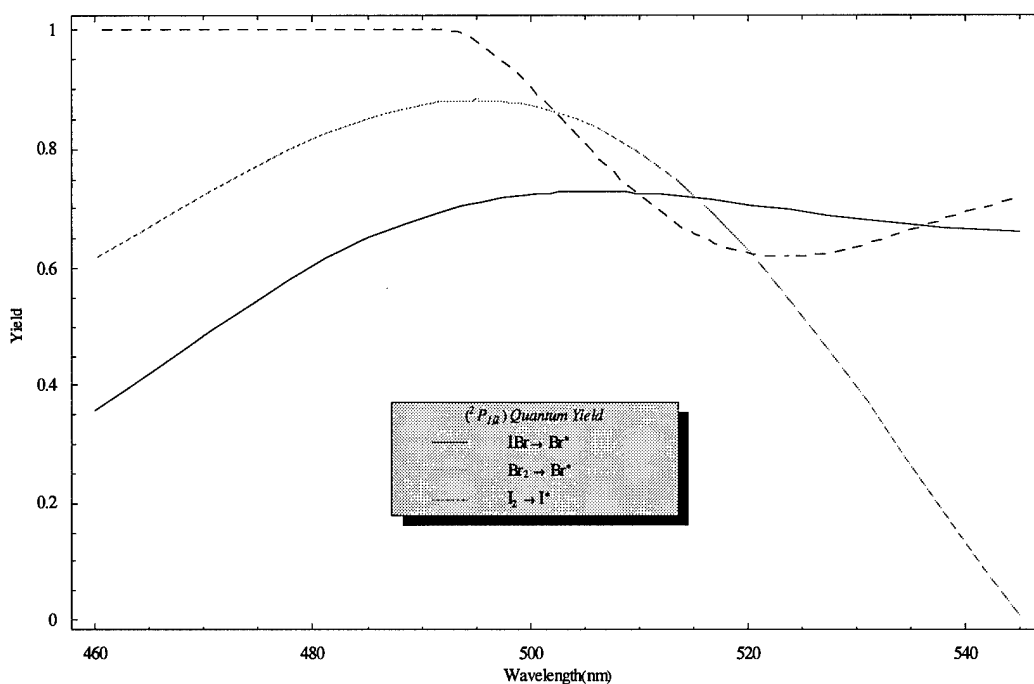


Figure 3-3. Comparison of (${}^2P_{1/2}$) quantum yields from photodissociation of IBr, Br₂, and I₂ molecules as a function of incident wavelength

Quantum yield (ϕ) is defined, for each molecule at various wavelengths, as that proportion of photodissociation events which result in exactly one excited atom. By including this term within the integral of equation (3-13), the expression can be converted from a total absorption rate into a total Br (${}^2P_{1/2}$) or I (${}^2P_{1/2}$) pumping rate:

$$R_{p(i)t} = \frac{S_e N_i}{D_p} \int_{\lambda_1}^{\lambda_2} \frac{F(\lambda) \phi_i(\lambda) \sigma_i(\lambda)}{\xi(\lambda)} \left[1 - e^{-\xi(\lambda) D_p} \right] d\lambda \quad (3-14)$$

Equation (3-14) therefore represents the production rate ($\text{mol}/\text{cm}^3 \cdot \text{s}$) of spin-orbit excited atoms due to the photodissociation process. It is valid for each of the three molecular precursors (IBr, Br₂ and I₂) when the appropriate parameters are used.

In the case of IBr, corresponding production rates for ground state bromine and iodine atoms are easily obtained by replacing ϕ_{IBr} within the integral with $[1 - \phi_{\text{IBr}}]$ and

[1.0], respectively. That is, since one iodine atom is always liberated by IBr photodissociation, it has an effective quantum yield of unity. Production rates for the unexcited daughter atoms of Br₂ and I₂ precursor are treated similarly: at least one unexcited atom will emerge from each dissociative event. Therefore, for both these ground state cases, the effective quantum yield is $[2-\phi]$.

The issue of quantum yield is central to the viability of any photolytic laser, and must be considered within the context of population inversion. Because of inherent hyperfine degeneracies within the Br (²P_{1/2}) and Br (²P_{3/2}) energy levels (2 and 4, respectively), the requirement for inversion, $\Delta N = [\text{Br}^*] - (g^*/g) [\text{Br}]$, is relaxed from $[\text{Br}^*] \geq [\text{Br}]$ to $[\text{Br}^*] \geq \frac{1}{2} [\text{Br}]$. Thus, the effective quantum yield ϕ must be greater than or equal to 0.33 to contribute to inversion [36]. As current data indicates that these cutoffs occur at the 457.7–545.3 nm wavelength boundaries, this is the spectral region that will be initially considered in this thesis. It is assumed that, during laser operation, wavelengths external to this band are excluded by some manner of bandpass discrimination.

3.5. Kinetic Interaction of Chemical Species

The rate with which a given chemical reaction occurs is proportional to the number density of each parent species, as well as a unique reaction constant k applicable to that specific process [42]. For instance, in the generic exchange (e_1) reaction $\text{AB} + \text{C} \rightarrow \text{AC} + \text{B}$, the rate of the reaction is defined as $\text{Re}_1 = [\text{AB}] \cdot [\text{C}] \cdot k_{e_1}$. Since the yield of AC and B from this reaction is unity, production rates for each of these species (due to reaction e_1 only) are Re_1 as well. A similar methodology applies to the process of three-

body recombination, in which an assisting agent M acts as a collisional energy sink between two atoms. By providing a transfer mechanism for latent kinetic energy of the colliding atoms, the assisting agent makes chemical assembly of the atoms energetically possible. The frequency of a specific recombination event (M defined uniquely) is proportional to the product of its three colliding partners, such that the process $A+B+M_i \rightarrow AB+M_i$ has a frequency of occurrence of $R_{r_1}=[A] \cdot [B] \cdot [M_i] \cdot k_{r_1}$. The units of two- and three-body reaction coefficients are necessarily different: cm^3/s and cm^6/s , respectively.

For chemical systems containing energetically-excited atoms, another two-body interaction process is significant: that of atomic quenching. In the case of long-lived metastable atoms like Br ($^2P_{1/2}$) and I ($^2P_{1/2}$)—each of which demonstrates a spontaneous emission lifetime (τ_{21}) on the order of a second—de-excitation predominantly results via collisions with adjacent particles [18-19, 21]. Because laser performance is driven by inversion of excited- and ground-state lasant populations, the undesirable effect of atomic quenching must be accurately described. Since quenching involves the interaction of two distinct molecules ($A^* + B \rightarrow A + B$), the quenching process is characterized by two-body rate coefficients similar to those involved in exchange reactions.

By iteratively applying these reaction coefficients to a chemical system, the temporal development of all species can be obtained [37]. The result is a method for confidently evaluating a system much too complicated for closed-form analysis. Even in this full kinetic treatment, however, it is unreasonable and unnecessary to include each distinct process to obtain extremely accurate results. Doing so would require the development and application of nearly one hundred independent rate coefficients. For

reasons of practicality, therefore, the "full" ILSA model has invoked the following approximations.

1. *Three-body recombination.* Recombination is assisted not only by other chemical species, but by the interior surface of the gain cell as well. In fact, any third-body medium can serve as a combination enabler for two appropriate atoms. But, under most circumstances, chemically-assisted recombination is the dominant facilitation process [29]. For this reason, surface effects are not considered in the kinetic model. Furthermore, because IBr is by far the most populous chemical species within the gain cell, only IBr-assisted recombination reactions are addressed in the model. By eliminating all but this most common collisional partner, the number of required recombination reactions is reduced by a factor of seven. This is a desirable result, in that (a) many recombination rate coefficients are poorly documented and therefore cannot be adopted with high confidence, and (b) full inclusion of the 50+ remaining recombination reactions would prove a severe burden to the kinetic code. At any rate, current literature suggests that the cumulative effects of recombination, when compared with exchange and quenching processes described above, are kinetically minor [9, 37].

2. *Rare ($^2P_{1/2}$)-partner reactions.* While it is possible for excited atoms to participate in all exchange or recombination reactions, the coefficients of such reactions are roughly 1-2 orders of magnitude less than those of their unexcited counterparts [22, 38]. By far, quenching is the reaction most likely to consume a spin-orbit excited atom. For this reason, exchange reactions involving Br* or I* species have been excluded from the model. In the case of recombination, the central phenomenon of *energy transfer* justifies consideration of some ($^2P_{1/2}$) interaction. Therefore, recombination processes

involving as many as one excited atom are modeled; those involving the extremely rare recombination of *two* excited atoms are excluded.

3. *Collisional dissociation.* Concurrent with photolytically-driven dissociation, the halogen molecules within the gain cell also undergo *collisional* dissociation of the form $AB+M \rightarrow A+B+M$ [39]. However, under typical laser pumping, this rate is far eclipsed by that of photodissociation and shall not be included in the model.

It is an unfortunate fact that—from all indications of present research—quantified rate coefficients have been experimentally determined for only two of four important exchange reaction processes [9, 40]. More specifically, coefficients for forward and reverse directions of the reaction $Br + IBr \rightleftharpoons I + Br_2$ are established; those for $Br + I_2 \rightleftharpoons IBr + I$ are not.[†] In their computational treatment, Harries and Meador explicitly included only the *forward* processes of each reaction, presumably because the exothermic, “downhill” nature of these reactions signify larger rate coefficients than the reverse scheme [9].

This limited representation of IBr laser cell kinetics, however, does not reflect, even in heuristic terms, the proper kinetic relationship between IBr, Br_2 , and I_2 molecular species. The execution of kinetic code with well-developed rate coefficients should, in the absence of an excitation source and at 298.2 K, restore randomized population distributions of IBr, Br_2 , and I_2 to an equilibrium ratio determined by the law of mass action: 100:4:4 [9, 41]. Associated populations of atomic iodine and bromine should be

[†] Although there exist other exchange reactions involving spin-orbit excited atoms of bromine or iodine, such reactions are relatively infrequent (due to energy barriers) and therefore are not considered here.

likewise depleted, as these atoms pursue increased stability through recombination into one of the three diatomic molecules.

Harries and Meador attempted a reconciliation of their kinetic code by incorporating the inherent equilibrium balance between IBr, I₂, and Br₂ into an artificial kinetic rate coefficient that governs chemical interaction of the three species. They reasoned [9]:

At room temperature, by the law of mass action (assuming no photodissociation), the concentration of I₂ and Br₂ in IBr is 0.04. It then follows that if the forward reaction $2\text{IBr} \rightarrow \text{I}_2 + \text{Br}_2$ has a rate coefficient K_7 , then [sic] the reverse coefficient K_8 is $(0.04)^2 \times K_7$.

While the law of mass action does *reflect* the eventual state of equilibrium between iodine and bromine species, it does not describe the process by which this occurs. The kinetic interaction that yields this result is driven by the net effect of *all* relevant reaction rates, particularly those represented by exchange processes. Given that all other significant reaction rates have been at least approximately defined, a proper quantification for the reversible $\text{Br} + \text{I}_2 \rightleftharpoons \text{IBr} + \text{I}$ process should result in the expected distribution of IBr, Br₂, and I₂ populations (absent a photolysis source). Because the exchange reactions also involve atomic radicals, ancillary effects upon atomic populations—not reflected in the Harries/Meador study—would be anticipated as well.

Relative rates for forward and backward processes of a given exchange reaction can be approximated in a straightforward manner. Using the difference in Gibbs free energy between reactants and products on either side of a chemical equation, a proportionality constant—reflecting the difference in magnitude between forward and reverse rate coefficients—can be defined for a given temperature [42]. For the exchange

reaction presently under investigation, it was determined that the forward process $\text{Br} + \text{I}_2 \rightarrow \text{IBr} + \text{I}$ is exothermic, and therefore “downhill” in nature. The rate coefficient for this process was computed to be larger than its endothermic counterpart by a factor of 7.6×10^4 [29, 41].

Suitability of this analysis was tested by performing similar calculations upon the experimentally-established, reversible exchange reaction $\text{Br} + \text{IBr} \rightleftharpoons \text{I} + \text{Br}_2$. The resulting proportionality factor of 1.67×10^2 is closely in agreement with a 1.71×10^2 ratio calculated from data measured by Clyne/Cruse and Haugen *et al* for forward and reverse reaction rates, respectively [20, 4].

With *relative* magnitudes of these coefficients established, only one remaining element—the approximate frequency of either process—is needed to quantify the value of both rate coefficients. Gruebele *et al* insisted on the absence of coefficient data for either direction of this reaction, but conjectured that, due to its small energy barrier to formation, the forward process occurs rapidly: “within a small order of the collisional rate [40].” In this vein, the present study assigned rate coefficient values between 10^{-11} and 10^{-10} mol/cm³·s to the forward reaction; corresponding reverse coefficients were assigned in accordance with the proportionality factor defined previously. Model simulation (absent pumping) was subsequently used as a means of selecting a base value that produces experimentally expected results. A middle value of approximately 5×10^{-11} was chosen due to its agreement with the law of mass action.

With reasoning thus defined, central reaction processes included in the ILSA model are the following:

Table 3-3. Rate Coefficients Used in Numerical Model of IBr Laser

Eqn	Reaction Process	Rate Coefficient	Units	Reference (Endnote #, Author)
[kq1]	$\text{Br}^* + \text{IBr} \rightarrow \text{Br} + \text{IBr}$	1.0×10^{-12}	cm^3/s	[18] Pastel <i>et al</i> ('94)
[kq2]	$\text{Br}^* + \text{I} \rightarrow \text{Br} + \text{I}$	1.9×10^{-11}	cm^3/s	[18] Pastel <i>et al</i> ('94)
[kq3]	$\text{Br}^* + \text{I}_2 \rightarrow \text{Br} + \text{I}_2$	1.9×10^{-12}	cm^3/s	[19] Hofmann/Leone ('78)
[kq4]	$\text{Br}^* + \text{Br}_2 \rightarrow \text{Br} + \text{Br}_2$	1.2×10^{-12}	cm^3/s	[21] Johnson <i>et al</i> ('96)
[kq5]	$\text{Br}^* + \text{Br} \rightarrow \text{Br} + \text{Br}$	6.8×10^{-13}	cm^3/s	[18] Pastel <i>et al</i> ('94)
[kq6]	$\text{Br}^* + \text{Br} \rightarrow 2\text{Br}$	2.5×10^{-14}	cm^3/s	[18] Pastel <i>et al</i> ('94)
[kq7]	$\text{I}^* + \text{IBr} \rightarrow \text{I} + \text{IBr}$	6.0×10^{-11}	cm^3/s	[9] Harries/Meador ('83)
[kq8]	$\text{I}^* + \text{I}_2 \rightarrow \text{I} + \text{I}_2$	3.5×10^{-11}	cm^3/s	[9] Harries/Meador ('83)
[kq9]	$\text{I}^* + \text{Br}_2 \rightarrow \text{I} + \text{IBr}_2$	5.6×10^{-11}	cm^3/s	[9] Harries/Meador ('83)
[ke1]	$\text{Br} + \text{IBr} \rightarrow \text{I} + \text{Br}_2$	4.6×10^{-11}	cm^3/s	[4] Haugen <i>et al</i> ('85)
[ke2]	$\text{Br} + \text{I}_2 \rightarrow \text{IBr} + \text{I}$	5.0×10^{-11}	cm^3/s	[40] Gruebele <i>et al</i> ('91)
[ke3]	$\text{I} + \text{Br}_2 \rightarrow \text{IBr} + \text{Br}$	2.1×10^{-13}	cm^3/s	[4] Haugen <i>et al</i> ('85)
[ke4]	$\text{I} + \text{IBr} \rightarrow \text{I}_2 + \text{Br}$	4.6×10^{-16}	cm^3/s	Present Study
[kr1]	$\text{Br} + \text{Br} + \text{IBr} \rightarrow \text{Br}_2 + \text{IBr}$	3.0×10^{-30}	cm^6/s	[9] Harries/Meador ('83)
[kr2]	$\text{Br}^* + \text{Br} + \text{IBr} \rightarrow \text{Br}_2 + \text{IBr}$	4.0×10^{-32}	cm^6/s	[9] Harries/Meador ('83)
[kr3]	$\text{Br} + \text{I} + \text{IBr} \rightarrow 2\text{IBr}$	1.0×10^{-32}	cm^6/s	[9] Harries/Meador ('83)
[kr4]	$\text{Br}^* + \text{I} + \text{IBr} \rightarrow 2\text{IBr}$	1.0×10^{-32}	cm^6/s	[20] Clyne/Cruze ('72)
[kr5]	$\text{I}^* + \text{Br} + \text{IBr} \rightarrow 2\text{IBr}$	3.0×10^{-32}	cm^6/s	[9] Harries/Meador ('83)
[kr6]	$\text{I} + \text{I} + \text{IBr} \rightarrow \text{I}_2 + \text{IBr}$	3.0×10^{-30}	cm^6/s	[9] Harries/Meador ('83)
[kr7]	$\text{I}^* + \text{I} + \text{IBr} \rightarrow \text{I}_2 + \text{IBr}$	3.0×10^{-32}	cm^6/s	[9] Harries/Meador ('83)

3.6. Photon Emission

Photon emission—by both spontaneous and stimulated processes—is central to the operation of all conventional lasers. However, given that laser physics theory is well established and universally understood, this topic will be only briefly considered here.

The time rate of change of N_p , the intracavity photon population (in photons/ $\text{cm}^3 \cdot \text{s}$) is given as [43]:

$$\frac{\partial N_p}{\partial t} = \{A_{sp} N_{Br^*}\} + \left\{ \left(\frac{I_g}{I_c} \right) c \sigma_{SE} (\Delta N - N_{th}) N_p \right\} \quad (3-15)$$

where the first and second bracketed quantities correspond to cavity contributions by spontaneous and stimulated emission, respectively. The rate of stimulated emission is directly proportional to total photon density, stimulated emission cross section σ_{SE} , and

the difference between instantaneous ($\Delta N = N^* - \frac{1}{2} N$) and threshold (ΔN_{th}) inversion densities. The ratio of gain length to cavity length (l_g/l_c) is necessary to account for that fraction of time in which photon propagation between cavity mirrors is outside the gain cell and therefore not capable of interacting with excited bromine atoms. Consistent with previous treatments of the Br lasing process, the line shape function $g(\nu)$, an implicit element of the stimulated emission cross section, was derived as exclusively Doppler in nature [44, 45].

The spontaneous emission contribution is given as the product of total Br ($^2P_{1/2}$) population density N_{Br^*} , and a mode-specific spontaneous emission coefficient A_{sp} . This constitutes the photon "noise," caused by spontaneous relaxation of metastable bromine atoms, and is required as a feed for the buildup of stimulated emission within the cavity. Ultimately, upon reaching a respectable photon cavity population, spontaneous emission becomes kinetically negligible and output power is almost entirely determined by the stimulated emission process.

3.7. Lasant Circulation Processes

The family of processes heretofore derived is entirely sufficient for modeling a *static-cell* IBr laser system. Properly assembled, these elements accurately predict population dynamics within the gain cell over time. This is indeed the method embraced in past studies examining the nature of IBr laser pulses [9]. However, since it is suspected that a free-running, closed-cell IBr photodissociation laser cannot sustain prolonged population inversion, any attempt to treat the continuous-wave case must include a chemical restoration mechanism as well.

Due both to lasant precursor depletion and buildup of photofragment byproducts, photodissociative lasers often experience bottlenecking difficulties not shared by other lasers. An appropriate chemical restoration process, then, must address both these effects over extended periods of time. In practice, this amounts to the *simultaneous* (a) removal of photofragment products and (b) reintroduction of lasant precursor in the gain cell. Fortunately, in the case of iodine monobromide, these two demands are complementary: the law of mass action strongly favors IBr production over that of Br₂ and I₂ in the equilibrium density proportion of 100:4:4 [41]. Thus, it is clear that a lasant transit system—whereby the cell contents are allowed to flow out via circulation mechanism, recombine in the absence of stimulating radiation (possibly under high pressures), and return to the cell as dominantly-IBr precursor—is an attractive method of obtaining CW oscillation.

Precise modeling of a circulation process would require rigorous application of the Navier-Stokes transport equations, with attendant scrutiny of surface-induced viscous effects, local population density variations, and other dynamic considerations. Such attention to detail is excessively (albeit commendably) diligent for the purposes of this study. Therefore, the ILSA model invokes a truncated approach that retains only the most central tenets of fluid flow analysis.

The removal rate of chemical species from a vessel—driven by induced pressure differentials or mechanical fanning—is proportional to the induced velocity of the gas, as well as the average population density of the chemical species. Moreover, for a given flow velocity, the removal rate is *inversely* proportional to the length of flow path from

end to end. In this sense, the circulation loss behaves much like any generic decay expression. The removal constant, β , applies simultaneously to all chemical species as

$$\left(\frac{\partial N_i}{\partial t}\right)_{\text{outflow}} = -N_i \cdot \beta = -N_i \frac{v_{\text{flow}}}{l_{g(l)}}, \quad (3-16)$$

where $l_{g(l)}$ represents the length of the gain cell along the path of gas flow. Depending upon the engineering geometry used, this direction could be either parallel or perpendicular to the longitudinal orientation of the cavity.

In balance of this circulation outflow, principles of conservation require that the total atomic density loss be matched by a corresponding atomic gain in the form of input IBr precursor. That is, any pragmatically supportable laser system must avoid a net depletion or growth over time. Furthermore, it bears repeating that it is the total *atomic* rather than *molecular* density that must be balanced in detail. The continuity condition for a lasant circulation process is thus:

$$\left(\frac{\partial N_{\text{Atom}_T}}{\partial t}\right)_{\text{flow}} = 0 = \sum_m^{\text{IBr,Br}_2,\text{I}_2} 2 \left(\frac{\partial N_m}{\partial t}\right)_{\text{flow}} + \sum_n^{\text{Br,Br}^*,\text{I,I}^*} \left(\frac{\partial N_n}{\partial t}\right)_{\text{flow}} \quad (3-17)$$

Zapata's results indicate that sealed-cell, IBr laser performance is highly reproducible when sufficient time ($\sim 60+$ seconds) elapses between pumping events [8]. This suggests a strong photofragment affinity towards recombination in the same IBr/Br₂/I₂ proportion as that of initial precursor. A comparison of the relative rate coefficient magnitudes certainly supports this observation. Therefore, it is fair to assume and model a circulation system that invokes the process of recombination, outside the gain cell, as a basis for establishing a steady inflow of lasant precursor. This total

molecular inflow rate, matched on an atomic scale to the velocity-dependent outflow rate, is equal to $\frac{\beta \cdot \Psi}{2I_{g(l)}}$, where Ψ , the total atomic concentration, is defined as:

$$N_{\text{Atom}_T} = \Psi = 2 \sum_m^{\text{IBr, Br}_2, \text{I}_2} N_m + \sum_n^{\text{Br, Br}^*, \text{I, I}^*} N_n \quad (3-18)$$

Again assuming a fully-recombined population ratio of 100:4:4 (IBr:Br₂:I₂) as precursor feed, the inflow rate is split between the three species in these proportions:

$$\left(\frac{\partial N_{\text{IBr}}}{\partial t} \right)_{\text{Inflow}} = \left(\frac{1.00}{1.08} \right) \Psi \beta, \quad \left(\frac{\partial N_{\text{I}_2, \text{Br}_2}}{\partial t} \right)_{\text{Inflow}} = \left(\frac{0.04}{1.08} \right) \Psi \beta \quad (3-19), (3-20)$$

It is thus demonstrated that the introduction of a flow regimen requires application of the universal loss coefficient, $-\beta$, to all studied molecular species, as well as three source terms for IBr, Br₂, and I₂ given by equations (3-19) and (3-20).

IV. Computer Models of the IBr Photolysis Laser

The IBr Laser Simulation Algorithm (ILSA) is a Mathematica[®]-based computational package, written by the author, that solves for kinetic behavior of a Br ($4^2P_{1/2} \rightarrow 4^2P_{3/2}$) laser, pumped by photolysis of IBr via concentrated solar radiation. Based upon system parameters input by the user (i.e., gain cell temperature and pressure, solar amplification, reflectivity/transmittance of optical components, cavity dimension, bandpass filter range, and laser flow velocity), the algorithm calculates and plots population concentrations and resulting output power for a standing-wave laser cavity.

Two versions of ILSA code were developed in the course of this study. The first version—ILSA1, intended for general use—includes a guided interface that prompts the user for relevant parameters to be used in obtaining a solution. Analysis and output is then executed according to these user-defined preferences. The second version (ILSA2) is unedited source code that also contains internal hyperlinks to key portions of the document and several ancillary charts that were used to validate the model. Due to its accessibility and completeness, ILSA2 is appropriate for the design-oriented user who wishes to introduce modifications to the programming package. A printed version of this code is included as Appendix B.

4.1. Model Overview

The ILSA program is designed to effectively model all processes relevant to the IBr laser, based upon parameters input by the user. The first eighteen pages of source code are devoted to elements of the laser pumping mechanism (IBr photolysis by solar

concentration). This is followed by the introduction of eight nonlinear, coupled, time-dependent differential equations that represent the temporal dynamics of all chemical and photon populations within the gain cell under solar pumping. Numerical solutions to these equations are obtained using Mathematica's[®] native NDSolve algorithm. To assist with sensitivity analysis, each solution is then broken down into its constituent processes and plotted as a function of time.

Because the IBr photodissociation laser may require removal, recombination, and reintroduction of lasant to maintain continuous-wave behavior, ILSA performs additional analysis of long-term, non-excited chemical interaction between photofragment species. This is designed to simulate the intermediate recombination process that would be induced outside of the gain cell. It provides insight into the system's recirculation demands, particularly the time scale required for reestablishing a high-concentration IBr precursor.

An additional section of ILSA code, dedicated to obtaining a closed-form solution for CW laser performance, reflects a distillation of all data produced by the time-dependent kinetic model. While it is only approximate in nature, the analytic model allows a more immediate analysis not offered by the kinetic model. This can prove useful in design studies concerned with a laser's engineering requirements.

In the course of analyzing data, it became rapidly apparent that the ILSA code, as originally developed, was exceedingly laborious in its execution time. After some computational reconstruction, three alternate versions of code were produced. Each version is designed to match particular user requirements of time and accuracy.

Appendix A, *Modifications to ILSA Code*, presents the methods and reasoning behind these code adjustments, as well as a general comparison of each version's merits.

4.2. Time-Dependent Kinetic Model

In an attempt to fully exploit the usefulness of the ILSA model, the author executed full kinetic code several hundred times, with various parameter combinations, thereby extracting insight into fundamental behavior of the IBr laser. While doing so, two objectives were simultaneously pursued: (1) characterization of the basic nature of a solar-pumped laser pulse, and (2) an understanding of its underlying kinetic processes. Results of both these efforts, as well as an experimental validation of results, follow.

4.2.1. Results of Kinetic Simulation

Qualitatively speaking, the typical ILSA-modeled laser pulse is kinetically consistent with experimental results from previous IBr laser studies. Under nominal conditions, the laser cavity rapidly builds up an intense photon population—peaking after less than 20 microseconds—and then presides over an “underdamped”-type moderation of photon population levels. As shown in Figure 4-1, this oscillatory behavior is clearly observable in the short interval following initial gain saturation. Further analysis indicates that the extent of underdamping is dependent upon output coupler reflectivity. Optimally-coupled cavities demonstrate minimal oscillatory behavior; poor coupling results in three or more cycles of underdamped oscillation.

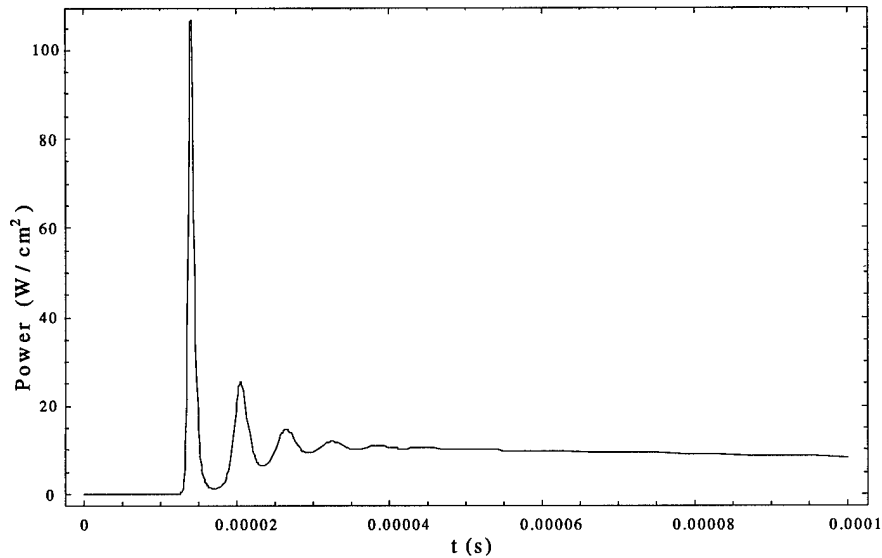


Figure 4-1. Typical temporal behavior of a poorly-coupled ILSA-modeled output pulse.

The end destination of this dampened photon population is conspicuously dependent upon the set of operating conditions selected for the module. Rigorous analysis of parameter interplay will be deferred to the following discussion section; however, one qualitative observation bears introduction here. For low pumping rates and no lasing recirculation, continuous-wave operation is not obtainable and photon density within the cavity drops to noise (spontaneous emission) levels only. This is an expected result, as is the fact that introducing ample flow velocity *does* lead to a continuous-wave capability. However, somewhat unexpected is the finding that a closed gain cell, given a sufficiently high solar concentration, will achieve continuous wave operation under most conditions. It has been postulated in previous studies—and heretofore accepted as fact—that a *sealed-cell* IBr laser is incapable of continuous-wave operation. Evidently, high pumping intensities can serve to overwhelm deleterious kinetic effects within the gain cell, achieving the desirable result of CW oscillation.

4.2.2. Sensitivity Analysis

With the exception of certain unavoidable approximations, the kinetic model developed here is as complete and exhaustive as practical. Even in the case of the mathematically-expedited alternatives, accessibility of the model has been sacrificed in favor of accuracy. This is an important first step in proper characterization of the IBr laser. Having done this, however, it is advisable to examine the numerical importance of each individual contribution to the complete kinetic solution. By doing so, the researcher can conduct an effective sensitivity analysis of the modeled system and then simplify the representation by eliminating processes which are kinetically trivial. If it can be done without sacrificing fundamental accuracy of the full kinetic model, repeated elimination of peripheral processes will ultimately lead to a system which can be represented entirely by closed-form, analytic solutions. Inasmuch as this is the desired result—providing a measure of convenience, timeliness, and simplicity—sensitivity analysis is an important exercise in kinetic model development.

Numerical solutions representing the temporal development of all distinct chemical species in the IBr kinetic model have been separated into their constituent processes and individually plotted as a function of time in the *Sensitivity Analysis* section of Appendix B. For purposes of clarity, each of the seven species is represented by a pair of charts. The first chart represents positive (“production”) contributions; the second, negative (“loss”) contributions. Both quantities are given in units of $[\text{mol}/\text{sec}\cdot\text{cm}^3]$. By observing the competing charts for a given species, one can visually assess the relative significance of each kinetic process contained in the full ILSA model. An extended kinetic analysis shall be presented in Section IV of this thesis, and thus interpretation of

these plots will not be undertaken here. However, as before, one glaring result deserves advance mention. Almost without exception, the general process of recombination is relatively infrequent; in terms of overall reaction rates, quenching and exchange processes consistently dominate kinetics of the gain cell. However, for the case of iodine dimerization ($I+I+M \rightarrow I_2+M$), a dramatically higher occurrence rate is exhibited. Indeed, in addition to achieving a steady-state reaction rate that is several orders of magnitude higher than that of its nearest recombination competitor, the iodine dimerization process is kinetically faster than several two-body reactions. This dynamic may have strong implications for resulting laser performance.

4.2.3. Experimental Validation

As previously mentioned, a bona fide solar-pumped IBr photodissociation laser has yet to be built and operated. For this reason, experimental validation of ILSA cannot be precisely achieved. Solar concentration is often simulated, however, by use of either xenon flashlamp or argon arc lamp, both of which closely approximate the spectral characteristics of solar radiation [8, 13]. More often, IBr lasers are often pumped by a frequency-doubled (532 nm) Nd:YAG system, due to the high Br^* quantum yield at this wavelength [15, 24-25]. With minor modifications to its computer code, ILSA has been adequately matched to each of these scenarios; comparison with experimental results tacitly confirms the model's accuracy in treating IBr laser kinetics. However, any validation gleaned by these approaches should be considered applicable only to non-pumping processes. As there is no current research available on actual solar pumping of iodine monobromide gas, this aspect of the IBr solar laser must stand on theoretical merits, without experimental comparisons.

The Nd:YAG-pumped, IBr photolysis laser presented by Johnson is somewhat removed from the directly solar-pumped case [15]. However, owing to this study's precise characterization of laser performance as a function of pressure, it is an effective means of testing the versatility of ILSA code under various IBr pressures. In this analysis, the stimulating pulse was *extremely* brief in duration (on the order of 10 ns), much shorter than any other event on the IBr laser time scale. For this reason, it is appropriate to simulate the Johnson study by (1) eliminating all pumping terms within the ILSA rate equations, (2) altering initial concentrations of IBr, Br*, and Br from $\{IBr_0, 0, 0\}$ to those generated by the Nd:YAG pulse according to Beer's Law and the quantum yield at 532 nm. All other aspects of the Johnson study—to include mode volume, gain cell pressure, and reflectance/transmittance of optical components—were input to the ILSA model.

While the Johnson paper did not measure actual output power of the IBr laser, it did chart temporal behavior and *relative* magnitudes of output pulses for varying partial pressures of IBr precursor. Figure 4-2, an ILSA simulation plot, reflects this same pressure-dependent behavior.

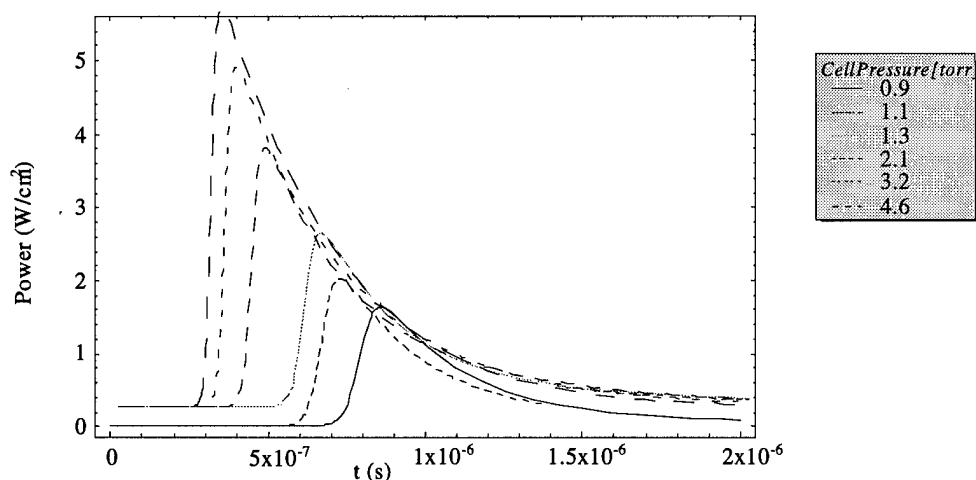


Figure 4-2. IBr-pressure dependence of an instantaneously-pumped laser

The “instantaneous” pumping approximation is appropriate for situations in which short-duration pulses are used to excite the lasant. In limiting the subsequent kinetic dynamics of the cell, this scenario also allows one to more exactly monitor the process of population equilibration. *Continual* pumping, with its resulting dissociation of all three molecular species, tends to mask the nature of ambient molecular interaction by rapidly “flooding” the gain cell with iodine and bromine atoms. By removing this pumping contribution, it can be confirmed—at least anecdotally—that the arrangement of rate coefficients produces expected results within the gain cell populations.

From previous studies of IBr photodissociation, it is known that—upon removal of a stimulating source—system equilibrium is quickly reestablished by the IBr photofragments. IBr, Br₂, and I₂ molecules are regenerated directly via atomic recombination and indirectly via exchange reactions, until the molecules achieve a

100:4:4 density distribution consistent with the law of mass action.[†] In their serial firing of a sealed-cell IBr laser, Zapata and DeYoung found that one-minute intervals were sufficient to obtain a full recovery of IBr precursor [8]. Thus, one would expect similar results to be demonstrated by the ILSA kinetic model.

In large measure, these kinetic effects are indeed reflected in model results. Over a sixty-second plotting period, populations of atomic bromine and iodine are depleted to relatively low levels. Total number density of Br₂ and I₂ species drop appreciably, but still remain above four percent of IBr density. Concurrent with these results, IBr density necessarily increases, in asymptotic fashion, towards initial (pre-stimulated) levels.

These results, *qualitatively-defined*, are true irrespective of operating conditions. Yet *quantitative* agreement between the ILSA model and experimental results is found to vary strongly with selection of total cell pressure. Lower pressures (less than 5 Torr) produce exceptionally well-behaved results; at 1 Torr, a sixty-second recombination period restores IBr precursor to 93% of its initial concentration; proportions of [Br₂] and [I₂] species each asymptotically approach 5% of final IBr concentrations. These results are certainly favorable, given the fact that their foundational equations are based on an incomplete (albeit dominant) set of reaction coefficients. Under higher pressures, however, numerical agreement begins to falter. In many cases, IBr recovery is limited to 80% or less of its initial concentration. Correspondingly, asymptotic limits for Br₂ and I₂ populations remain well above 5% of [IBr], often as much as 10-15% apiece. Thus, although IBr and Br₂/I₂ densities are properly driven in opposite directions of

[†] Under contaminant-free conditions and an ambient temperature of 298 K.

stabilization, higher pressures evidently hamper convergence toward a *numerically* correct steady-state distribution.

An explanation for this inconsistent kinetic behavior can be found by scrutinizing the concurrent roles played by exchange and recombination reactions. In general terms, the exchange reactions do not collectively contribute to a net change in atomic or molecular populations. Iodine atoms are effectively interchanged with bromine atoms; I_2/Br_2 molecules with IBr molecules. Relative magnitudes of the four reaction coefficients determine the ultimate equilibrium proportions. But, as evidenced by the functional form of the exchange reactions themselves, atomic iodine or bromine must be present for such reactions to occur. A strong recombination influence within the gain cell, by serving to deplete the number density of atomic radicals, can therefore impact the frequency with which exchange reactions occur.

High cell pressures provide this recombination influence. Under such conditions, recombination events become more frequent (relative to two-body processes) and the proportionality typically established by exchange reactions is compromised. As a result, the ILSA model restores molecular densities, but not in the expected proportions.

These ILSA-predicted effects of pressure upon kinetic equilibrium are not consistent with laboratory results. Practically speaking, final molecular distributions at 298 K should not be dependent upon cell pressure [41]. It is postulated that the model's deficiency in this respect is due to its exclusion of collisional dissociation processes in kinetic rate equations. The two-body dissociation process $XY+M \rightarrow X+Y+M$, applicable to each of the three diatomic molecules, allows for continual liberation of atomic bromine and iodine even in the absence of a photolysis source.

While high-pressure systems do favor atomic recombination over dissociation, it is suspected that inclusion of a collisional dissociation process in the ILSA model would remove much of the pressure-dependent behavior. By effectively slowing the net rate of atomic recombination, the important role played by exchange reactions would be given due weight and final population distributions made consistent with the law of mass action.

This kinetic omission, while detrimental to treatment of the unexcited case, is not of particular importance to the more relevant case of solar excitation. Under concentrated solar incidence, collisional dissociation is minor when compared to contributions from molecular photolysis. In the context of general laser analysis, the assemblage of kinetic rate coefficients should therefore be regarded with high confidence.

4.3. Analytic Model: Continuous-Wave IBr Laser

4.3.1. Kinetic Assumptions

The ease (or difficulty) with which one can develop an accurate, closed-form model for any CW laser system is almost exclusively decided by the degree of competition among its constituent kinetic processes. Lasers that lend themselves most convincingly to analytic solution exhibit dominant processes that are few in number, and easily represented mathematically. Although there may be literally hundreds of kinetic reactions contributing to the laser's overall dynamic behavior, effects of many of these reactions can be considered peripheral (and thus ignored) they are relatively small in magnitude. The resulting numeric solutions for chemical and photon densities will normally be very close to results obtained using iterative, fully inclusive methods [46].

Unfortunately, no such dominance is immediately recognizable for the case of a static-cell IBr laser. Initially, the pumping process is strongly dominated by photodissociation of IBr rather than Br_2 or I_2 , and small populations of atomic iodine and bromine contribute insignificantly to quenching, exchange, and recombination reactions. With the progressive depletion of IBr, however—and the photofragment liberation that accompanies it—steady state population densities are shifted towards dramatically different proportions. The final state of dynamic equilibrium reflects a general assimilation of several kinetic processes, thus complicating the modeling process.

In many previous studies of this laser, it has been noted that the IBr precursor is only minimally depleted by laser or solar-simulator pumping sources [8, 15, 16]. If this result were true under the conditions of continual solar pumping, steady-state populations of Br_2 and I_2 could be approximated by their initial values, and analytic treatment of exchange reactions would be considerably assisted. However, it is clear from consideration of ILSA data that both these molecular species may, depending upon pumping intensity, grow dramatically in population (to 15% or more of IBr number density). Thus, the prospective analytic model is further complicated by the need to consider population development of these two species.

The “closed form” model ultimately developed includes the three majority quenching processes (IBr, Br_2 , and I), each direction of the two exchange reactions, and atomic iodine dimerization. I_2 and Br_2 populations were not explicitly solved for in steady-state; rather, they were assigned typical IBr proportions in the cell (~15%) to properly weight the rate equations.

4.3.2. Accuracy and Applicability

Upon review of the above results, confidence in the analytic laser model is substantially compromised. It is true that, under select conditions, a clear kinetic dominance will surface and allow accurate modeling of both populations and output power. For such situations, this closed-form solution is applicable and valuable; it allows circumvention of the full kinetic model and the time investment that accompanies it. However, the observed degradation in model precision under other conditions renders it ill-suited for use as a wide-sweeping analytic tool.

V. Results and Analysis

5.1. Attainment of CW Oscillation

An immediately striking result of the ILSA computational analysis lies in the apparent ability to achieve continuous-wave oscillation without introduction of a laser flow mechanism. Conventional wisdom, developed from past IBr laser studies and previously assumed here, has contended that a *static-cell* IBr laser is incapable of CW operation [8, 9]. Despite the presence of exchange and recombination reactions that allow for removal of atomic iodine through dimerization or IBr production, such reactions were thought to be eclipsed by the rapid rate of [I] production from IBr and I₂ photodissociation. As a result, the theory continued, population densities of atomic iodine grew rapidly within the gain cell, ultimately achieving so severe a Br* quenching effect that population inversion was terminated. Furthermore, thermal increases within the gain cell were suspected of simultaneously enhancing this quenching mechanism and inhibiting the removal rate of ground state bromine atoms. Pumping intensity could be increased as a means of augmenting Br* production to a rate that overcame such quenching effects, but would likely not be sustainable over time due to the rapid depletion of IBr precursor.

The deleterious effects of iodine buildup are real, and they exact a price on laser performance. With a Br* quenching coefficient of $1.9 \times 10^{-11} \text{ cm}^3/\text{s}$ (the fastest of all the bromine relaxation coefficients), atomic iodine is one of the greatest kinetic threats to sustainment of the upper lasing population [18]. But quenching is not the sole process by

which this radical disrupts laser oscillation. The exchange reactions ke_3 and ke_4 , both identified as removal mechanisms for atomic iodine populations, each yield ground-state bromine atoms as one of two reaction products. Therefore, even those processes largely credited with allaying quenching sources, discourage lasing by other avenues.

Thus it is clear that a large iodine buildup results in inversion spoiling not only through increased Br^* quenching effects, but also through the increased frequency of ke_3 and ke_4 exchange reactions. This leads to the question that is fundamental to establishing a CW IBr laser: which kinetic process *is* primarily responsible for allowing the system to continually lase without the assistance of vacuum flow?

As confirmed during development of the analytic model, the process evidently responsible for restraining iodine populations is that of dimerization: $I+I+M \rightarrow I_2+M$. It is a fortunate fact that ke_3 and ke_4 exchange reactions are endothermic in nature. The uphill character of these reactions, signified by smaller rate coefficients, allows more rapid iodine removal to occur via the favored dimerization process. The dynamic of IBr recombination likewise has positive effects on inversion, due to removal of atomic bromine and iodine, but generally occurs at a much slower rate [9].

Iodine dimerization does not, in itself, sufficiently explain the observance of static cell, continuous-wave lasing. No flashlamp- or solar-simulated system has ever reported such results under these conditions. However, it is also true that no previous study has used bandpass methods to truncate the wavelength range of incident pumping energy. A cursory examination of IBr (and, to a lesser degree, Br_2) quantum yield curves reveals the potentially destructive effects of using full-band spectral irradiance as an IBr laser pump source. Beyond both extremes of the 457-545 nm bandpass range used in this model, Br^*

quantum yields from IBr photolysis drop below the "inversion-generating" value of 0.33 [36]. In fact, above a threshold wavelength of 545 nm, production of Br ($^2P_{1/2}$) is energetically impossible and quantum yield is zero [4]. It is contended that, without preferential photolytic generation of Br ($^2P_{1/2}$), quenching effects ultimately overwhelm lasing inversion and extinguish photon buildup. The result is a pulsed output beam, typically shorter than 10 μ s in duration.

5.2. Resonator Design

5.2.1. Pumping Geometry/Photolysis Path Length

While the ILSA computer algorithm will attempt to solve for laser kinetics under literally any combination of input parameters, a heavy measure of pragmatism is required, on the part of the user, to avoid the design of impracticable or patently unrealistic systems. Nowhere is this consideration more important than with respect to pumping geometry. Although many innovative pumping methods have been previously proffered by the literature, this thesis has confined its analysis to three established methods. These are the longitudinally-, transversely-, and frustum-pumped systems. Each system has intrinsic advantages and disadvantages that may carry different weight under different design constraints. Therefore, each candidate is viable, and deserves individual consideration.

The optical path length of an incident photon within the gain cell (D_p) is the only laser parameter driven exclusively by pumping geometry. If one assumes for simplicity a tetragonally-shaped gain cell under side-pumped conditions, the optical path length is merely the depth of the cell along this direction (assuming normal incidence). Under

longitudinal pumping, path length is either the full length of the gain cell (for pure axial pumping) or a portion of that length (for oblique pumping incidence). In the case of a frustum-type pumping arrangement, no *uniform* path length. Rather—as a consequence of the solar reflector’s quasi-parabolic design—the path length of an individual photon is dependent upon its entry location on the gain tube, and, correspondingly, its original reflection point from the solar collector [7]. Full accounting of this situation requires a rigorous mathematical treatment. However, since such precision is excessive for the purposes at hand, it is sufficient to use a *median* path length determined by the gain cell’s (1) length/width aspect ratio, and (2) separation distance from the solar reflector. Choi *et al* found that, for a typical configuration, this distance can be adequately estimated as 150% of the tube diameter [7].

In short, photolysis path length is not a quantity that can be optimized independently of other factors; it is inextricably linked to design configuration. For the most part, selection of one configuration or the other as “preferable” will be deferred to the concluding section of this paper. On the basis of available model data, however, it is possible to *eliminate* one geometry type from further consideration. Under most conditions, the longitudinal pumping approach is only partially successful in obtaining CW laser oscillation. This is doubtless due to severe attenuation effects encountered by the photolysis beam as it propagates over the entire gain cell length. Consequently, a large portion of the gain medium is unaffected by the incident photon stream, and gain is frustrated. While drastic reductions in the scale of laser tube length may relieve this failure, the efficiency of this method is clearly inferior to that of its two alternatives.

5.2.2. Gain Cell Dimensions

Consistent with expectations, a lengthening of the gain cell yields linear improvements in output power (Figure 5-1). It follows that, theoretically speaking, exceedingly long gain tubes are capable of outputting several kilowatts of power under 20,000 SCs. Unfortunately, the limitations of direct solar reflection place a practical limit upon such scalability. The side-pumped configuration is extremely inflexible in this respect. Under frustum pumping, however, a gain length of 3 meters appears reasonable [6]; therefore, this length was invoked for use in the ensuing parameter evaluations.

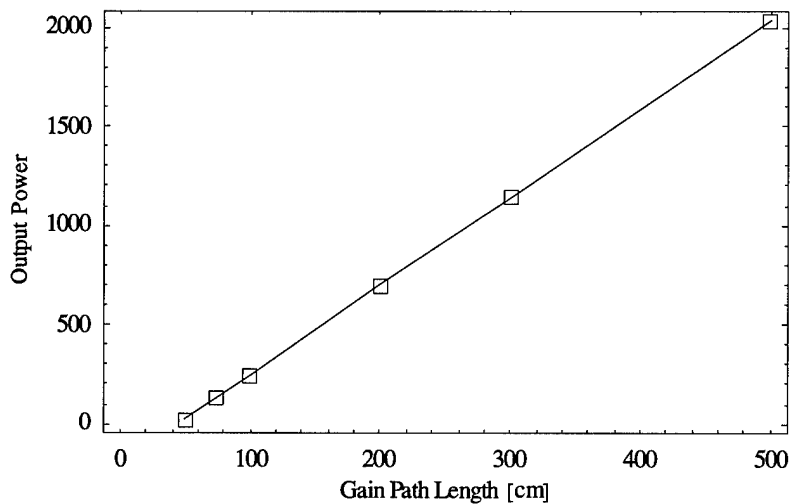


Figure 5-1. Output power as a function of gain cell length.

5.3. Parametric Optimization

5.3.1. Precursor Concentration

Of all system parameters, perhaps none boast a more fundamental impact on IBr laser dynamics than does gain cell pressure. With the attendant increase in frequency of particle interaction, higher cell pressures drive an acceleration of both two- and three-

body reaction rates. More important, however, is the nonuniform manner in which these reaction rates are altered. Because three-body reactions are given as the product of three, rather than two, "parent" population densities, changes in cell pressure affect these rates more dramatically. That is, exchange and quenching reactions are implicitly quadratic functions of cell pressure; recombination exhibits third-order pressure dependence. To some degree, it is therefore possible for one to use pressure selection as a means of molding kinetic behavior: encouraging certain reaction types over others.

Selection of a gain cell operating pressure is largely driven by the laser's pumping configuration. High densities of gain material provoke greater attenuation effects upon an incident beam, and thus limit the propagation depth of individual photons.

Consideration of the precursor's absorption cross section, in this context, allows an effective matching of pressure and penetration depth. For a gain cell one meter in length, longitudinally-oriented pumping favors relatively low IBr partial pressures (~3 Torr). Conversely, frustum- and side-pumped scenarios, which typically enjoy only short photolysis path lengths, require higher IBr pressures for sufficient energy absorption (~ 40-70 Torr under identical system dimensions). As suggested by Figure 5-2, the most expeditious method of identifying optimal cell pressure for a given system design is to simply plot output power vs. various IBr pressures, and note the resulting maximum value.

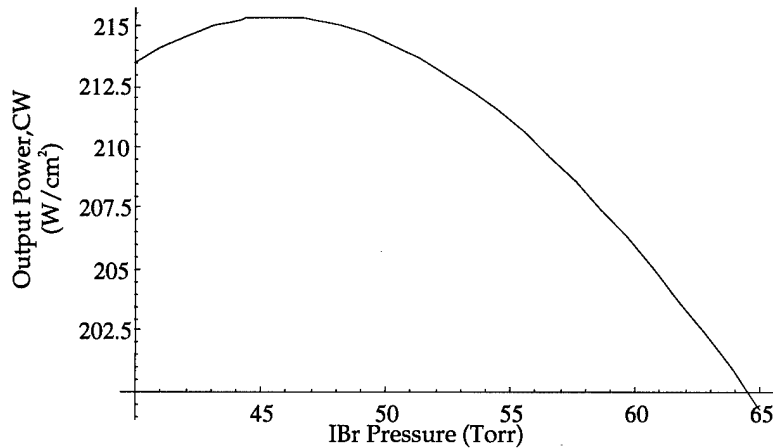


Figure 5-2. Laser performance as a function of initial IBr partial pressure.

Further investigation reveals that IBr pressure selection must also consider the intensity of the solar source. It shall be shown that, depending upon the relevant solar concentration factor, ideal pressures can vary as much as 30 Torr.

5.3.2. Gain Flow Velocity

Although lasant flow is not the indispensable enabler of CW laser performance originally proposed, some degree of recirculation is still desirable. Temperature effects, while not directly considered in the ILSA model, are a pervasive concern in intensely-pumped systems. By outflowing the cell contents through an external heat sink, average temperatures of the gain material can be appreciably reduced. The other benefit afforded by flow, continual recombination of atomic iodine and bromine into IBr precursor, also enhances overall laser performance by reducing system dependence upon internal kinetic processes. In net terms, recirculation reduces steady-state populations of the lower laser level both directly (through Br ($^2P_{3/2}$) removal) and indirectly (via removal of strong quenching agents: i.e., atomic iodine).

Computer analysis demonstrates the effects of various flow velocities on output power (Figure 5-3). In this representation, the flow process is defined as transverse in orientation (across the width of the gain cell), but can be easily modified to reflect longitudinal flow.[‡] Under moderate flow conditions, output intensity is sharply improved with increasing velocity. The beneficial effects of both Br ($^2P_{3/2}$)/quenching agent removal and IBr replenishment outweigh the negative effects of Br ($^2P_{1/2}$) removal.

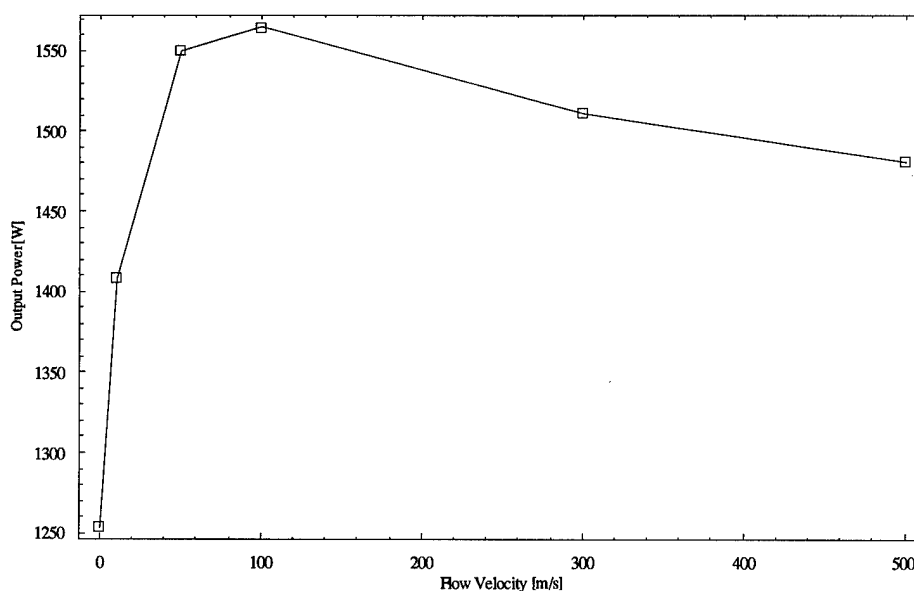


Figure 5-3. Output power as a function of transverse flow velocity.

Conversely, laser performance *suffers* under aggressive flow conditions. Velocities above roughly 100 m/s impart such rapid removal rates that the steady-state Br ($^2P_{1/2}$) population is notably depleted; inversion density and photon emission is therefore affected similarly. Under typical laser configurations, a flow velocity of

[‡] If practical from a design standpoint, transverse flow is generally preferable to longitudinal methods, in that identical removal rates can be effected with a comparatively slower flow velocity.

100 m/s appears to optimize kinetic balance in the gain cell. However, such an enhancement must be considered in light of economic and engineering constraints. Should this scale of lasant flow require extraordinary complications in design, more nominal rates of 10-20 m/s can be implemented with success. Under this scheme—given the steep slope of Figure 5-3—output power can still be appreciably improved; flow-related cooling effects can be exploited as well.

5.3.3. Bandpass Design

Results of this computer model reaffirm the need to discriminate against “destructive” wavelengths emitted by a solar source. While *pulsed* operation of the IBr laser is certainly possible with unrestricted solar pumping, continuous-wave oscillation is evidently frustrated by excessive Br ($^2P_{3/2}$) production under this scenario. Although the ILSA model is designed with this premise in mind, and does not generally allow pumping outside of theoretically-established boundaries (as defined in Section III), the kinetic code was altered by the author to allow such broadband incidence. Under these modified circumstances, modeled laser intensity was indeed short-lived, and qualitatively matched the experimental results reported by Guiliano/Hess and Zapata/De Young [8, 16]. With this premise established as valid, further analysis was performed to determine whether total output power could be improved by narrowing the bandpass range from its theoretically-determined limits.

Review of kinetic model results tends to support the mathematically-based methodology used in selecting “optimal” wavelength limits. Total output power, when calculated and charted as a function of upper and lower wavelength limits, attains maximum values very close to those limits previously calculated from IBr

photodissociation yield curves. That is, merely selecting the wavelength range which corresponds to an $\text{IBr} \rightarrow \text{I} + \text{Br}^*$ quantum yield greater than 0.33 is nearly adequate for maximizing total output power.

Although most proposed applications of a space-based laser are decidedly CW in nature [1], it is a worthwhile exercise to consider the effects of bandpass on (unsustainable) laser *pulses* as well. Under this optimization scenario, it is the *ratio*, rather than the difference, of Br^* and Br production which proves critical to obtaining a high peak power. Accordingly, this demand narrows the ideal bandpass range to those regions of the electromagnetic spectrum in which Br^* quantum yields from IBr photodissociation are at near-maximal values. Although this adjustment will not increase total pulse power in *absolute* terms, an improvement is recognized relative to the pump intensity committed to the system. For instance, in one model, altering the bandpass range from 457-545 nm to 465-525 nm reduced maximal output intensity by only five percent. These findings have notable implications for laser design. If a particular application rendered pulsed operation desirable, narrowing of the bandpass range could allow virtually unchanged power output under lower pumping intensities. Consequently, thermal increases within the gain cell could be mitigated.

5.3.4. Optimum Coupling

Selection of a laser's optimal output coupling can be obtained by analyzing the mathematical relationship between small-signal gain and cavity optics [43]. Although it requires solution of a transcendental equation in R_{coup} , this is a fairly straightforward exercise for the typical laser. In the case of the IBr laser, small signal gain is not easily obtainable and thus a graphical approach is preferable.

Because of its implicit dependence upon small signal gain, optimum coupling for the IBr laser is likewise driven by such central factors as pumping intensity, cell pressure, and gain length. Generally, lower pressures and higher solar concentrations required heavier output couplings (often with reflectivities as low as 90%). Of course, any conclusions drawn about optimum coupling are also heavily rooted in the optical parameters of the cavity. Changes in window transmittances or reflectivity of the second mirror will affect these conclusions accordingly.

5.3.5. Solar Concentration

As might be mathematically expected, incremental increases in solar concentration are accompanied by a linear improvement in output power. Of more significance, however, is the fact that progressively higher pumping intensities are likewise rewarded with improved *efficiencies*. An increase from 3,000 to 5,000 SCs, for example, was observed to boost total efficiency nearly fifty percent in the frustum-pumped case. Notwithstanding this fact, it is noted that such efficiency increases are subject to a law of diminishing returns. As displayed in Figure 5-4, efficiency margins near the upper practical limit (20,000 SC) are much more modest than those arising under near-threshold conditions.

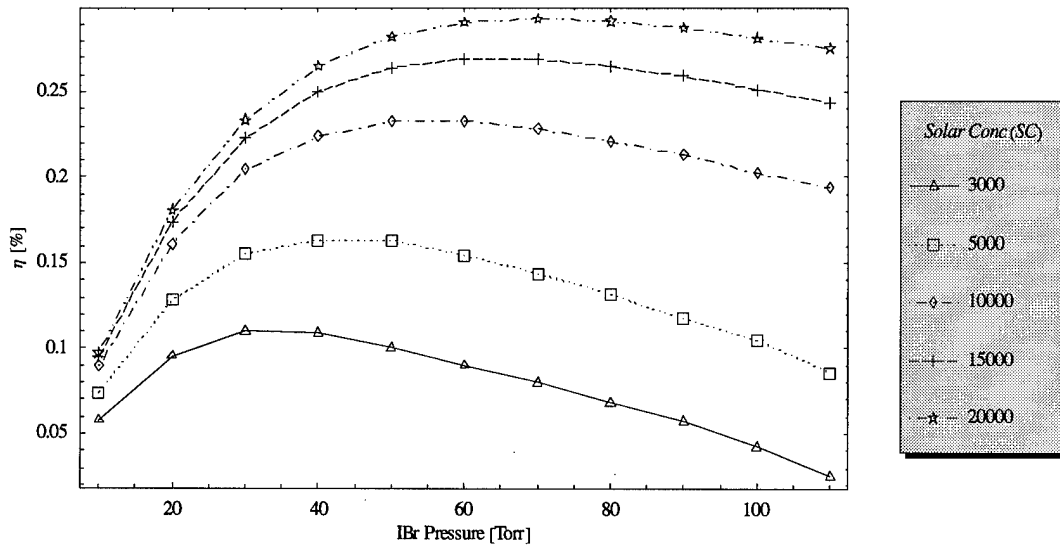


Figure 5-4. Total laser efficiency as a function of solar concentration and IBr partial pressure.

While sterile computational analysis clearly indicates that the highest achievable solar concentration results in optimal laser output, there are practical limits upon the degree to which this can be engineered. Terrestrial concentration modules boasting a capability of 50,000 solar constants (SC) have been successfully produced and operated [47], but it is doubtful that such an ambitious system could be similarly deployed on a space platform. For this reason, a reasonable concentration factor of 10,000 SC was assumed in most computational examinations within this thesis. It should be noted, however, that a concentration factor of 20,000—frequently cited as a high but achievable index for a space station—is capable of generating a laser output exceeding 1.2 kilowatts under a frustum-type geometry. Such scaling issues should be considered, as appropriate, in future design efforts.

An equal, if not more important consideration for this laser system is the issue of threshold. Under extremely limiting environmental constraints, it may be preferable to

opt for a smaller, more reliable laser module, the output beam of which can be amplified by other established methods. Again, thermal effects may also motivate such a conclusion. In this scenario, it is helpful to ascertain minimum pumping standards for continuous-wave operation. Again invoking the frustum-oriented model—with 3-m gain length, dual mirror reflectivities of 0.998 and window transmittances of 0.99—ILSA results indicate that threshold lasing is achieved at approximately 550 solar constants. Comparatively low IBr concentrations, on the order of 35 Torr, are noted to assist threshold attainment under low-intensity pumping conditions. Thus, higher cell pressures effectively raise the solar concentration factor that is needed to attain threshold oscillation.

5.4. Temperature Effects

The optimistic predictions presented here, in support of the IBr laser, come with an important caveat attached. All kinetic processes modeled by the ILSA algorithm presume operation under room temperature (298.15 K) conditions. To the extent that thermal effects within the gain cell can be mitigated by aggressive system design, this is not a *purely* unreasonable assumption. But the detrimental effects of higher temperatures on laser dynamics are well documented and pervasive [8-9], and deserve at least cursory analysis in this thesis.

In the absence of some internal or external cooling mechanism, continual solar incidence—amplified to as much as 20,000 times its normal intensity—has a demonstrated potential for dramatically heating the contents of a gain cell. Thermal increases are primarily driven by the translational energy imparted to IBr photofragments

upon dissociation; high cell pressures contribute to this effect by permitting greater absorption of incident photons. Previous estimates indicate that, under a comparatively moderate pumping intensity of only 2000 solar constants, the temperature of a gain cell held at 5 Torr can exceed 1000 K [9].

As a matter of scale, the typical laser systems presented here—employing up to 70 Torr of precursor partial pressure and a concentrated insolation of 10,000—are even *more* apt to thermally agitate the gain cell. These effects can strongly influence system kinetics, since each of the three reaction types exhibits some degree of thermal sensitivity. Piecemeal compilation of available research on the temperature dependence of quenching, recombination, and exchange reactions [8, 9, 39, 41] indicate that (as might be intuitively expected) recombination is the process most sharply impacted by temperature variations. With a temperature increase from 300 to 1000 K, rate coefficients for the important reaction $I+I+M \rightarrow I_2+M$ experience a reduction by three full orders of magnitude. The effects of temperature on Br ($^2P_{1/2}$) quenching have not been explicitly quantified, but comparable studies on I ($^2P_{1/2}$) deactivation by I_2 suggest that the same 700 K temperature rise effectively reduces this coefficient by a factor of 20 [9].

Forward and backward rates of an exchange reaction, denoted by $R(k_e)$ and $R(k_{-e})$ respectively, are strongly influenced by absolute temperature [8, 42]. In accordance with the law of detailed balance, these rates are related by the expression:

$$\frac{R(k_{-e})}{R(k_e)} \propto \exp(-\Delta E/kT), \quad (5-1)$$

where ΔE is the energetic difference between products and reactants, and k is the Boltzmann constant. A temperature increase from 300 to 1000 K, therefore, results in a

fifteen-fold increase in the reverse-to-forward rate proportion. A corresponding reduction in Br ($^2P_{3/2}$) removal rates by the ke_1 and ke_2 processes would be anticipated.

In an attempt to simulate these kinetic temperature effects, alternate rate coefficients—corresponding to a cell temperature of 1000 K—were constructed by the author and incorporated into the ILSA program. The results of this simulation, depicted in Figure 5-5, confirm the ruinous effects of high temperature operation.

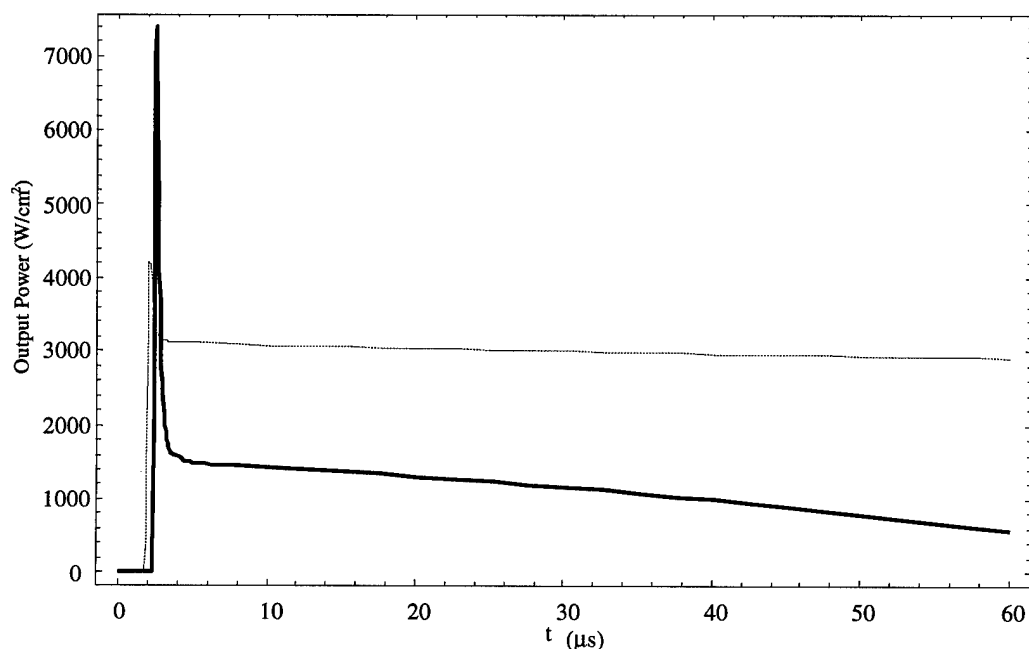


Figure 5-5. Relative output power from IBr laser systems under simulated temperature conditions of 298.2 K (gray) and 1000K (black).

Although quenching is mitigated under these conditions, the impaired rates of recombination and forward exchange serve to undermine overall laser performance. Steady-state intensity is compromised by more than fifty percent; furthermore, analysis of long-term population dynamics indicates that unrestrained growth of all non-IBr species ultimately terminates the Br* inversion at roughly 100 μs. Clearly, because an actual

gain cell would not *instantaneously* warm 700 degrees upon pumping, it is more likely that an uncooled laser would exhibit room temperature behavior initially, then take on high-temperature effects with increasing kinetic energy.

5.5. Comparisons with Competing Systems

As is true in any process involving the selection of a technical system, attractiveness of the IBr laser is predicated not only upon its own merits, but those of its competitors as well. It has been well established in this paper that, at present, a class of perfluoroalkyl iodides—having been thoroughly investigated for the solar pumping scenario—enjoys industry approval as the choice for space deployment. It is therefore essential that both candidate systems be compared, on even terms, in the areas of efficiency, power, and sustainability. Efficiency, being the most objective of these criteria, will be considered first and with the most rigor. Also, since the specific *t*-C₄F₉I-precursor system has been declared (from multiple fronts) as the pragmatic frontrunner of its class [5-7], it is this system which will be the basis of comparison.

5.5.1. Efficiency

As previously mentioned, “solar-absorptive” efficiency of the IBr laser—defined as the fraction of energy successfully transferred from an incident solar stream to molecular absorption within the gain cell—is visibly superior to that of the competing class of perfluoroalkyl iodides. In addition to the fact that their absorptive properties are confined to a poorly represented region of the solar spectrum (250-350 nm), C_xF_yI precursors are also limited by a lower peak absorption coefficient [6]. This does not necessarily foreclose the issue of *overall* laser efficiency, however. There are desirable

features of the $t\text{-C}_4\text{F}_9\text{I}$ laser that could constitute, on balance, a superior process of power conversion. These include near-unity yield of I^* upon $t\text{-C}_4\text{F}_9\text{I}$ photodissociation, as well as a shorter lasing wavelength (1.3 μm) and less destructive quenching effects. For this reason, efficiencies of both lasers should be scrutinized in detail.

By virtue of the numerous studies published on perfluoroalkyl iodide lasers, operating efficiencies of these systems are well documented. Despite slightly differing absorption profiles, members of the $\text{C}_x\text{F}_y\text{I}$ family exhibit similar overall quantum efficiencies of roughly 0.1 percent.[§] This value serves as an important benchmark for evaluating the IBr system, and is ultimately the one of most importance. But it is also useful to deconstruct each laser candidate into its constituent processes. By identifying the series of “micro-efficiencies” that comprise overall operating efficiency, relative strengths and weaknesses can be assessed.

Composite efficiencies are defined as follows. *Spectral efficiency* is that proportion of insolation radiation that falls within the optimal bandpass range for each laser. In the case of $t\text{-C}_4\text{F}_9\text{I}$, this precursor’s uniformly high quantum yield precludes the need for wavelength discrimination and spectral efficiency is therefore defined by its full range of absorption. *Absorptive efficiency* is defined as that proportion of incident radiation that is actually absorbed by a “precursor” molecule. In the case of the IBr laser, both IBr and Br_2 species are included under this criterion, since Br_2 photolysis also contributes to the upper laser level. This dynamic is highly dependent upon precursor

[§] Interestingly, reported efficiencies for both flashlamp- and solar concentrator-pumped systems are virtually identical, testifying to the suitability of xenon as a solar surrogate [6, 14].

density and photolysis path length; therefore, these variables are stipulated in Table 5-1. *Kinetic efficiency*, the proportion of absorption events that ultimately result in a cavity photon, is a euphemistic tool that reveals the extent to which collateral kinetic events (such as quenching or chemical reaction) interfere with stimulated emission. Finally, *cavity efficiency*—the proportion of cavity photons that are eventually output-coupled into the laser beam—is a metric that is driven almost entirely by resonator design, and thus is largely trivial for purposes of comparison. But it does provide reassuring closure to the task of efficiency deconstruction; when multiplied in series, constituent efficiencies yield the same *overall* value that would be obtained from a simple $P_{\text{out}}/P_{\text{in}}$ computation.

Buried as an element of kinetic efficiency is the fundamental quantity of *quantum efficiency*, defined as the ratio of lasing frequency to pumping frequency [46]. In that it reflects the absolute limit of a laser's total operating efficiency, quantum efficiency is a valuable metric. For both IBr and *t*-C₄F₉I systems, pumping frequencies are not uniquely defined. Rather, they are contained within absorption bands of the precursor. Therefore, for purposes of this analysis, chosen frequencies are those corresponding to *peak* quantum yields for each laser system.

Table 5-1 encapsulates all pertinent efficiency data for the two laser systems under consideration. For reasons of economics, normal convention is to report a laser's efficiency in terms of energy so that it can be compared to others on a level basis. Solar-pumped lasers have the inherent advantage that pumping energy is essentially "free" to the developer. For this reason, it is worthwhile to also note the photonic efficiency of each device. Under this convention, quantities classically measured in watts (J/s) are

instead tracked in photons/sec. An overall photonic efficiency, then, is given as the fraction of lasing to incident photons.

Table 5-1. Operating Efficiencies of IBr and *t*-C₄F₉I Laser Systems.

Efficiency Type	IBr (p _{IBr} =70 Torr, D _o =1.5 cm)		C ₄ F ₉ I (p _{C₄F₉I} =20 Torr, D _o =7.5 cm)	
	Energetic	Photonic	Energetic	Photonic
Spectral (η _s)	11.4%	6.2%	6.02%	0.481%
Absorptive (η _a)	76.5%	76.4%	~60.0%	~60.0%
Kinetic (η _k)	6.73%	37.4%	9.5%	43.0%
Quantum	(18.2%)	(100%)	(22.0%)	(100%)
Other	(37.0%)	(37.4%)	(~43.0%)	(~45.0%)
Cavity	37.5%	37.5%	35.0%	35.0%
Total (η _t)	0.22%	0.65%	0.12%	0.043%

Total efficiency [1] of the IBr laser is given simply by the ratio of total output beam power to the total incident power provided by solar reflector. The ILSA model reports both these quantities as power densities (W/cm²); therefore, efficiency computations require conversion to *absolute* terms. A standard Gaussian beam treatment is sufficient for calculating total output laser power. For the TEM₀₀ mode [43],

$$P_{\text{Tot}} = P_{\text{den}} \left(\frac{\pi w_o^2}{2} \right). \quad (5-2)$$

where P_{Tot} , P_{dens} , and w_o are the total power (W), power density (W/cm²), and waist of the output beam respectively. If the resonant beam is mode-matched to the cross sectional area of a cylindrical gain tube, the radius of this tube can be substituted for the waist in this expression. For the case of the 1-cm diameter considered previously, a large

Rayleigh range is obtained and divergence of the Gaussian beam can be neglected in mode volume calculations.**

Total incident power, that power channeled by the solar concentrator onto the gain cell, can, under most configurations, be obtained by a trivial calculation. The simple side-pumped case, for instance, entails an elliptically-shaped reflector focusing the solar image onto the facing side of the gain cell. Total incident solar power is thus given by the product of terrestrial-incident solar density (0.136 W/cm^2), exposed area of the gain cell, and solar concentration factor:

$$P_{\text{inc}_T} = (0.136 \text{ W/cm}^2) [l_g \cdot w_g] S_c. \quad (5-3)$$

This is the power incident upon the system *prior* to discrimination by the bandpass filter. An axially-pumped system would be treated similarly, with the expression for exposed cell area modified from $[l_g \cdot w_g]$ to $[d_g \cdot w_g]$ (rectangular channel design) or $[\pi r_g^2]$ (cylindrical tube design). For clarification, the quantities l_g , w_g , d_g , and r_g are the respective length, width, depth and radius of the gain tube.

Due to its complicated pumping geometry, the frustum design does not lend itself to a straightforward, two-dimensional conversion. For reasons of economy, details of such a computation will not be provided here. However, a fair approximation of this quantity can be obtained by dividing the total frustum volume by the mean photolysis path length.

** Calculations indicate that mode-matching of a 1-cm diameter tube, in a 330-cm confocal/planar resonator cavity, translates to a minimum radius of curvature for the mirror of 260-m.

The remaining mathematics are straightforward. Consolidating these results into an overall value, it is apparent that the IBr laser is, in energy terms, nearly twice as efficient than its *t*-C₄F₉I counterpart (0.22% vs 0.12%). If full use is made of the efficiency dividends offered by the “upper” pumping limit of 20,000 SC, this efficiency can be further boosted to 0.29%. In relative terms, this improvement is appreciable as well as encouraging. But it is minor when compared to the difference in *photonic* efficiencies for the two systems. As documented in Table 5-1, photonic efficiency of the IBr laser system is more than fifteen times greater than that of *t*-C₄F₉I. Under a pumping intensity of 20,000 solar constants, this difference becomes a factor of *twenty*.

In addition to these reported laser efficiencies, there are, of course, operational factors that introduce further losses to each laser system. Imperfect power transference associated with mechanical losses from cooling jackets, reflector geometry, etc. can and should be factored into a comprehensive efficiency analysis. On the basis of their research, Choi et al estimated a combined ancillary efficiency for the frustum-pumped system as 86% [7]. Since both IBr and *t*-C₄F₉I lasers would be similarly impacted by these operational losses, such effects do not serve as a performance discriminator between the two systems.

With regard to efficiency estimates, it is important to remark on the apparent chasm that exists between this and previous studies of the solar-pumped IBr laser. For instance, on the basis of their computational model, Harries and Meador asserted a typical operating efficiency of 1.2% [9]; Zapata and De Young’s results suggested an intrinsic laser efficiency of 0.9% [8]. Aside from immediately apparent differences in laser design and pulse criteria (both studies used pulsed, rather than CW output as the

source of their computations), the difference can be traced to discrepant interpretations of quantum yield. Harries and Meador assumed a wavelength-invariant Br ($^2P_{1/2}$) yield of 70% per photolysis event; Zapata and De Young effectively assumed a quantum yield of unity. In that the present model has both assumed a variable quantum yield and limited incident solar flux on the basis of this variability, it is to be expected that resulting efficiencies be considerably lower than those developed in these studies.

A final efficiency observation bears heavily upon the issues of gain temperature and bandpass design. While it is true that the 457-545 nm range does provide for optimal output power (and, by extension, a higher *overall* laser efficiency), it can be logically argued that the metric $I_{\text{abs}}/I_{\text{output}}$ is more pragmatically useful than $I_{\text{inc}}/I_{\text{output}}$. That is, although more narrow bandpass ranges realize an inferior output power, such a trade-off may still be preferable. A reduction in the energy allowed to interact with the gain cell will translate into less severe thermal effects. Indeed, as depicted in Figure 5-6, absorptive-output efficiency increases notably when the bandpass range (centered about the IBr absorption peak of ~ 495 nm) is incrementally narrowed. Depending upon the importance of thermal management to the IBr laser system, overall design may ultimately benefit from implementation of this principle.

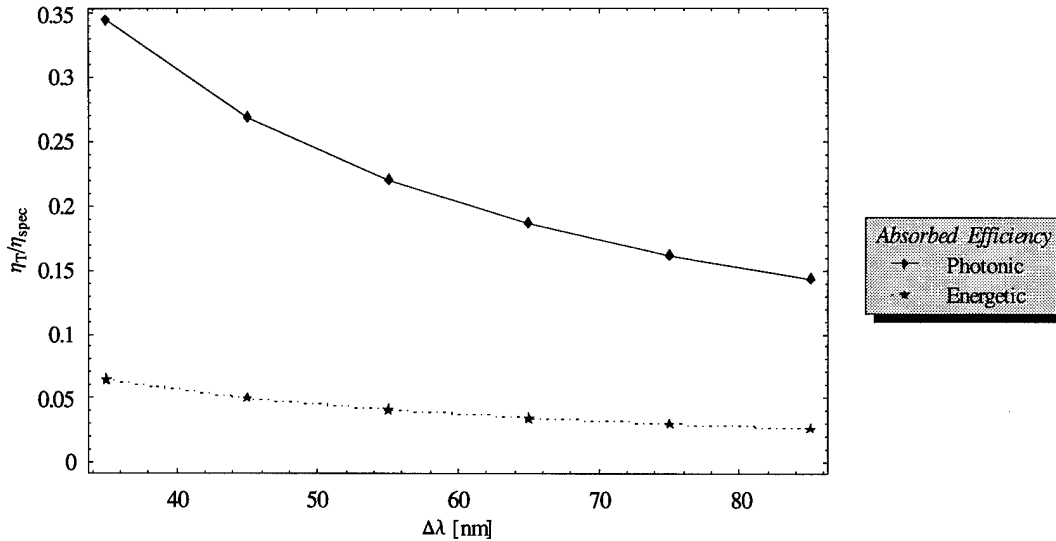


Figure 5-6. Absorbed efficiency of the IBr laser as a function of bandpass width (centered at 495 nm).

5.5.2. Output Power

Comparisons of output laser power must be both presented and interpreted with caution. Each laser system considered here is uniquely designed and functions under distinct parameter conditions. On the basis of computer modeling, however, it is apparent that the IBr laser is capable of generating kilowatt-level power in continuous-wave fashion. This capacity is suitable for some, but not all, of the space-based missions envisioned in recent literature. For instance, the power beaming function has been estimated to require 25-kW of output power [7]. Unless multiple lasers were phase-arrayed to meet this requirement, an IBr laser of this dimension would prove inadequate. Some form of power amplification would certainly be advisable.

5.5.3. Design Costs

Given that IBr and *t*-C₄F₉I lasers share almost identical engineering demands, the costs of sustaining either system on a space platform are practically indistinguishable.

The IBr laser's higher pumping threshold, however, would seem to necessitate a more ambitious scale of solar concentrator. One would expect to incur higher development and deployment costs under this scenario.

VI. Conclusions and Recommendations

6.1. Conclusions

The search for an “ideal” set of operating conditions—upon which design of the IBr laser can be incontrovertibly founded—is a somewhat myopic pursuit. There are numerous combinations of module parameters that have proven, if only in mathematical terms, sufficient for supporting an intrinsically efficient and successful laser. Furthermore, the standards against which *superior* performance is judged are certainly not universally defined; rather, they are subject to the biases and needs of the developer. However, exhaustive interpretation of ILSA output results *has* suggested a general developmental preference for certain regions of the parametric envelope. By way of engineering guidance, then, the following design recommendations are offered.

1. While both side- and frustum-pumped laser systems appear promising, superior efficiency and geometric economy of the latter module makes it comparatively preferable. In addition, the frustum design exhibits an inherent symmetry that is not shared by the side-pumped method.
2. Cavity design characterized by a mode-matched cylindrical gain cell (perhaps 3 meters long and 1-cm in diameter), under 70 Torr of IBr partial pressure and modest 10-20 m/s longitudinal flow velocity, appears to be profoundly effective in achieving near-ideal laser performance for a pumping intensity of 20,000 SC.
3. Insolation upon the gain cell should be of as high a solar concentration as is practical. At a minimum, the threshold requirement of roughly 550 SC *must* be met in

order to obtain CW oscillation. Incident radiation should be spectrally constrained—by bandpass methods or otherwise—to a wavelength bandwidth of 457-545 nm.

6.2. Recommendations

6.2.1. Applications

The potential applications of a solar-pumped, space-based IBr laser system are many in number, but not particularly unique in character. Assuming a sufficiently high output power capability, any infrared, continuous-wave laser system is well suited to the three functions mentioned in the introduction. Deployment on an earth-orbiting, heliostationary platform would ensure the opportunity for uninterrupted solar collection. However, the intractable nature of a large reflection-laser module (as opposed to a compact, chemically fueled laser) does seem to discourage compatibility of the IBr laser with non-stationary mission types. For this reason, it would appear that power beaming, rather than communications or satellite debris annihilation, is the application most amenable to the IBr laser system. The ability of other spacecraft to maneuver within arbitrary range of an orbiting—but otherwise stationary—energy source largely eliminates the need for dexterity in laser aiming.

6.2.2. Pursuit of a Space-Based, Solar-Pumped IBr Laser

As supported by results of the ILSA computational model, it is the author's recommendation that further investigations of the solar-pumped, IBr photolytic laser be pursued. Although a lower quantum yield and more pronounced quenching effects do detract from the *kinetic* efficiency of the IBr laser, spectral and absorptive efficiencies favor this prospective system over the perfluoroalkyl alternative. Its intrinsic affinity for

the solar spectrum makes the IBr photodissociative laser particularly well suited to a directly solar-pumped scenario.

Efficiency is a central criterion in laser appraisal, and its importance cannot be understated. But an equally compelling argument for adoption of the IBr system lies in its operational simplicity. Whereas members of the perfluoroalkyl laser class require at least moderate lasant removal rates to prevent accumulation of molecular iodine, ILSA model results suggest that the IBr system is essentially self-sufficient – capable of neutralizing CW lasing threats by virtue of its own chemical processes. While pragmatic concerns such as temperature may still deem a flow mechanism desirable, it is indeed encouraging that such a design feature is not necessary on the basis of inherent kinetics alone.

Absent any future proceedings to the contrary, it is further recommended that the parameter guidelines offered here be considered in any future design efforts of the IBr laser. Perhaps the most important—and yet easily implemented—element of this guidance is a spectral discrimination against solar wavelengths falling outside of the 457-545 nm envelope. Additionally, in light of the kinetic importance of iodine recombination to laser performance, experimental efforts should be undertaken to identify buffer agents with a preferential affinity for atomic iodine interaction. In this same vein, it is highly desirable to pursue the use of materials that exhibit cohesive preference for atomic iodine as an inner gain cell coating. Integration of one or both of these facilitators into IBr laser design should prove profitable in terms of laser performance. Indeed, the already-respectable CW power output could be boosted to still higher levels.

In short, the IBr photodissociative laser is uniquely suited for direct solar pumping. On the basis of computational analysis performed here, the technical limitations of an IBr system are not as acute as originally believed. Further exploration of this system, in an experimental context, may provide interested parties with an attractive alternative to the present line of photolytic precursors.

Appendix A. Modifications to ILSA Kinetic Code

In the realm of kinetic modeling, uncompromising mathematical rigor often incurs more than its share of liability. The original, fully-inclusive ILSA model contains numerous sources of complexity that serve to slow the process of numerical convergence. In particular, expressions for solar photolysis involve integration over several wavelength-dependent quantities, some of which are contained in exponential functions. These include quantum yield, solar incidence, and absorption cross section. Because the pumping expressions also involve transient quantities (i.e., time-varying populations of IBr, Br₂, and I₂), complicated integrals must be calculated individually for each step of the numerical solution.

These computations are observed to significantly delay the time needed for obtaining numerical solutions. For instance, a typical run of the full ILSA model—involving a nominal 500 μs of kinetic dynamics—requires nearly one thousand iterative steps and consumes over eight hours of processing time on a (Pentium™-II) 300 megahertz processor. While the patient user is assured of an eventual solution, this scale of computation time is exceedingly inconvenient for most practical purposes.

Elimination of this expediency issue, without any corresponding loss in numerical precision, was achieved by fundamentally restructuring the ILSA kinetic code. Because it is the *pumping* expressions that are most computationally intensive, only this aspect required correction; all other kinetic processes were allowed to stand as originally coded. Using Mathematica's® native *FunctionInterpolation* function, the modified version numerically maps individual (²P_{1/2}) and (²P_{3/2}) pump rates (for iodine and bromine atoms

alike) as a function of IBr, Br₂, and I₂ concentrations. These maps are then used, in lieu of individual mathematical expressions, in iterating the kinetic rate equations.

The time advantage of this approach is twofold. Firstly, an interpolation function must only be computed *once* before it can be used expeditiously in all code that follows it. Because Mathematica[®] is able to return interpolated values faster than virtually any mathematical operation, code execution is extremely efficient; no significant difference exists between the processing time for “long” (milliseconds) and “short” (microseconds) kinetic solutions. Secondly, under some circumstances an existing interpolation map may be reused on a differently-configured laser system, as long as the new input parameters do not impact the pumping expression.^{††} Under this approximation scheme, processing time for a single set of data is shortened to roughly 30 minutes.

Further reconstruction enabled the development of two additional laser simulators. Model B constitutes little more than a bookkeeping change, but improves processing time by better than 50% with only a minor increase in associated error.

Taking advantage of the reasonable approximation

$$\left(\frac{\int_{\lambda_1}^{\lambda_2} \bar{F}(\lambda) \phi_i(\lambda) d\lambda}{\int_{\lambda_1}^{\lambda_2} \bar{F}(\lambda) d\lambda} \right) \cdot \int_{\lambda_1}^{\lambda_2} \frac{\sigma_i(\lambda)}{\xi(\lambda)} [1 - e^{-\xi(\lambda)D_p}] d\lambda \approx \int_{\lambda_1}^{\lambda_2} \frac{F(\lambda) \phi_i(\lambda) \sigma_i(\lambda)}{\xi(\lambda)} [1 - e^{-\xi(\lambda)D_p}] d\lambda, \quad (6-1)$$

an integrated quantum yield for the three molecular dissociation processes can be computed initially, then used as a multiplier to convert IBr, Br₂, and I₂ dissociation into

^{††} By name, these parameters include photolysis path length, temperature, IBr partial pressure, and upper/lower bandpass wavelength limits. Because solar concentration contributes to pump rate in simple linear fashion, it has been removed from the interpolation effort so as to further improve flexibility of the model.

($^2P_{1/2}$) and ($^2P_{3/2}$) production rates. Since, under this methodology, only one interpolation map is then required for all production processes associated with a parent molecule, considerable time savings can be realized.

The second alternative (Model C) is faster still in execution time, but much more convoluted in development. Though respectable, accuracy of this model is inferior to that of both the above alternatives. Its solutions are obtained by deconstructing and simplifying the integrals associated with solar pumping. Because wavelength-dependent quantities are not wildly varying within the spectral range of interest, many of these integrands can be spectrally averaged once (as demonstrated in Model B) then used as prefactors in future calculations. Furthermore, the attenuation factor ξ can be approximated by its dominant contribution $[I_{Br}] \cdot \sigma_{IBr}$ when it appears in the exponent of the pumping expression.

Under this revised pumping approach, the photolysis fraction $[1 - \exp(-\xi \cdot D_p)]$ was replaced by $[1 - \exp(-[I_{Br}] \cdot \sigma_{IBr})]$ and then fitted to an interpolation curve exhibiting the same functional dependence upon IBr concentration. Figure A-1 shows the agreement between exact and modeled pumping expressions.

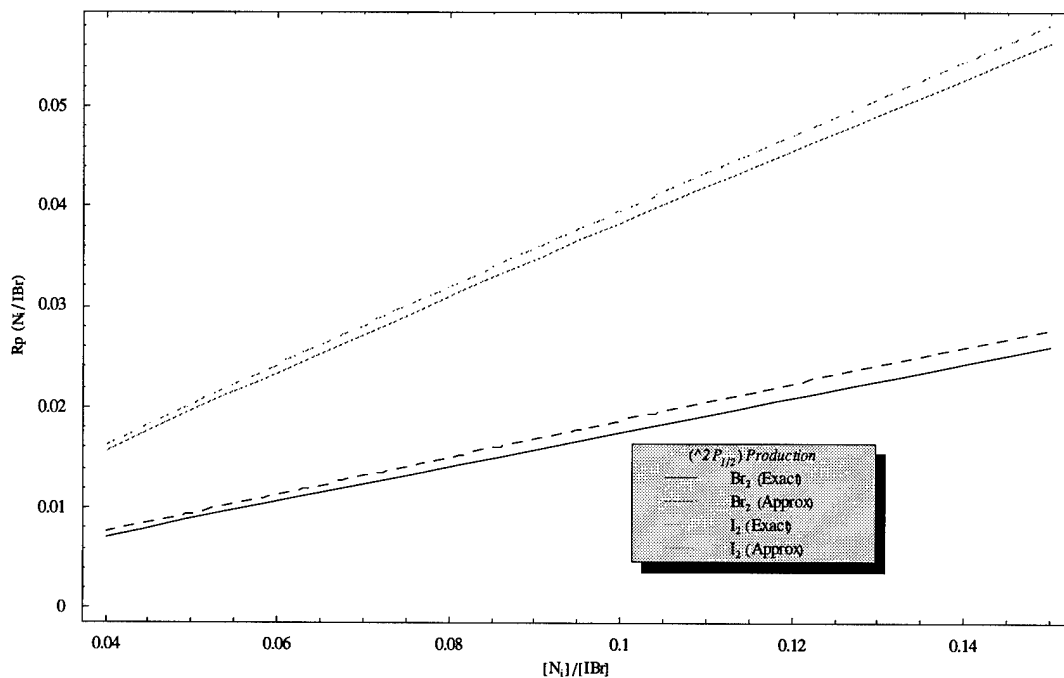


Figure A-6-1. Comparison of exact and approximate representations of Br (${}^2P_{1/2}$) and I (${}^2P_{1/2}$) production from Br_2 and I_2 photolysis, respectively.

The end product of this approximation is encouraging. As reflected in Table A-1, Model C yields results that are reasonably close to those generated by the full kinetic method. Still, the most judicious blend of economy and precision appears to be offered by Model B.

Table A-1. Steady-State Comparisons of ILSA-Modeled Parameters. Values are computed for a frustum-pumped system under 10K SC; processing times correspond to the duration of code execution on a Pentium®-II, 300 MHz personal computer.

Parameter	Units	Model #1 ("Exact")	Model B (Integrated ϕ)	Relative Error (%)	Model C (Averaging)	Relative Error (%)
IBr	mol/cm ³	1.0362 x 10 ¹⁸	1.0362 x 10 ¹⁸	0.00%	1.0428 x 10 ¹⁸	6.37%
Br ₂	mol/cm ³	2.8997 x 10 ¹⁸	2.8997 x 10 ¹⁸	0.00%	2.8667 x 10 ¹⁸	1.14%
I ₂	mol/cm ³	2.8577 x 10 ¹⁸	2.8577 x 10 ¹⁸	0.00%	2.8263 x 10 ¹⁸	1.10%
Br (² P _{1/2})	mol/cm ³	2.8636 x 10 ¹⁸	2.8636 x 10 ¹⁸	0.00%	2.8252 x 10 ¹⁸	1.34%
Br (² P _{3/2})	mol/cm ³	1.4063 x 10 ¹⁸	1.4063 x 10 ¹⁸	0.00%	1.3295 x 10 ¹⁸	5.46%
I (⁴ P _{1/2})	mol/cm ³	2.3518 x 10 ¹⁸	2.3783 x 10 ¹⁸	1.34%	2.1954 x 10 ¹⁸	6.65%
I (⁴ P _{3/2})	mol/cm ³	8.4132 x 10 ¹⁸	8.4132 x 10 ¹⁸	0.00%	8.1002 x 10 ¹⁸	3.72%
N _p	photons/cm ³	1.2317 x 10 ¹⁸	1.2448 x 10 ¹⁸	1.06%	1.1219 x 10 ¹⁸	8.91%
Power _{out}	watts	531.13	536.76	1.06%	483.78	8.91%
Process Time	minutes	58	18	N/A	3.8	N/A

The flexibility offered by three kinetic simulators—each exhibiting a unique mixture of expediency and precision—is intended to match changing user demands. On the specific issue of engineering design, for instance, Model C can be used for top-level review of rough design concepts; more refined data can then be extracted via the interpolation map models. Overall, a combination of these three approaches can streamline the process of laser system investigation.

Appendix B. ILSA: Mathematica® Source Code

■ Barry N. Behnken, Capt, USAF
 Air Force Institute of Technology
IBr Laser Simulation Algorithm (ILSA)

■ Load Required Packages/ Set Code Design Preferences

```
Off[Unset::norep]
Off[FindRoot::"frmp"]
Off[General::"spell1"]
Off[NIntegrate::"inum"]

Remove[ShowProgress]
Needs["Graphics`Graphics3D`"]
Needs["NumericalMath`PolynomialFit`"]
Needs["NumericalMath`InterpolateRoot`"]
Remove[ShowProgress]
Needs["Statistics`NonlinearFit`"]
Needs["Graphics`Graphics`"]
Needs["Graphics`Legend`"]
Needs["Statistics`LinearRegression`"]
Needs["Graphics`MultipleListPlot`"]

$TextStyle = {FontFamily -> "Times", FontSize -> 8};
```

■ Clear Notebook Functions/ Variables

```
ClearAll[UserTag, q, h,
c, k, Na, R_sun, SunEarth, n, t, v, λ, vlib, em, Δv, e, IBrAbsv,
IBrAbsλ, σabs, PowerOut, λPeakSolar, λcutHi, Me, Mq, SolarMe, SolarMq, τrt, τp, Rp,
IBr,
BrStar, Br, Br2, Iod, Iod2, Photon, BrStarData, BrData, IodData, PhotonData, Γ, φ,
ΔN, ΔNth, γ, γth, σse, λlase, vlase, Rmir, A21, Asp, Rmir, Tcell, ρ, tmax]

q = 0; While[(q = q + 1) <= 6, em0q = .; v0q = .; Δv0q = .; emB0q = .; vB0q = .; ΔvB0q = .;
Tq = .; Pcellq = .; Lgq = .; Scq = .; Rcoupq = .; Atubeq = .;
Dpq = .;
λcutLoq = .; λcutHiq = .; vFlowq = .; Setq = .;]; q = .; a1 = a2 = a3 = a4 = a5 = a6 = a7 = 1;
temp1 = temp2 = press1 = press2 = path1 = path2 = λ11 = λ12 = λh1 = λh2 = 0; UserTag = 2;
```

Hyperlink (*Skip User Interface*)

Skip Interface

■ Prompt User for Laser Parameters/Computation Preferences (Optional)

```
T0 = 298.2; Pcell0 = 1.0; Lg0 = 100; Sc0 = 20000; Rcoup0 = 0.98; Atube0 = 20;
Dp0 = 60; λcutLo0 = 457.7; λcutHi0 = 545.3; vFlow0 = 3000;
Rmir = 0.998; Tcell = 0.99; ρ = 0.85; tmax = 0.1;
```

```
ClearAll[a1, a2, a3, a4, a5, a6, a7, Choose, prompt, Prompt, w, SelectMults];
q = 0; While[(q = q + 1) <= 11, {promptq = ., variableq = ., prompt2q = .}]; UserTag = 1;
```

```
ParameterLabel = {"Operating Temperature [K]", "IBr Partial Pressure [Torr]",
  "Gain Path Length [cm]", "Solar Concentration",
  "Output Coupler Reflectivity", "Area/ Laser Tube [cm^2]",
  "Pumping Path Length [cm]", "Upper Cutoff Wavelength [nm]",
  "Lower Cutoff Wavelength [nm]", "Flow Velocity [m/s]"};
VarList = {T, Pcell, Lg, Sc, Rcoup, Atube, Dp, λcutLo, λcutHi, vFlow};
VarList2 = {Rmir, Tcell, ρ, tmax};
PLabel = {"Mirror 1 Reflectivity", "Cell Window Transmittance",
  "Ratio: Gain/Cavity Length", "Plotting Duration [sec]"};
a1 = 0; While[((a1 > 6) || (a1 < 1) || (IntegerQ[a1] == False)),
  a1 = Input["Enter Number of Curves to be Computed\n\n[1-6]"];]
```

```
Prompt[w_] :=
  ColumnForm[{"PARAMETER ASSIGNMENTS\n\nPlease Enter:", ParameterLabel[[w]],
    "", SequenceForm["[ENTER] for... (Default = ", (VarList[[w]])0, ")"}];
q = 0; While[(q = q + 1) < 11,
  While[((promptq == Null || (NumberQ[promptq] && promptq >= 0)) != True),
    promptq = Input[Prompt[q]]];
  q = 0; While[(q = q + 1) < 11, If[promptq == Null, promptq = (VarList[[q])0]];
  SelectMults[w_] := SequenceForm["(", w, ") ", ParameterLabel[[w]]];
  q = 0; While[(q = q + 1) < 11, (VarList[[q])0 = promptq];
    λcutHi0 = 10-9 λcutHi0; λcutLo0 = 10-9 λcutLo0;
```

```
Prompt2[w_] :=
  ColumnForm[{"PARAMETER ASSIGNMENTS\n\nPlease Enter:", PLabel[[w]],
    "", SequenceForm["[ENTER] for... (Default = ", (VarList2[[w]]), ")"}];
q = 0; While[(q = q + 1) < 5,
  While[((prompt2q == Null || (NumberQ[prompt2q] && prompt2q >= 0)) != True),
    prompt2q = Input[Prompt2[q]]];
  q = 0; While[(q = q + 1) < 5, If[prompt2q == Null, prompt2q = VarList2[[q]]];
  SelectMults2[w_] := SequenceForm["(", w, ") ", PLabel[[w]]];
  q = 0; While[(q = q + 1) < 5, VarList2[[q]] = prompt2q];
  ShowParam1 = TableForm[Table[{d, ParameterLabel[[d]]}, {d, 1, 5}],
    TableSpacing -> {0, 0.5}];
  ShowParam2 = TableForm[Table[{d, ParameterLabel[[d]]}, {d, 6, 10}],
    TableSpacing -> {0, 0.5}];]
```

```
If[a1 == 1, Goto [BypassMult]];
Choose = 0; While[((Choose > 10) || (Choose < 1) || (IntegerQ[Choose] == False)),
```

```

Choose = Input[ColumnForm[{"SELECT VARIABLE PARAMETER:", "",
  TableForm[ShowParam1], "", "...or [ENTER] for other variables..."}]];
If[(Choose == Null), (Choose = Input[ColumnForm[{"SELECT VARIABLE PARAMETER:",
  "", TableForm[ShowParam2],
  "", "...or [ENTER] for other variables..."}]]]);

q = 0; While[(q = q + 1) <= a1],
  While[((NumberQ[variableq] && variableq >= 0) != True),
    variableq = Input[SequenceForm[ParameterLabel[[Choose]], ": Set #", q]]];
  series = a1; d = 0;
  While[(d = d + 1) <= series, {Td = prompt1, Pcelld = prompt2,
    Lgd = prompt3, Scd = prompt4, Rcoupld = prompt5, Atubed = prompt6,
    Dpd = prompt7, λcutLod = 10-9 * prompt8, λcutHid = 10-9 * prompt9, vFlowd = prompt10,
    (VarList[[Choose]]d = variabled, Setd = variabled)}]; d =.;
  ParameterLabel[[6]] = "Area/ Laser Tube [\\(cm^2\\)";
  ParameterLabel[[8]] = "λcutoff (lower) [m]";
  ParameterLabel[[9]] = "λcutoff (upper) [m]"; Parameter = ParameterLabel[[Choose]];

Label[BypassMult];
a2 = 0; While[((a2 > 2) || (a2 < 1) || (IntegerQ[a2] == False)),
  a2 = Input["Display Absorption/Emission Plots?\n\n[1] Yes\n[2] No"];
a3 = 0; While[((a3 > 3) || (a3 < 1) || (IntegerQ[a3] == False)),
  a3 = Input["Select:\n\n[1]
  Full,\n[2] Interpolation or\n[3] Approx.\n\nKinetic Model"];
a4 = 0; While[((a4 > 2) || (a4 < 1) || (IntegerQ[a4] == False)),
  a4 = Input["Generate/Display Sensitivity Plots?\n\n[1] Yes\n[2] No"];
a5 = 0; While[((a5 > 2) || (a5 < 1) || (IntegerQ[a5] == False)),
  a5 = Input["Perform Closed-Form Analysis?\n\n[1] Yes\n[2] No"];
a6 = 0; While[((a6 > 2) || (a6 < 1) || (IntegerQ[a6] == False)),
  a6 = Input["Perform Recombination Analysis?\n\n[1] Yes\n[2] No"];
a7 = -1; While[((a7 > 6) || (a7 < 0) || (IntegerQ[a7] == False)),
  a7 = Input["Animate Laser Graphics? [0] No\n\nYes. Show:
  \n\n[1] Output Power\n[2] IBr\n[3] BrStar\n[4] Br\n[5] Gain
  Coefficient"];

```

■ Standard Physical Constants:

```

h = 6.626 * 10-34; (* J s *)
c = 3.0 * 1010; (* cm/s *)
k = 1.38 * 10-23; (* J/mol K *)
Na = 6.022 * 1023; (* mol/mole *)
Rsun = 6.96 * 108; (* m *)
SunEarth = 1.49 * 1011; (* m *)
MassBr = 79.9 * 1.67 * 10-27; (* kg *)

```

■ Absorption/Quantum Yield Curves for IBr, Br₂ and I₂

■ IBr Absorption (using Britton/Seery Gaussian Overlap Model):

$\nu_{\text{vib}} = 267.4 \text{ c;}$
 $\epsilon m_{0_1} = 169.8; \nu_{0_1} = 19715 \text{ c; } \Delta\nu_{0_1} = 1132 \text{ c;}$
 $\epsilon m_{0_2} = 288; \nu_{0_2} = 20951 \text{ c; } \Delta\nu_{0_2} = 2211 \text{ c;}$
 $\epsilon m_{0_3} = 78.9; \nu_{0_3} = 37289 \text{ c; } \Delta\nu_{0_3} = 3848 \text{ c;}$

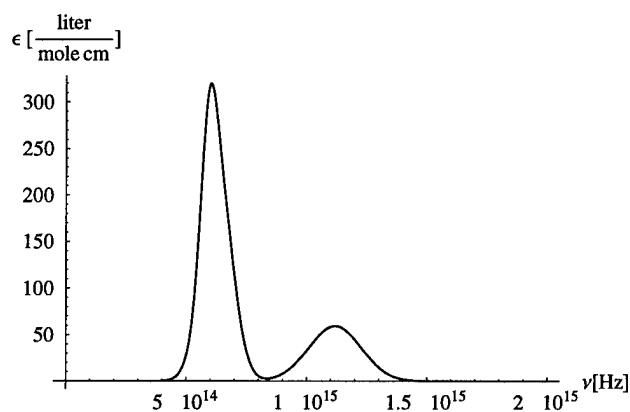
$$\epsilon m[n_, T_] := \epsilon m_{0_n} \left(\text{Tanh} \left[\frac{h \nu_{\text{vib}}}{2 k T} \right] \right)^{1/2}$$

$$\Delta\nu[n_, T_] := \Delta\nu_{0_n} \left(\text{Tanh} \left[\frac{h \nu_{\text{vib}}}{2 k T} \right] \right)^{-1/2}$$

$$\epsilon[n_, \nu_, T_] := \epsilon m[n, T] \text{Exp} \left[- \left(\frac{\nu - \nu_{0_n}}{\Delta\nu[n, T]} \right)^2 \right]$$

$$\text{IBrAbs}[\nu_, T_] := \epsilon[1, \nu, T] + \epsilon[2, \nu, T] + \epsilon[3, \nu, T]$$

If [a2 != 2, Plot [IBrAbs[\nu, 298.2], {\nu, 0, 2 * 10¹⁵}, PlotRange -> All,
 AxesLabel -> {" \nu[Hz] ", "\epsilon [$\frac{\text{liter}}{\text{mole cm}}$] "}, ImageSize -> {300, 270}]];

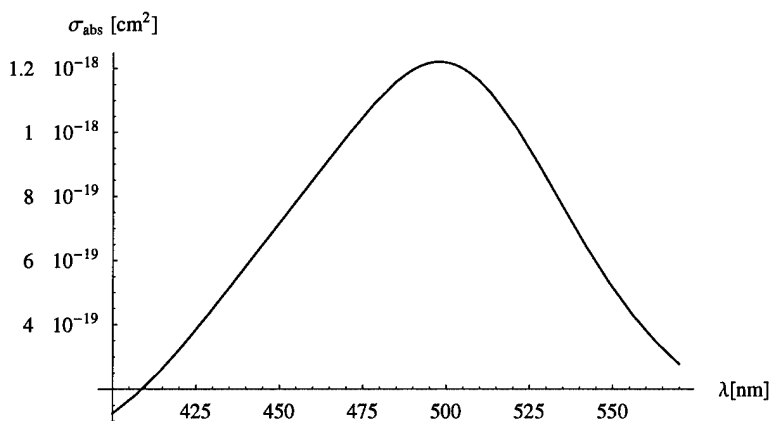
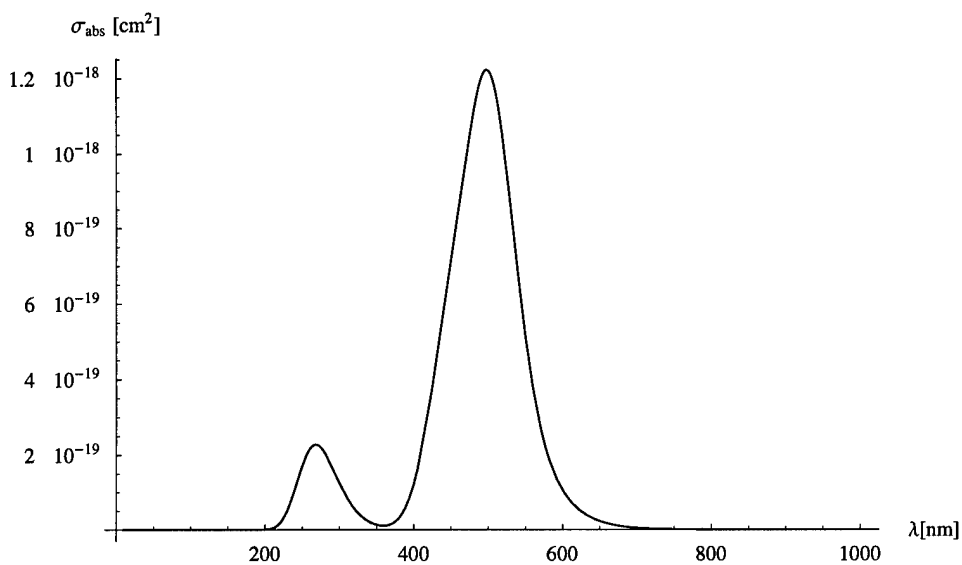


Conversion: IBr Extinction Coefficient (ν) \rightarrow Absorption Cross Section (λ)

$$\text{IBrAbs}\lambda[\lambda_ , T_] := \text{IBrAbs}\nu\left[\frac{c}{100 \lambda} , T\right]$$

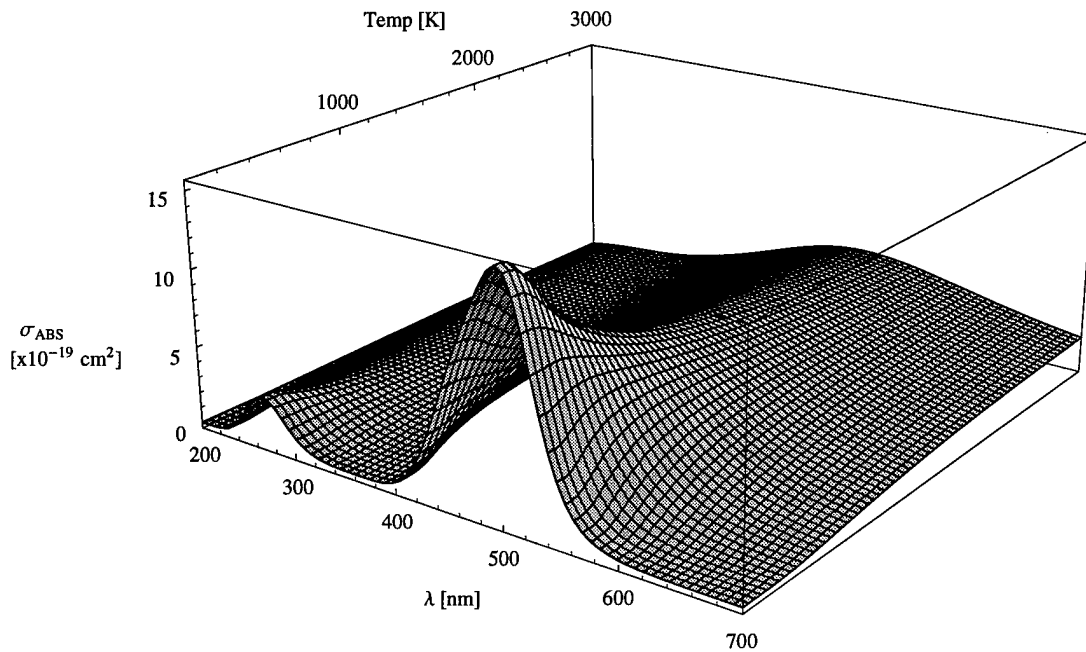
$$\sigma_{\text{abs}}[\lambda_ , T_] := \left(\frac{10^3}{\text{Na}}\right) \left(1 + \text{Log}\left[\frac{10}{E}\right]\right) \text{IBrAbs}\lambda[\lambda , T]$$

```
If[a2 != 2, {Plot[ $\sigma_{\text{abs}}[\lambda * 10^{-9}, 298.2]$ , { $\lambda$ , 10, 103}, PlotRange -> All,
  AxesLabel -> {"  $\lambda$ [nm]", " $\sigma_{\text{abs}}$  [cm2"]}, ImageSize -> {460, 320}},
  Plot[ $\sigma_{\text{abs}}[\lambda * 10^{-9}, 300]$ , { $\lambda$ , 400, 570}, PlotRange -> All,
  AxesLabel -> {"  $\lambda$ [nm]", " $\sigma_{\text{abs}}$  [cm2"]}, ImageSize -> {370, 230}]]];
```



3-D Representation of σ_{ABS} as a Function of Incident Wavelength and Ambient Temperature:

```
If[a2 != 2,
Plot3D[1019  $\sigma_{abs}[\lambda * 10^{-9}, T]$ , { $\lambda$ , 200, 700}, {T, 10-4, 3 * 103}, PlotRange -> All,
PlotPoints -> 70, ViewPoint -> {1.849, -2.582, 1.168},
AxesLabel -> {" $\lambda$  [nm]", "Temp [K]", " $\sigma_{ABS} \backslash n [x10^{-19} \text{ cm}^2]$ "},
ImageSize -> {600, 500}];
```



Peak Absorption @ Room Temperature, 298.2K (497.8 nm):

```
{ $\sigma_{abs}[497.8 * 10^{-9}, 298.2]$ , IBrAbs $\lambda[497.8 * 10^{-9}, 298.2]$ }
```

```
{1.22196 * 10-18, 319.582}
```

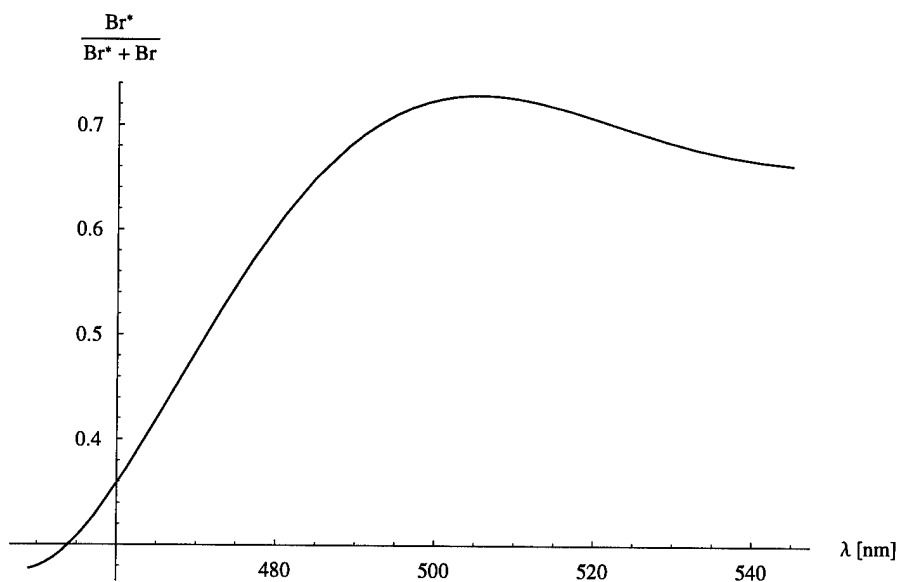
■ Br* Quantum Yield from IBr Photodissociation

*Mathematical Model of IBr + hν → I + Br(P_{1/2}) Yield Curve,
derived from data within Haugen et al (1985)*

```

φ = PolynomialFit[{{450, 0.28}, {455, 0.30}, {457, 0.33}, {460, 0.36},
  {465, 0.44}, {470, 0.46}, {475, 0.54}, {480, 0.62}, {490, 0.68}, {500, 0.73},
  {510, 0.72}, {520, 0.71}, {530, 0.68}, {540, 0.67}, {545.5, 0.66}}, 5];
If[a2 != 2, Plot[φ[λ], {λ, 449, 545}, AxesLabel -> {" λ [nm]", "  $\frac{Br^*}{Br^* + Br}$ "},
  ImageSize -> {427, 400}]];

```



Solve for Theoretically-Optimal ($\Delta N \geq 0$) Lower Wavelength Cutoff (nm):

* $\Delta N = N_1 - 1/2 N_2$; $\phi \geq \frac{1}{3}$ for $\Delta N \geq 0$

```

Extract[Solve[φ[λ] == 1/3, λ], 2]

```

```

{λ → 457.716}

```

■ Br₂: Minority Species Absorption Profile (Britton/Seery)

$$\begin{aligned} \nu_{\text{vibB}} &= 323.2 \text{ c}; \quad \epsilon_{\text{mB}0_1} = 90.1; \quad \nu_{\text{B}0_1} = 20452 \text{ c}; \\ \Delta\nu_{\text{B}0_1} &= 1582 \text{ c}; \quad \epsilon_{\text{mB}0_2} = 204.2; \quad \nu_{\text{B}0_2} = 24159 \text{ c}; \quad \Delta\nu_{\text{B}0_2} = 2102 \text{ c}; \end{aligned}$$

$$\epsilon_{\text{mB}}[n, T] := \epsilon_{\text{mB}0_n} \left(\text{Tanh} \left[\frac{h \nu_{\text{vibB}}}{2 k T} \right] \right)^{1/2};$$

$$\Delta\nu_{\text{B}}[n, T] := \Delta\nu_{\text{B}0_n} \left(\text{Tanh} \left[\frac{h \nu_{\text{vibB}}}{2 k T} \right] \right)^{-1/2};$$

$$\epsilon_{\text{B}}[n, \nu, T] := \epsilon_{\text{mB}}[n, T] \text{Exp} \left[- \left(\frac{\nu - \nu_{\text{B}0_n}}{\Delta\nu_{\text{B}}[n, T]} \right)^2 \right];$$

$$\text{Br2Abs}\nu[\nu, T] := \epsilon_{\text{B}}[1, \nu, T] + \epsilon_{\text{B}}[2, \nu, T];$$

$$\text{Br2Abs}\lambda[\lambda, T] := \text{Br2Abs}\nu \left[\frac{c}{100 \lambda}, T \right];$$

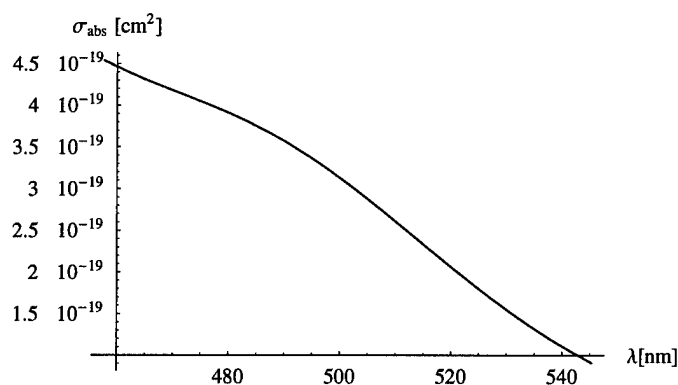
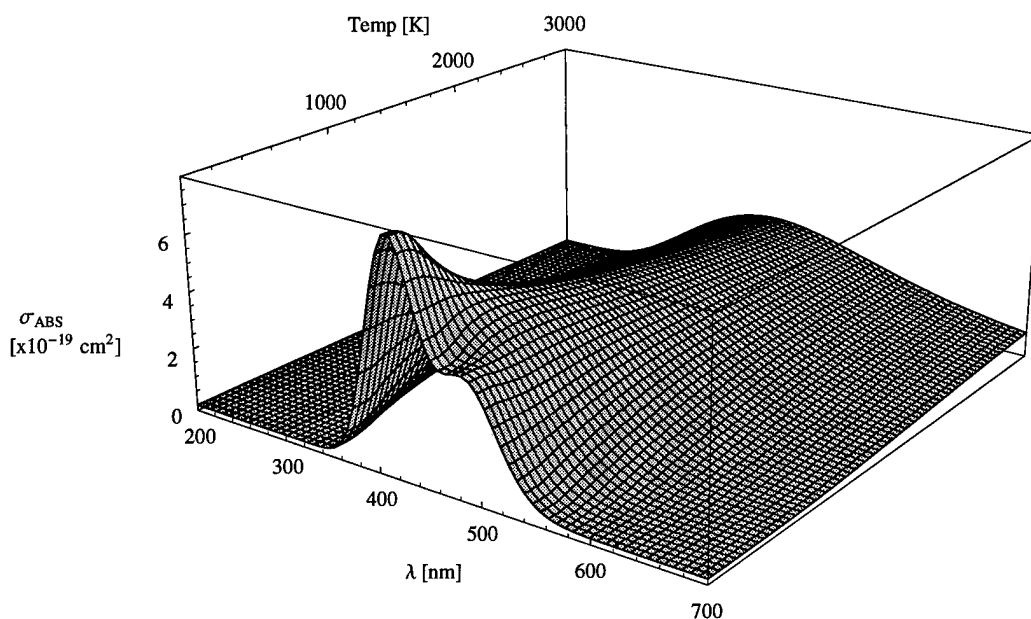
$$\sigma_{\text{abs}2}[\lambda, T] := \left(\frac{10^3}{\text{Na}} \right) \left(1 + \text{Log} \left[\frac{10}{E} \right] \right) \text{Br2Abs}\lambda[\lambda, T];$$

Br₂ Absorption Plots: (a) 3-D, for all wavelengths; (b) at 298 K, for 456-545 nm

```

If[a2 != 2, Plot3D[1019 σabs2[λ * 10-9, T], {λ, 200, 700}, {T, 10-4, 3 * 103},
  PlotRange -> All, PlotPoints -> 70, ViewPoint -> {1.849, -2.582, 1.168},
  AxesLabel ->
  {"λ [nm]", "Temp [K]", " σABS\n[x10-19 cm2"]}, ImageSize -> {494, 372}]];
If[a2 != 2, Plot[σabs2[λ * 10-9, 298.2], {λ, 457.7, 545.3}, PlotRange -> All,
  AxesLabel -> {" λ [nm]", "σabs [cm2"]}, ImageSize -> {323, 228}]];

```



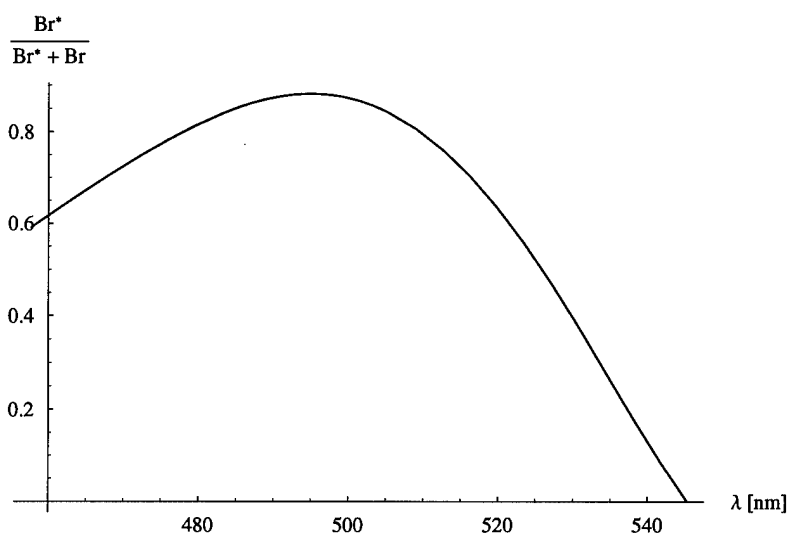
■ Br* Quantum Yield from Br₂ Photodissociation

*Mathematical Model of Br₂ + hν → Br(P_{3/2}) + Br(P_{1/2}) Yield Curve,
derived from data within Haugen et al (1985)*

```

φ2 = PolynomialFit[{{445, 0.44}, {450, 0.49}, {460, 0.62}, {466, 0.67},
  {470, 0.74}, {475, 0.78}, {480, 0.83}, {490, 0.84}, {500, 0.87}, {510, 0.83},
  {518, 0.67}, {520, 0.61}, {530, 0.40}, {545.3, 0}}, 5];
If[a2 != 2, Plot[φ2[λ], {λ, 457.7, 545.3}, AxesLabel -> {" λ [nm]", "  $\frac{Br^*}{Br^* + Br}$ "},
  ImageSize -> {379, 306}, PlotRange -> All]];

```



■ I₂: Minority Species Absorption Profile

Derived From Data Contained in Tellinghuisen, Using Methods From Britton/Seery

```

v vibI = 214 c;
I2Data = {{420, 6.9}, {430, 16.9}, {440, 34.5}, {450, 61}, {460, 93}, {470, 127},
{480, 153}, {490, 168}, {500, 167}, {510, 154}, {520, 131}, {530, 106},
{540, 81}, {550, 59}, {560, 41}, {570, 27.9}, {580, 18.4}, {590, 11.8},
{600, 7.4}, {610, 4.6}, {620, 2.8}, {630, 1.7}, {640, 0.8}, {650, 0.4}};
NonlinearRegress[

I2Data, emIOFit  $\left( \text{Tanh}\left[ \frac{h \text{v vibI}}{2 k 298.2} \right] \right)^{1/2} \text{Exp}\left[ -\left( \frac{\frac{c}{100 \lambda \cdot 10^{-9}} - \text{vIOFit}}{\Delta \text{vIOFit} \left( \text{Tanh}\left[ \frac{h \text{v vibI}}{2 k 300} \right] \right)^{-1/2}} \right)^2 \right]$ ,

λ, {{emIOFit, 246}, {vIOFit, 20231 c}, {ΔvIOFit, 4.1 1013}},
MaxIterations -> 200, WorkingPrecision -> 40]

{BestFitParameters -> {emIOFit -> 244.723,
vIOFit -> 6.06534 × 1014, ΔvIOFit -> 4.10001 × 1013}, ParameterCITable ->



|         | Estimate                   | Asymptotic SE              | CI                                                         |
|---------|----------------------------|----------------------------|------------------------------------------------------------|
| emIOFit | 244.723                    | 0.336667                   | {244.023, 245.423}                                         |
| vIOFit  | 6.06534 × 10 <sup>14</sup> | 6.74584 × 10 <sup>10</sup> | {6.06393 × 10 <sup>14</sup> , 6.06674 × 10 <sup>14</sup> } |
| ΔvIOFit | 4.10001 × 10 <sup>13</sup> | 6.49149 × 10 <sup>10</sup> | {4.08651 × 10 <sup>13</sup> , 4.11351 × 10 <sup>13</sup> } |



EstimatedVariance -> 0.220236,



|                      | DF | SumOfSq           | MeanSq    |
|----------------------|----|-------------------|-----------|
| ANOVA Table -> Model | 3  | 174720.           | 58239.8   |
| Error                | 21 | 4.624952200796178 | 0.220236, |
| Uncorrected Total    | 24 | 174724.           |           |
| Corrected Total      | 23 | 84060.8           |           |



AsymptoticCorrelationMatrix ->  $\begin{pmatrix} 1. & -0.000338715 & -0.572234 \\ -0.000338715 & 1. & 0.140267 \\ -0.572234 & 0.140267 & 1. \end{pmatrix}$ ,

FitCurvatureTable -> $Failed}

```

Least Squares Fit Results for emI0, vI0, ΔvI0 Parameters of I₂ Gaussian Absorption Model

```

{Evaluate[ΔvIOFit /. %[[1, 2]]], Evaluate[ΔvIOFit /. %[[1, 2]]] / c}
{4.10001 × 1013, 1366.67}

{Evaluate[vIOFit /. %[[1, 2]]], Evaluate[vIOFit /. %[[1, 2]]] / c}
{6.06534 × 1014, 20217.8}

```

```

emI0 = 246; ΔvI0 = 1366.67 c; vI0 = 20217.8 c;
emI[T_] := emI0 (Tanh[(h v vibI) / (2 k T)]) ^ (1 / 2);
ΔvI[T_] := ΔvI0 (Tanh[(h v vibI) / (2 k T)]) ^ (-1 / 2);
I2Absλ[λ_, T_] := emI[T] Exp[-((c / (100 λ) - vI0) / ΔvI[T]) ^ 2];
σabs3[λ_, T_] := (10 ^ 3 / Na) (1 + Log[10 / E]) I2Absλ[λ, T];

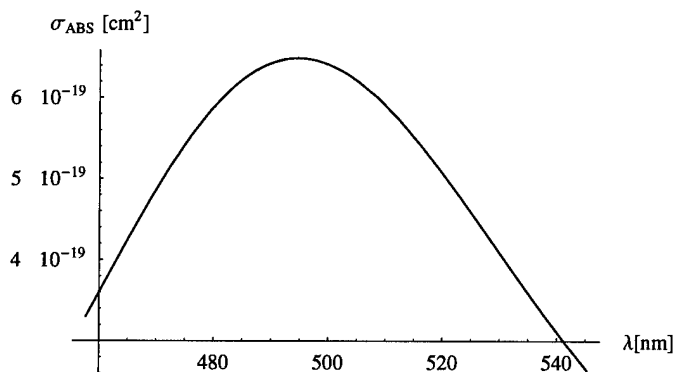
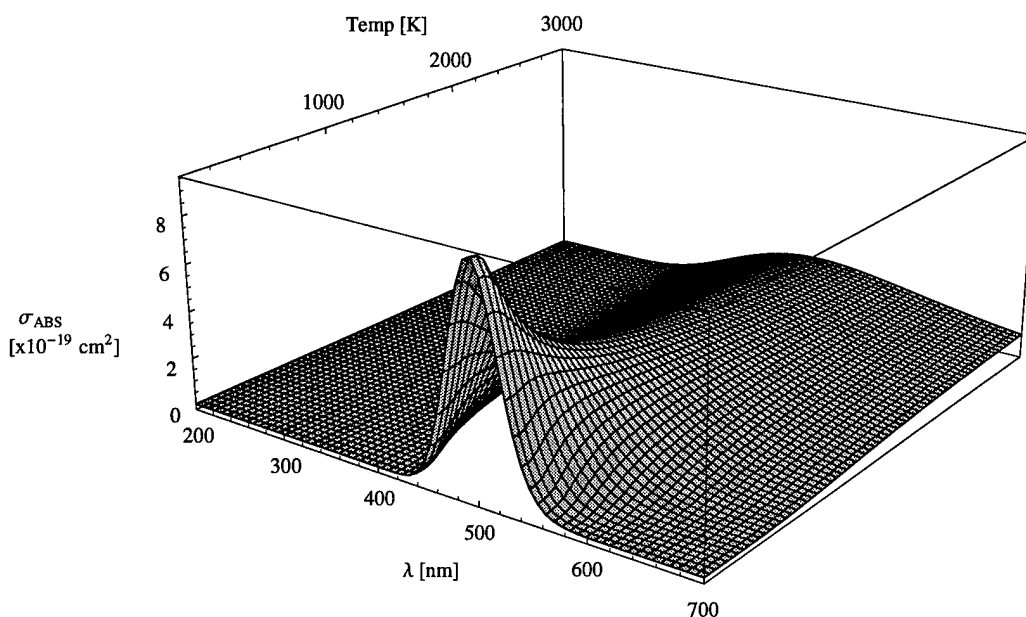
I2Extinct = Interpolation[I2Data];
TableForm[Table[{N[λ], I2Extinct[λ], N[I2Absλ[λ 10 ^ (-9), 298.2], 3]},
{λ, 420, 650, 10}],
TableHeadings -> {None, {StyleForm["λ [nm]", FontWeight -> "Bold"],
StyleForm["ε (Literature)", FontWeight -> "Bold"],
StyleForm["ε (Modeled)", FontWeight -> "Bold"]}}]

```

λ [nm]	ε (Literature)	ε (Modeled)
420.	6.9	6.36
430.	16.9	16.2
440.	34.5	34.2
450.	61.	61.
460.	93.	94.1
470.	127.	128.
480.	153.	154.
490.	168.	168.
500.	167.	168.
510.	154.	154.
520.	131.	132.
530.	106.	107.
540.	81.	81.3
550.	59.	59.1
560.	41.	41.1
570.	27.9	27.5
580.	18.4	17.8
590.	11.8	11.2
600.	7.4	6.85
610.	4.6	4.1
620.	2.8	2.41
630.	1.7	1.39
640.	0.8	0.791
650.	0.4	0.445

I₂ Absorption Plots: (a) 3-D, for all wavelengths; (b) at 298 K, for 456-545 nm

```
If[a2 != 2, {Plot3D[1019 σabs3[λ * 10-9, T], {λ, 200, 700}, {T, 10-4, 3 * 103},
  PlotRange -> All, PlotPoints -> 70, ViewPoint -> {1.849, -2.582, 1.168},
  AxesLabel ->
    {"λ [nm]", "Temp [K]", " σABS\n[x10-19 cm2"]}, ImageSize -> {494, 380}},
  Plot[σabs3[λ 10-9, 298.2], {λ, 457.7, 545.3}, PlotRange -> All,
  AxesLabel -> {" λ [nm]", "σABS [cm2"]}, ImageSize -> {323, 228}]]];
```

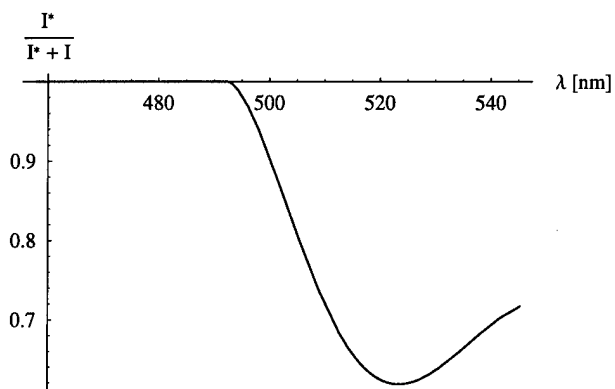
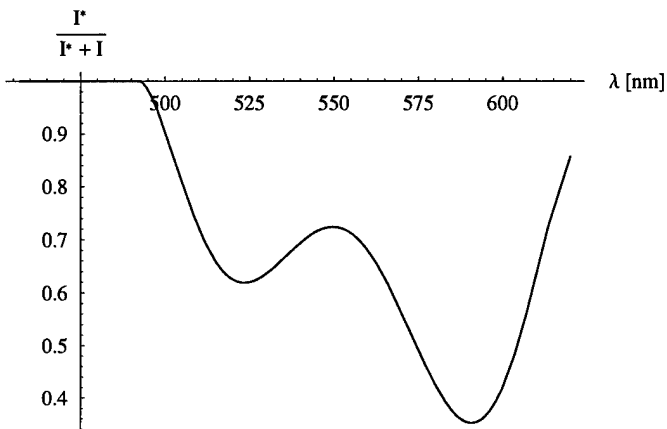


■ I* Quantum Yield from I₂ Photodissociation

Mathematical Model of I₂ + hν → I(P_{3/2}) + I(P_{1/2}) Yield Curve, derived from Tellinghuisen/Brewer

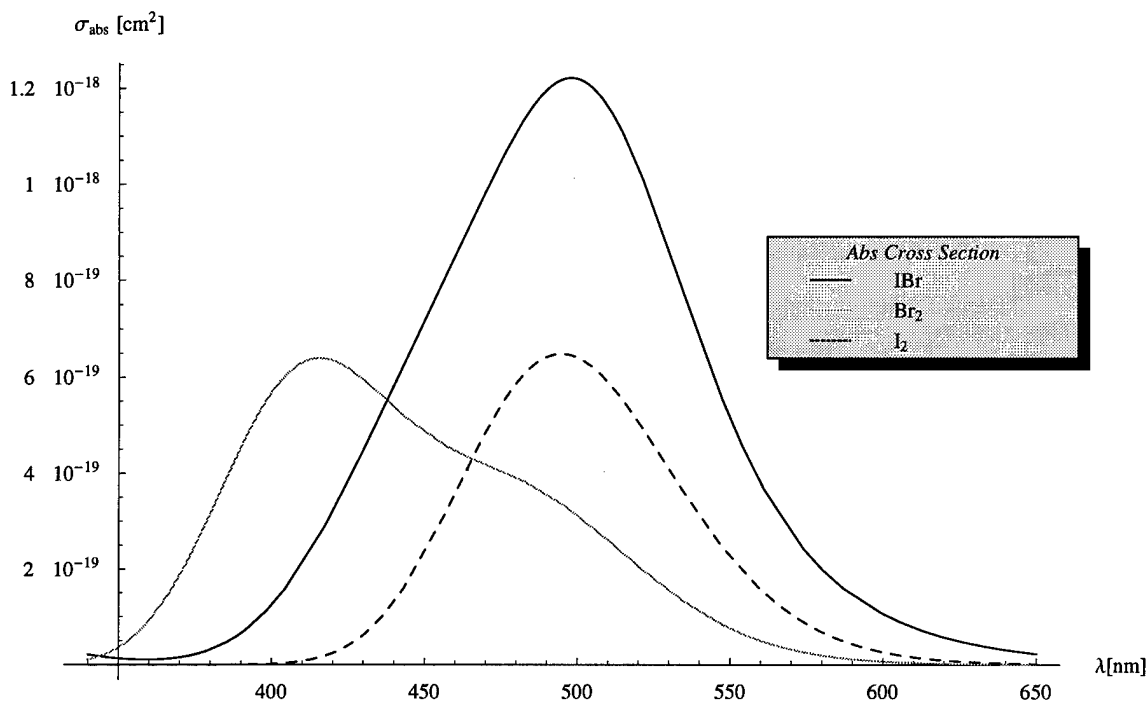
```

φ3a = PolynomialFit[{{491, .99}, {501, 0.93}, {509.1, 0.70}, {516.6, 0.62},
  {527.7, 0.66}, {546.2, 0.72}, {559.4, 0.67}, {569, 0.59}, {589.6, 0.33},
  {592.2, 0.35}, {603.7, 0.54}, {612.9, 0.67}, {623.9, 0.88}}, 6];
φ3[λ_] := If[λ > 492.6, φ3a[λ], 1.0]; If[a2 != 2, {Plot[φ3[λ], {λ, 457, 620},
  AxesLabel -> {" λ [nm]", " $\frac{I^*}{I^* + I}$ "}, ImageSize -> {318, 257}, PlotRange -> All],
  Plot[φ3[λ], {λ, 457.7, 545.3}, AxesLabel -> {" λ [nm]", " $\frac{I^*}{I^* + I}$ "},
  ImageSize -> {293, 236}, PlotRange -> All]}}];
  
```



■ Relative Absorption Cross Sections for [IBr], [Br₂] and [I₂]

```
aa = Plot[{σabs[λ*10-9, 298.2], σabs2[λ*10-9, 298.2], σabs3[λ*10-9, 298.2]},
  {λ, 340, 650}, PlotRange -> All, AxesLabel -> {" λ[nm]", "σabs [cm2"]},
  PlotStyle -> {GrayLevel[0], GrayLevel[0.7], Dashing[{0.01}]},
  PlotLegend -> {"IBr", "Br2", "I2"},
  LegendSize -> {.54, .21}, LegendBackground -> GrayLevel[0.95],
  LegendPosition -> {0.33, 0}, LegendShadow -> {0.02, -0.02}, LegendLabel ->
  StyleForm["Abs Cross Section", FontSlant -> "Italic"],
  DisplayFunction -> Identity];
If[a2 != 2, Show[aa, DisplayFunction -> $DisplayFunction, ImageSize -> {575, 400}]];
```



■ **Modeling of Solar Emission Spectrum as a Function of Wavelength**

■ **Energy Exitance (Me) Spectrum for Generic Blackbody & Sun:**

$$\text{Me}[\lambda_, T_] := \frac{2 \pi h c^2}{10000 \lambda^5} \frac{1}{e^{\frac{hc}{1000 \lambda T}} - 1}$$

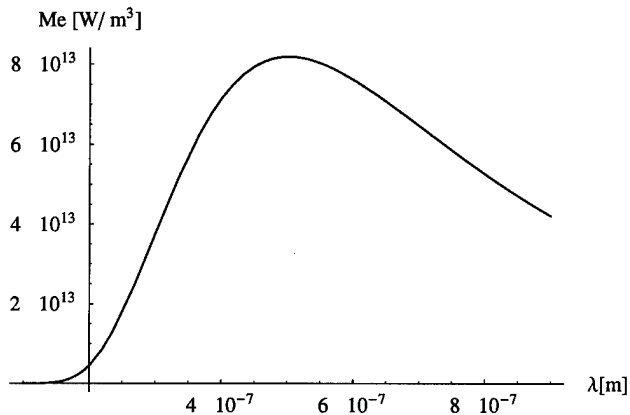
$$\text{SolarMe}[\lambda_] := (0.99) \text{Me}[\lambda, 5780]$$

Wavelength of Peak Energy Exitance using... {Wien's Law, Black Body Curve}:

```
{(2.8978 * 10^-3) / 5780, f = D[SolarMe[\lambda], \lambda];
  InterpolateRoot[f, {\lambda, 4 * 10^-7, 6 * 10^-7}, AccuracyGoal -> 10]}
{5.01349 * 10^-7, {\lambda -> 5.0055 * 10^-7}}
```

Solar Exitance vs Wavelength:

```
If[a2 != 2, Plot[SolarMe[\lambda], {\lambda, 10^-7, 9 * 10^-7}, PlotRange -> All,
  AxesLabel -> {" \lambda[m]", "Me [W/ m^3]"}, ImageSize -> {300, 270}]];
```



■ Photon Exitance (Mq) Spectrum for Generic Blackbody & Sun

$$M_q[\lambda, T] := \frac{100 \lambda M_e[\lambda, T]}{h c}$$

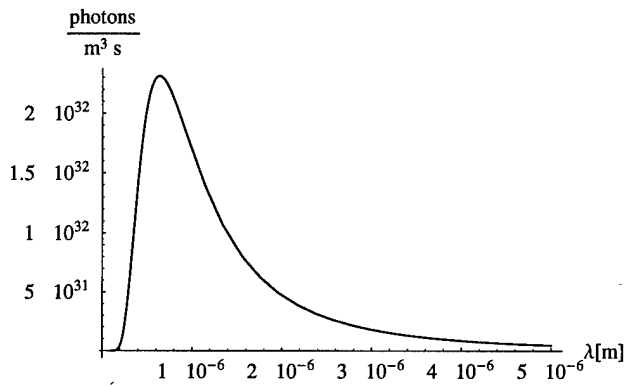
$$\text{SolarMq}[\lambda] := (0.99) M_q[\lambda, 5780]$$

Wavelength [m] of Peak SolarExitance:

```
f = ∂λ (SolarMq[λ]); InterpolateRoot[ f, {λ, 5 * 10-7, 7 * 10-7}, AccuracyGoal -> 10]
{λ -> 6.355668 * 10-7}
```

Solar Photon Exitance vs Wavelength:

```
If[a2 != 2, Plot [SolarMq[λ], {λ, 10-7, 5 * 10-6}, PlotRange -> All,
  AxesLabel -> {" λ[m]", "  $\frac{\text{photons}}{\text{m}^3 \text{ s}}$  "}, ImageSize -> {300, 270}]];
```



F := Solar Photon Incidence on Earth or Satellite Orbit [photons / s cm^2 per m wavelength]
 Solar {Eq [photons / s cm^2], Ee [W / cm^2]}: all wavelengths

$$F[\lambda_] := 10^{-4} \frac{R_{sun}^2}{SunEarth^2} SolarMq[\lambda]$$

$$\{SolarIncP = NIntegrate[F[\lambda], \{\lambda, 10^{-7}, 10^{-2}\}],$$

$$SolarIncW = NIntegrate[10^{-2} \frac{hc}{\lambda} F[\lambda], \{\lambda, 10^{-7}, 10^{-2}\}]\}$$

{6.3247 $\times 10^{17}$, 0.13627}

Solar {Eq [photons / s cm^2], Ee [W / cm^2]}:
 wavelengths which yield positive Br^*/Br inversion ($\Delta N > 0$)

$$\{NIntegrate[F[\lambda], \{\lambda, 457.7 * 10^{-9}, 545.3 * 10^{-9}\}],$$

$$NIntegrate[10^{-2} \frac{hc}{\lambda} F[\lambda], \{\lambda, 465 * 10^{-9}, 545.3 * 10^{-9}\}]\}$$

{3.92133 $\times 10^{16}$, 0.0142619}

Maximum Efficiency for IBr Laser {photonic, energy}:

$$\{NIntegrate[F[\lambda], \{\lambda, 457.7 * 10^{-9}, 545.3 * 10^{-9}\}] / NIntegrate[F[\lambda],$$

$$\{\lambda, 10^{-7}, 10^{-2}\}], NIntegrate[10^{-2} (hc) / \lambda F[\lambda], \{\lambda, 457.7 * 10^{-9},$$

$$545.3 * 10^{-9}\}] / NIntegrate[10^{-2} (hc) / \lambda F[\lambda], \{\lambda, 10^{-7}, 10^{-2}\}]\}$$

{0.0620002, 0.114055}

Maximum Efficiency for C_4F_9I Laser Competitors {photonic, energy}:

$$\{NIntegrate[F[\lambda], \{\lambda, 250 * 10^{-9}, 350 * 10^{-9}\}] / NIntegrate[F[\lambda],$$

$$\{\lambda, 10^{-7}, 10^{-2}\}], NIntegrate[10^{-2} (hc) / \lambda F[\lambda], \{\lambda, 250 * 10^{-9},$$

$$350 * 10^{-9}\}] / NIntegrate[10^{-2} (hc) / \lambda F[\lambda], \{\lambda, 10^{-7}, 10^{-2}\}]\}$$

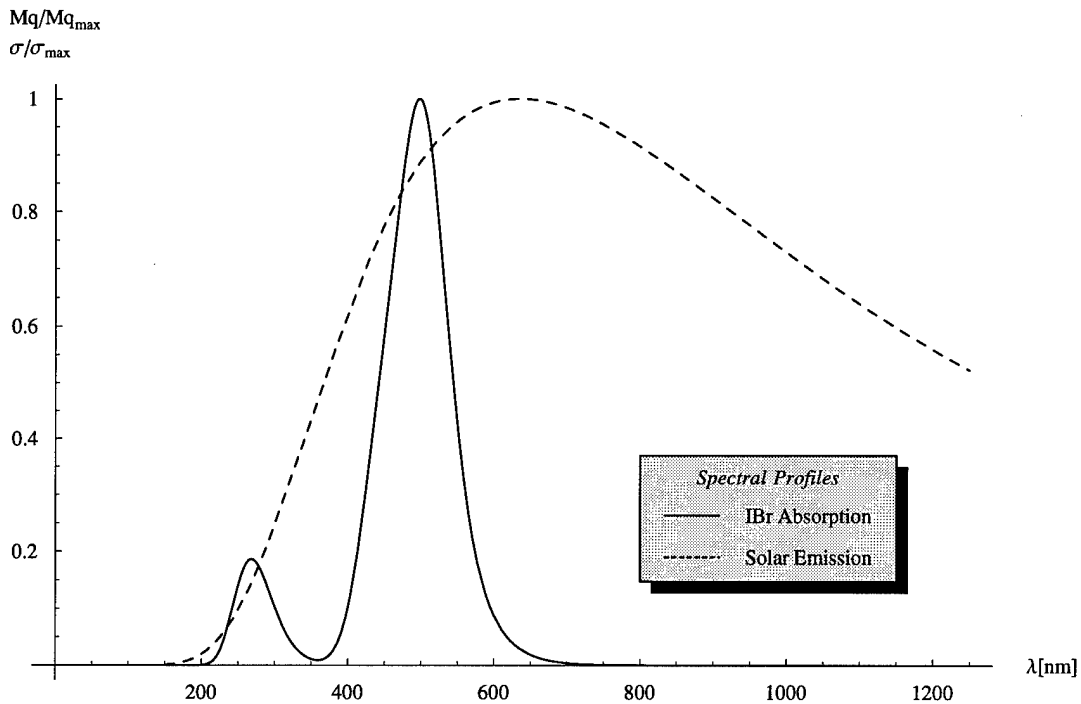
{0.00480755, 0.0601971}

Comparative Plot of Solar Exitance & IBr Absorption Spectrums

```

PlotTemp = Plot [ {σabs[λ * 10-9], 298.2] / σabs[497.8 * 10-9], 298.2] ,
SolarMq[λ * 10-9] / SolarMq[6.3557 * 10-7]],
{λ, 150, 1250}, PlotStyle -> {GrayLevel[0],
Dashing[{0.01}]}, AxesLabel -> {" λ[nm]", "Mq/Mqmax \nσ/σmax"}, PlotLegend ->
{"IBr Absorption", "Solar Emission"}, LegendSize -> {.45, .22},
LegendBackground -> GrayLevel[0.95], LegendPosition -> {0.17, -0.4},
LegendShadow -> {0.02, -0.02}, LegendLabel -> StyleForm["Spectral Profiles",
FontSlant -> "Italic"], DisplayFunction -> Identity]; If[a2 != 2,
Show[{PlotTemp}, DisplayFunction -> $DisplayFunction, ImageSize -> {580, 500}]];

```



■ Development of $IBr \rightarrow Br(P_{1/2}) \rightarrow Br(P_{3/2}) + h\nu$
Laser Rate Equations (Continuous Pumping)

■ Initialize Data Tables / Assign Rate Coefficients & Nominal Cavity Parameters

```
q = 0; Label[ClearTables];
  BrStarDataq = .;
BrDataq = .; IBrDataq = .; IodDataq = .; Iod2Dataq = .; Br2Dataq = .;
  IStarDataq = .; PhotonDataq = .;  $\gamma$ Dataq = .; PowerDataq = .; Laserq = .;
  If[UserTag != 1, (Tq = .; Pcellq = .; Lgq = .; Scq = .; Rcoupq = .; Dpq = .;
  Atubeq = .; Lcq = .;  $\lambda$ cutLoq = .;  $\lambda$ cutHiq = .;)]; q += 1; If[q <= 6, Goto[ClearTables]]
```

```
A21 = 0.63;  $\lambda$ lase = 2714 * 10^(-9);  $\nu$ lase = 0.01 c /  $\lambda$ lase; A21IStar = 7.69;
```

```
kq1 = 1.00 * 10^(-12) (* Br* quenching by IBr *) ;
kq2 = 1.90 * 10^(-11) (* Br* quenching by I *) ;
kq3 = 1.86 * 10^(-12) (* Br* quenching by I2 *) ;
kq4 = 1.20 * 10^(-13) (* Br* quenching by Br2 *) ;
kq5 = 6.75 * 10^(-13) (* Br* quenching by Br* *) ;
kq6 = 2.50 * 10^(-14) (* Br* quenching by Br *) ;
kq7 = 6.00 * 10^(-11) (* Br* quenching by IBr *) ;
kq8 = 3.50 * 10^(-11) (* I* quenching by I2 *) ;
kq9 = 5.60 * 10^(-11) (* I* quenching by Br2 *) ;

ke1 = 4.60 * 10^(-11) (* Br + IBr → I + Br2 *) ;
ke2 = 5.00 * 10^(-11) (* Br + I2 → IBr + I *) ;
ke3 = 2.69 * 10^(-13) (* I + Br2 → IBr + Br *) ;
ke4 = 6.607 * 10^(-16) (* I + IBr → I2 + Br *) ;

kr1 = 3.00 * 10^(-30) (* Br + Br + IBr → Br2 + IBr *) ;
kr2 = 4.00 * 10^(-32) (* Br* + Br + IBr → Br2 + IBr *) ;
kr3 = 1.00 * 10^(-32) (* I + Br + IBr → 2 IBr *) ;
kr4 = 1.00 * 10^(-32) (* I + Br* + IBr → 2 IBr *) ;
kr5 = 3.00 * 10^(-32) (* I* + Br + IBr → 2 IBr *) ;
kr6 = 3.00 * 10^(-30) (* I + I + IBr → I2 + IBr *) ;
kr7 = 3.00 * 10^(-32) (* I* + I + IBr → I2 + IBr *) ;
```

■ Preliminary View of Relevant Laser Parameters/Pumping Rates

Total IBr Photodissociation; Br(P_{1/2}) and Br(P_{3/2}) Generation Rates

```

If[UserTag == 1, Goto [Calc1]];
ClearAll[IBrN, Br2N, Iod2N];
T0 = 298.2; Pcell0 = 70; Lg0 = 300; Sc0 = 20000; Rcoup0 = 0.89; Atube0 = 0.785;
Dp0 = 1.5; λcutLo0 = 457.7 * 10-9; λcutHi0 = 545.3 * 10-9; vFlow0 = 0;
Rmir = 0.998; Tcell = 0.99; ρ = 1.1;
Label[Calc1];

series = 0; Ntag = 0; n = 0; Lcn = N[ρ * Lgn, 4];
ΔvD = 200 vlase √((2 k Tn Log[2]) / (MassBr c2)); gd = 2 / ΔvD √(Log[2] / π);
Aconc = 10-4 Scn Atuben Lgn Scn; trt = (2 Lcn) / c; τp = trt / (1 - (Tcell4 Rmir Rcoupn));
PumpPwrn = (SolarIncW * Scn * Lgn * Atuben / Dpn); IBr0 = 9.659 * 1018 (Pcelln / Tn);
ose = 104 (A21 λlase2) / (8 π) gd; Asp = (c ose) / (Lgn Atuben);
γth = 1 / (2 Lgn) Log[1 / (Tcell4 Rcoupn Rmir)]; ΔNth = γth / ose; Br20 = 0.04 IBr0;
I20 = 0.04 IBr0; β = (100 vFlown) / Lgn;

Rp[IBrN_, Br2N_, Iod2N_] :=
  (Scn / Dpn) NIntegrate[F[λ] (IBrN * σabs[λ, Tn) / (IBrN * σabs[λ, Tn]
    + Br2N * σabs2[λ, Tn] + Iod2N * σabs3[λ, Tn]) * (1 - Exp[-(IBrN * σabs[λ, Tn]
    + Br2N * σabs2[λ, Tn] + Iod2N * σabs3[λ, Tn]) Dpn)], {λ, λcutLon, λcutHin]];
Rpa[IBrN_, Br2N_, Iod2N_] :=
  (Scn / Dpn) NIntegrate[F[λ] φ[λ 109] (IBrN * σabs[λ, Tn) / (IBrN * σabs[λ, Tn]
    + Br2N * σabs2[λ, Tn] + Iod2N * σabs3[λ, Tn]) * (1 - Exp[-(IBrN * σabs[λ, Tn]
    + Br2N * σabs2[λ, Tn] + Iod2N * σabs3[λ, Tn]) Dpn)], {λ, λcutLon, λcutHin]];
Rpb[IBrN_, Br2N_, Iod2N_] :=
  (Scn / Dpn)
  NIntegrate[F[λ] (1 - φ[λ 109]) (IBrN * σabs[λ, Tn) / (IBrN * σabs[λ, Tn]
    + Br2N * σabs2[λ, Tn] + Iod2N * σabs3[λ, Tn]) * (1 - Exp[-(IBrN * σabs[λ, Tn]
    + Br2N * σabs2[λ, Tn] + Iod2N * σabs3[λ, Tn]) Dpn)], {λ, λcutLon, λcutHin]];
φIBr := NIntegrate[F[λ] φ[109 λ] σabs[λ, Tn],
  {λ, λcutLon, λcutHin}] / NIntegrate[F[λ] σabs[λ, Tn],
  {λ, λcutLon, λcutHin]];
φIBre[IBrN_, Br2N_, Iod2N_] := Rpa[IBrN, Br2N, Iod2N] / Rp[IBrN, Br2N, Iod2N];

Rp2[IBrN_, Br2N_, Iod2N_] :=
  (Scn / Dpn) NIntegrate[F[λ] (Br2N * σabs2[λ, Tn) / (IBrN * σabs[λ, Tn]
    + Br2N * σabs2[λ, Tn] + Iod2N * σabs3[λ, Tn]) * (1 - Exp[-(IBrN * σabs[λ, Tn]
    + Br2N * σabs2[λ, Tn] + Iod2N * σabs3[λ, Tn]) Dpn)], {λ, λcutLon, λcutHin]];
Rp2a[IBrN_, Br2N_, Iod2N_] :=
  (Scn / Dpn)
  NIntegrate[F[λ] φ2[λ 109] (Br2N * σabs2[λ, Tn) / (IBrN * σabs[λ, Tn]
    + Br2N * σabs2[λ, Tn] + Iod2N * σabs3[λ, Tn]) * (1 - Exp[-(IBrN * σabs[λ, Tn]
    + Br2N * σabs2[λ, Tn] + Iod2N * σabs3[λ, Tn]) Dpn)], {λ, λcutLon, λcutHin]];
Rp2b[IBrN_, Br2N_, Iod2N_] :=
  (Scn / Dpn)
  NIntegrate[F[λ] (2 - φ2[λ 109]) (Br2N * σabs2[λ, Tn) / (IBrN * σabs[λ, Tn]

```

```

+ Br2N* cabs2[λ, Tn] + Iod2N* cabs3[λ, Tn]) * (1 - Exp[- (IBrN* cabs[λ, Tn]
+ Br2N* cabs2[λ, Tn] + Iod2N* cabs3[λ, Tn]) Dpn]), {λ, λcutLo_n, λcutHi_n});
φBr2 := NIntegrate[F[λ] φ2[10^9 λ] cabs2[λ, Tn],
{λ, λcutLo_n, λcutHi_n}] / NIntegrate[F[λ] cabs2[λ, Tn],
{λ, λcutLo_n, λcutHi_n}];
φBr2e[IBrN_, Br2N_, Iod2N_] := Rp2a[IBrN, Br2N, Iod2N] / Rp2[IBrN, Br2N, Iod2N];

Rp3[IBrN_, Br2N_, Iod2N_] :=
(SCn / Dpn) NIntegrate[F[λ] (Iod2N* cabs3[λ, Tn]) / (IBrN* cabs[λ, Tn]
+ Br2N* cabs2[λ, Tn] + Iod2N* cabs3[λ, Tn]) * (1 - Exp[- (IBrN* cabs[λ, Tn]
+ Br2N* cabs2[λ, Tn] + Iod2N* cabs3[λ, Tn]) Dpn]), {λ, λcutLo_n, λcutHi_n}];
Rp3a[IBrN_, Br2N_, Iod2N_] :=
(SCn / Dpn)
NIntegrate[F[λ] φ3[λ 10^9] (Iod2N* cabs3[λ, Tn]) / (IBrN* cabs[λ, Tn]
+ Br2N* cabs2[λ, Tn] + Iod2N* cabs3[λ, Tn]) * (1 - Exp[- (IBrN* cabs[λ, Tn]
+ Br2N* cabs2[λ, Tn] + Iod2N* cabs3[λ, Tn]) Dpn]), {λ, λcutLo_n, λcutHi_n}];
Rp3b[IBrN_, Br2N_, Iod2N_] :=
(SCn / Dpn)
NIntegrate[F[λ] (2 - φ3[λ 10^9]) (Iod2N* cabs3[λ, Tn]) / (IBrN* cabs[λ, Tn]
+ Br2N* cabs2[λ, Tn] + Iod2N* cabs3[λ, Tn]) * (1 - Exp[- (IBrN* cabs[λ, Tn]
+ Br2N* cabs2[λ, Tn] + Iod2N* cabs3[λ, Tn]) Dpn]), {λ, λcutLo_n, λcutHi_n}];
φIod2 := NIntegrate[F[λ] φ3[10^9 λ] cabs3[λ, Tn],
{λ, λcutLo_n, λcutHi_n}] / NIntegrate[F[λ] cabs3[λ, Tn],
{λ, λcutLo_n, λcutHi_n}];
φIod2e[IBrN_, Br2N_, Iod2N_] := Rp3a[IBrN, Br2N, Iod2N] / Rp3[IBrN, Br2N, Iod2N];

RpTot[IBrN_, Br2N_, Iod2N_] :=
Rp[IBrN, Br2N, Iod2N] + Rp2[IBrN, Br2N, Iod2N] + Rp3[IBrN, Br2N, Iod2N];
BrStarTot[IBrN_, Br2N_, Iod2N_] := Rpa[IBrN, Br2N, Iod2N] + Rp2a[IBrN, Br2N, Iod2N];
BrTot[IBrN_, Br2N_, Iod2N_] := Rpb[IBrN, Br2N, Iod2N] + Rp2b[IBrN, Br2N, Iod2N];

φTot[IBrN_, Br2N_, Iod2N_] := (Rpa[IBrN, Br2N, Iod2N] + Rp2a[IBrN, Br2N, Iod2N]) /
(Rp[IBrN, Br2N, Iod2N] + Rp2[IBrN, Br2N, Iod2N]);

PList = {"Doppler-Broadened Linewidth ", "Δv_D:", ΔvD, "Hz"},
{"Peak Transition Lineshape ", "g(v_0):", gd, "s"},
{"Exposed Area of Solar Concentrator ",
"A_c:", Aconc, "\\(m^2\\)", {"Photon Round Trip ", "τ_rt:", τrt, "s"},
{"Photon Lifetime ", "τ_p:", τp, "s"}, {"Initial Concentration/ IBr ",
"[IBr]_0:", IBr0, "\\(cm^-3\\)", {"Stim Emission Cross-Section ",
"σ_st:", ose, "\\(cm^2\\)", {"Spontaneous Emission Rate ",
"ASP:", Asp, "\\(s^-1\\)",
{"Threshold Gain Coefficient ", "γ_th:", γth, "\\(cm^-1\\)",
{"Threshold Population Inversion ", "ΔN_th:", ΔNth, "\\(cm^-3\\)",
{"", "", "", ""}, {"Total Incident Solar Power", PumpPwr, "W"},
{"Initial IBr Photodissociation Rate ", "Rp_IBr:", Rp[IBr0, Br20, I20],
"\\(cm^-3\\) \\(s^-1\\)", {"Quantum Yield: IBr → I + \\(Br^*\\) ",
"φ_IBr:", φIBre[IBr0, Br20, I20], ""}, {"Initial Br2 Photodissociation Rate ",
"Rp_Br2:", Rp2[IBr0, Br20, I20], "\\(cm^-3\\) \\(s^-1\\)",

```

```

{"Quantum Yield: Br2 → Br + \!\(Br\^*\)",
  "φBr2:", φBr2e[IBr0, Br20, I20], ""},
{"Initial Photodissociation Rate (Total) ", "RpT:", RpTot[IBr0, Br20, I20],
  "\!\(cm\^-3\) \!\(s\^-1\)"},
{"\!\(Br\^*\) Quantum Yield (Combined) ", "φT:",
  φTot[IBr0, Br20, I20], ""}, {"Initial Br(P1/2) Pump Rate (Total) ", "RpBr*:",
  BrStarTot[IBr0, Br20, I20], "\!\(cm\^-3\) \!\(s\^-1\)"},
{"Initial Br(P3/2) Pump Rate (Total) ", "RpBr:",
  BrTot[IBr0, Br20, I20], "\!\(cm\^-3\) \!\(s\^-1\)"},
{"Initial Br2 Photolysis Contribution ",
  "RpBr2/T:", (100 Rp2[IBr0, Br20, I20]) / RpTot[IBr0, Br20, I20], "%"},
{"Initial I2 Photolysis Contribution ",
  "RpI2/T:", (100 Rp3[IBr0, Br20, I20]) / RpTot[IBr0, Br20, I20], "%"};
TableForm[PList, TableSpacing -> {1, 1}]

```

Doppler-Broadened Linewidth	Δv_D :	1.52374×10^8	Hz
Peak Transition Lineshape	$g(v_0)$:	6.16536×10^{-9}	s
Exposed Area of Solar Concentrator	A_c :	9.42×10^6	m ²
Photon Round Trip	τ_{rt} :	2.2×10^{-8}	s
Photon Lifetime	τ_p :	1.49885×10^{-7}	s
Initial Concentration/ IBr	$[IBr]_0$:	2.26737×10^{18}	cm ⁻³
Stim Emission Cross-Section	σ_{st} :	1.13836×10^{-17}	cm ²
Spontaneous Emission Rate	A_{sp} :	1.45014×10^{-9}	s ⁻¹
Threshold Gain Coefficient	γ_{th} :	0.000264562	cm ⁻¹
Threshold Population Inversion	ΔN_{th} :	2.32407×10^{13}	cm ⁻³
Total Incident Solar Power	PumpPwr	W	
Initial IBr Photodissociation Rate	$R_{P_{IBr}}$:	4.88849×10^{20}	cm ⁻³ s ⁻¹
Quantum Yield: IBr → I + Br*	ϕ_{IBr} :	0.640688	
Initial Br ₂ Photodissociation Rate	$R_{P_{Br_2}}$:	5.43725×10^{18}	cm ⁻³ s ⁻¹
Quantum Yield: Br ₂ → Br + Br*	ϕ_{Br_2} :	0.689597	
Initial Photodissociation Rate (Total)	R_{P_T} :	5.03999×10^{20}	cm ⁻³ s ⁻¹
Br* Quantum Yield (Combined)	ϕ_T :	0.641226	
Initial Br(P _{1/2}) Pump Rate (Total)	$R_{P_{Br^*}}$:	3.16949×10^{20}	cm ⁻³ s ⁻¹
Initial Br(P _{3/2}) Pump Rate (Total)	$R_{P_{Br}}$:	1.82774×10^{20}	cm ⁻³ s ⁻¹
Initial Br ₂ Photolysis Contribution	$R_{P_{Br_2/T}}$:	1.07882	%
Initial I ₂ Photolysis Contribution	$R_{P_{I_2/T}}$:	1.92728	%

Hyperlink To:

[Multiple Data Entry](#)

[Full Kinetic Model](#)

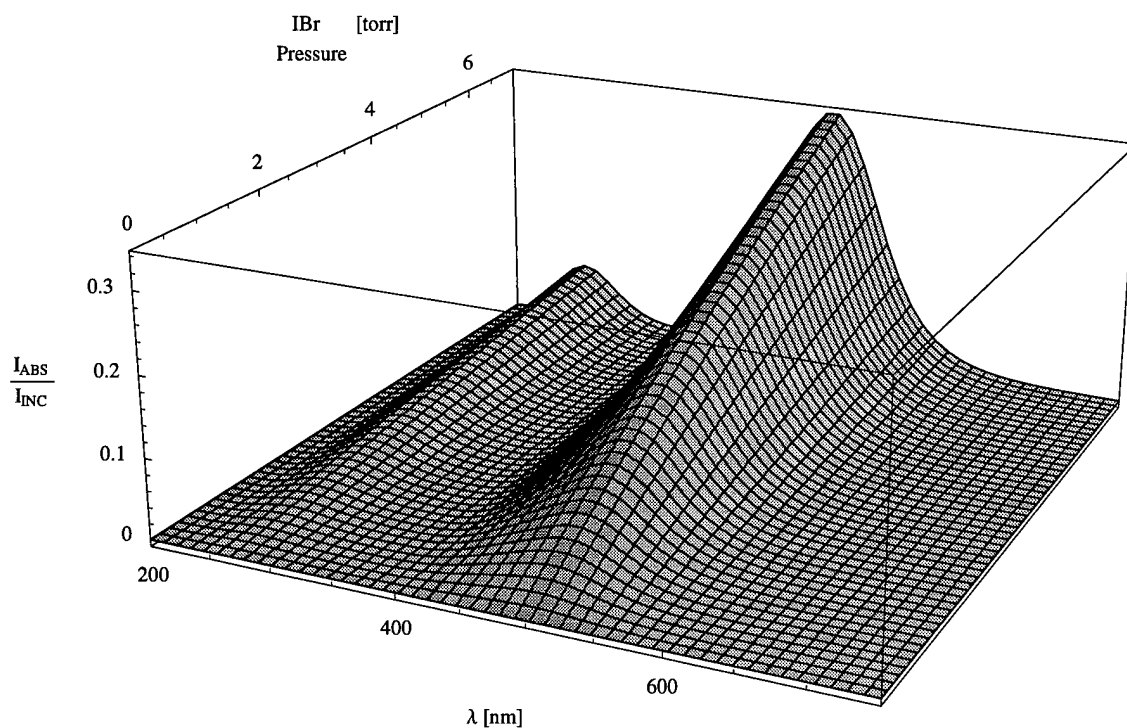
[Approx Kinetic Model](#)

3-D Representation of IBr Absorption of Incident Radiation vs $([IBr])_0$ and λ :

```

If[a2 != 2, Plot3D[ $1 - \text{Exp}[-\sigma_{\text{abs}}[10^{-9} \lambda, T_0] \left( \frac{9.659 \times 10^{18}}{T_0} \text{Press} \right) D_{P_0}]$ ],
  { $\lambda$ , 200, 750}, {Press, 0, 7}, PlotRange -> All, PlotPoints -> 50,
  ViewPoint -> {1.335, -2.882, 1.168}, AxesLabel ->
  {" $\lambda$  [nm]", " IBr      [torr]\nPressure", " $\frac{I_{\text{ABS}}}{I_{\text{INC}}}$ "}, ImageSize -> {550, 500}];

```

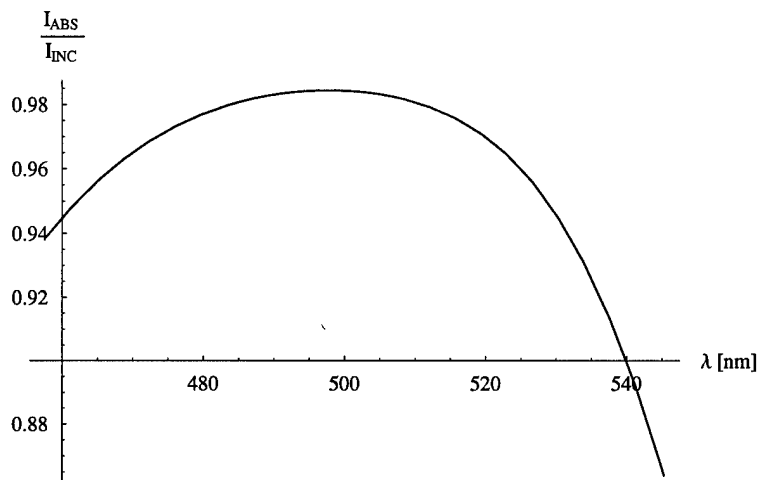


*I*Br Absorption Fraction for Incident Radiation within Wavelength Cutoffs:

```

If[a2 != 2,
Plot[(1 - Exp[-σabs[10-9 λ, T0] IBr0 Dp0]), {λ, (109 λcutLo0), (109 λcutHi0)},
AxesLabel -> {"λ [nm]", " $\frac{I_{ABS}}{I_{INC}}$ "}, PlotRange -> All, ImageSize -> {360, 270}]];

```

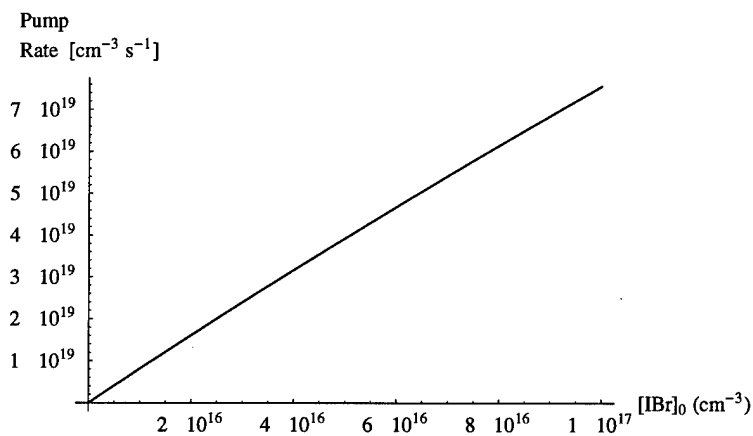


*Initial Photodissociation Pumping Rate via Solar Excitation for Varying [I*Br]₀:

```

If[a2 != 2, Plot[RpTot[IBrn, 0.04 IBrn, 0.04 IBrn], {IBrn, 1010, 1017}, AxesLabel ->
{" [I]Br0 (cm-3)", "Pump\nRate [cm-3 s-1]", ImageSize -> {360, 270}]];

```

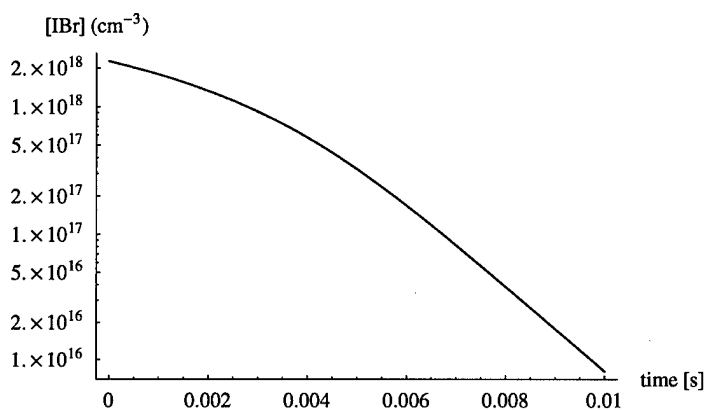


IBr Population Decline Upon Photodissociation by Solar Concentration/Excitation (Logarithmic Scale):

```

IBrOnly := NDSolve[{nIBr'[t] == -Rp[nIBr[t], 0.04 nIBr[t],
    0.04 nIBr[t]], nIBr[0] == IBr0}, nIBr[t], {t, 0, 10-2};
If[a2 != 2, LogPlot[Evaluate[nIBr[t] /. IBrOnly], {t, 0, 10-2},
    AxesLabel -> {"time [s]", "[IBr] (cm-3)"}, ImageSize -> {354, 258},
    PlotRange -> All];

```

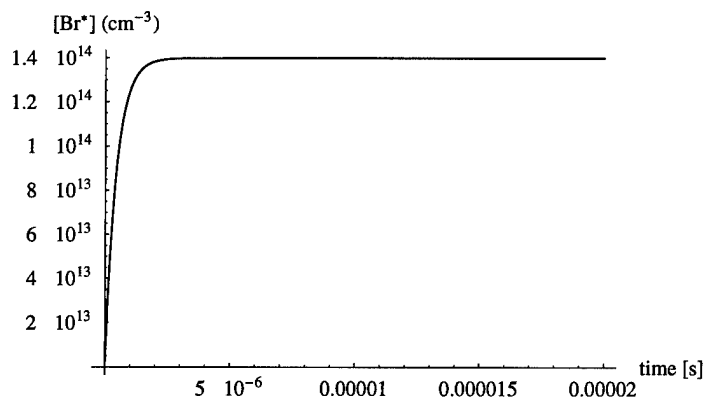


Production Rate of Br(P_{1/2}) upon IBr Photolysis, with Spontaneous Emission & IBr Quenching:

```

BrStarOnly := NDSolve[{BrS'[t] == BrStarTot[IBr0, Br20,
    I20] - A21 BrS[t] - (kq1 IBr0 BrS[t]), BrS[0] == 0}, BrS[t], {t, 0, 10-5};
If[a2 != 2, Plot[Evaluate[BrS[t] /. BrStarOnly], {t, 0, 2 * 10-5}, AxesLabel ->
    {"time [s]", "[Br*] (cm⁻³)"}, ImageSize -> {354, 258}, PlotRange -> All];

```

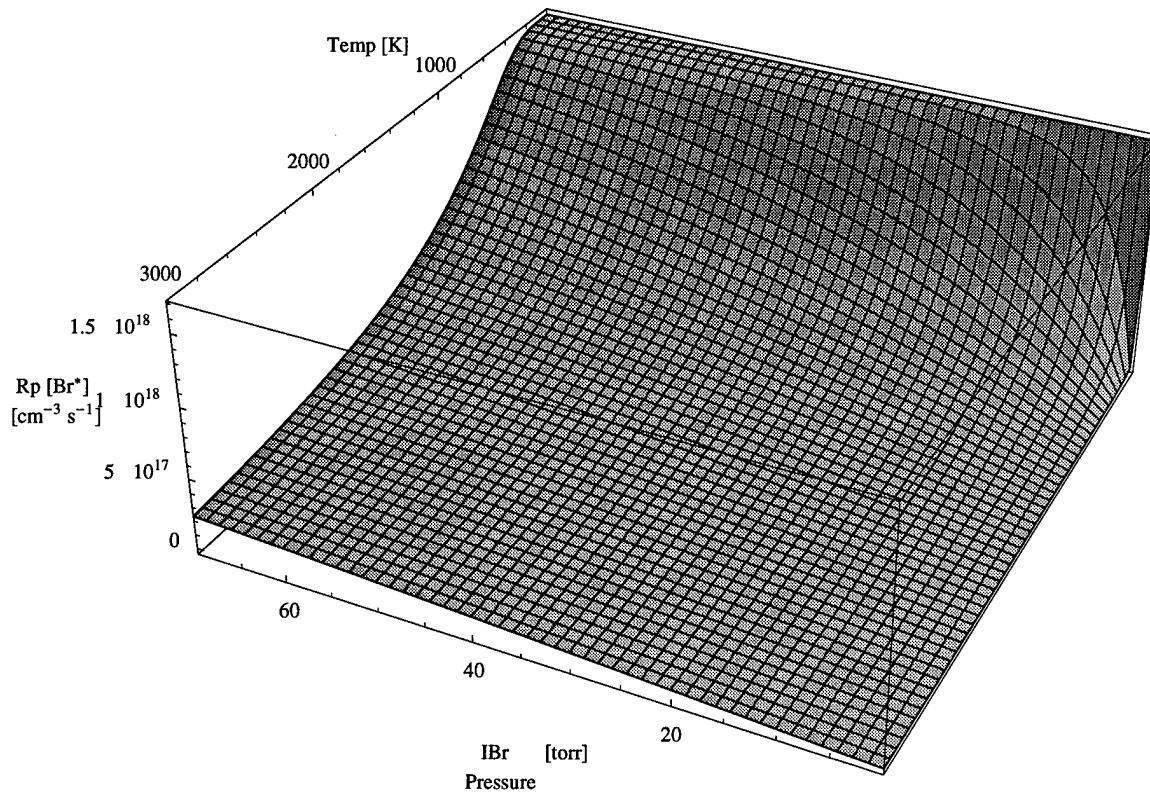


■ Pump Rate of Br($P_{1/2}$) as a Function of IBr Partial Pressure [Torr] and Gain Cell Temperature [K]

```

ppump2[IBr_, Temp_] := (Sc0 / Lg0) * (NIntegrate[phi[10^9 lambda] F[lambda] (1 - Exp[-sigma abs[lambda,
Temp] IBr Dp0]), {lambda, lambdaLo0, lambdaHi0}]);
If[a2 != 2, Plot3D[ppump2[(9.659 * 10^18 / Temp) Press], Temp], {Press, .1, 70},
{Temp, 0.1, 3000}, PlotPoints -> 50, AxesLabel ->
{" IBr [torr]\nPressure", "Temp [K]",
" Rp [Br*]\n[cm^-3 s^-1]"}, ImageSize -> {550, 500},
ViewPoint -> {-1.254, 2.593, 1.775}]];

```

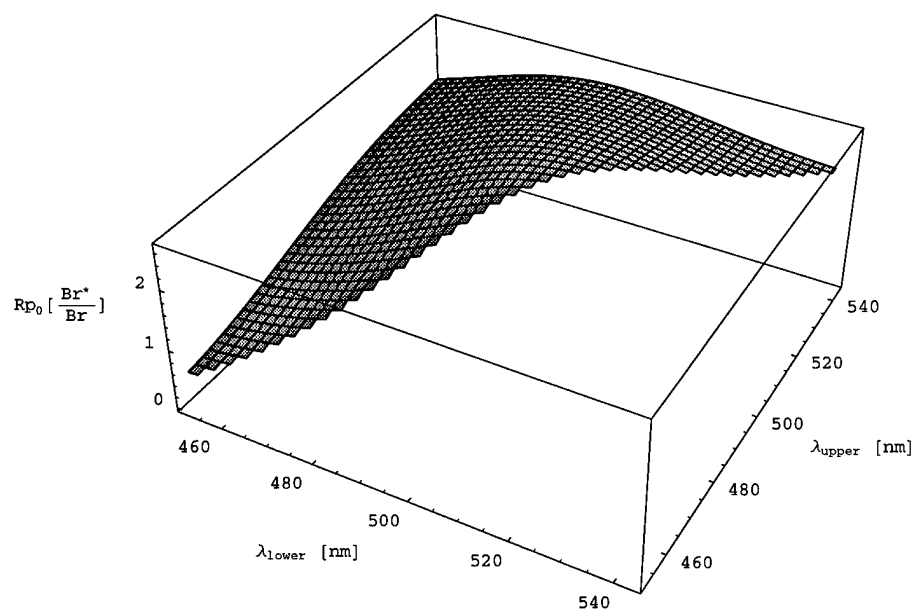
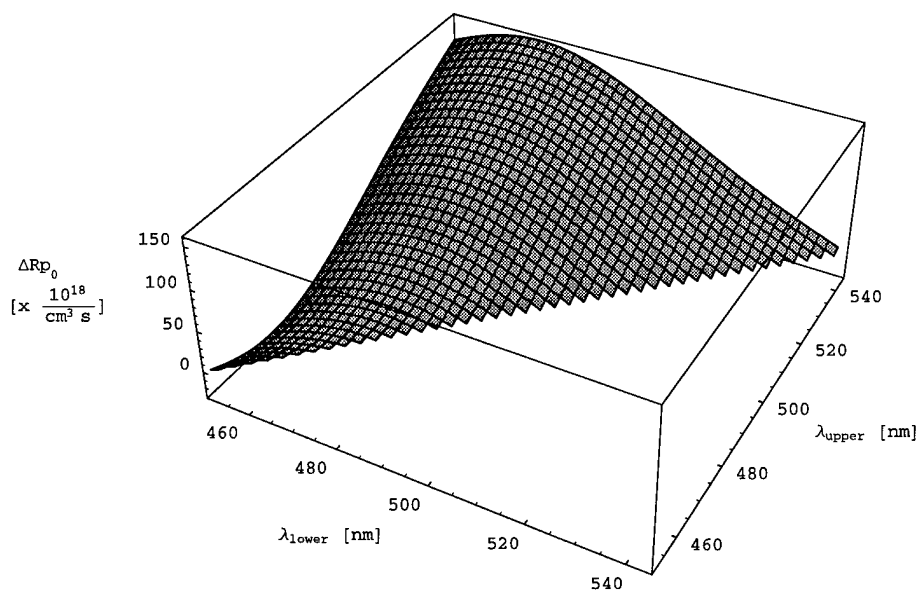


■ Comparison of Initial Br and Br* Pump Rates vs Insolant Wavelength Limits

```

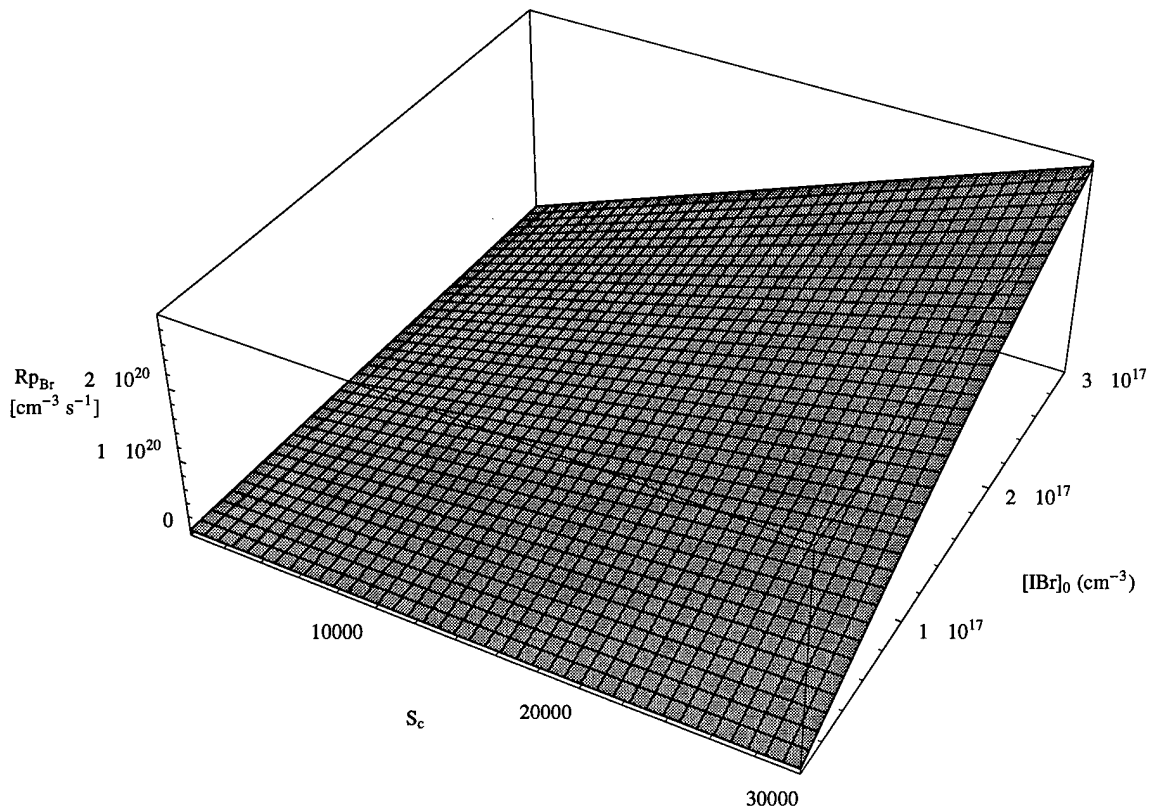
If[a2 != 2, {Off[Power::infy, ∞::indet, Plot3D::plnc, Plot3D::gval],
ppump3[λ1_, λ2_] := (If[λ1 < λ2, 1, Null]) * 10-18  $\left( \left( \frac{Sc_0}{Dp_0} \right) \right.$ 
    NIntegrate[φ[109 λ] F[λ] (1 - Exp[-σabs[λ, T0] IBr0 Dp0]), {λ, λ1, λ2}]
    -  $\left( \frac{Sc_0}{Dp_0} \right)$  NIntegrate[(1 - φ[109 λ]) F[λ] (1 - Exp[-σabs[λ, T0] IBr0 Dp0]),
    {λ, λ1, λ2}] ), aa = Plot3D[ppump3[λ1 * 10-9, λ2 * 10-9], {λ1, 450, 545},
    {λ2, 450, 545},
    AxesLabel -> {"λlower [nm]", "λupper [nm]", " ΔRp0 \ n[x  $\frac{10^{18}}{\text{cm}^3 \text{ s}}$ ] "},
    TextStyle -> {FontSize -> 7}, PlotPoints -> 45, ImageSize -> {440, 330}],
ppump4[λ1_, λ2_] := (If[λ1 < λ2, 1, Null]) *  $\left( \left( \frac{Sc_0}{Lg_0} \right) \right.$  NIntegrate[φ[109 λ] F[λ] (1 -
    Exp[-σabs[λ, T0] IBr0 Dp0]), {λ, λ1, λ2}] ) /  $\left( \left( \frac{Sc_0}{Lg_0} \right) \right.$ 
    NIntegrate[(1 - φ[109 λ]) F[λ] (1 - Exp[-σabs[λ, T0] IBr0 Dp0]), {λ, λ1, λ2}] ),
ab = Plot3D[ppump4[λ1 * 10-9, λ2 * 10-9], {λ1, 450, 545}, {λ2, 450, 545},
    AxesLabel -> {"λlower [nm]", "λupper [nm]", " Rp0 [ $\frac{Br^*}{Br}$ ]"}, TextStyle ->
    {FontSize -> 7}, PlotPoints -> 45, ImageSize -> {440, 330}],
On[Power::infy, ∞::indet, Plot3D::plnc, Plot3D::gval]};

```



■ Initial Br($P_{1/2}$) Pump Rate as a Function of Solar Concentration and $[IBr]_0$:

```
Pump5[Sconc_, IBr_] :=  $\frac{Sconc}{Sc_0}$  RpTot[IBr, 0.04 IBr, 0.04 IBr];
If[a2 != 2, Plot3D[Pump5[Sconc, IBr], {Sconc, 200, 30000}, {IBr,  $10^{12}$ ,  $3 \cdot 10^{17}$ },
AxesLabel -> {"Sc", "[IBr]0 (cm-3)", "RpBr \n[cm-3 s-1]", ImageSize -> {550, 500},
PlotPoints -> 40]];
```



■ Assign Multiple Parameter Series for Comparison (Optional):

```

If[UserTag == 1, Goto[CalcMany]];
series = 6;
d = 0; While[(d = d + 1) <= series,          (* Assign Data Sets *)
{Td = 298.2, Pcelld = 70, Lgd = 300, Scd = 20000, Rcoupd = 0.89, Atubed = 0.785,
  Dpd = 1.5, λcutLod = 457.7 * 10-9, λcutHid = 545.3 * 10-9, vFlowd = 0,
  Pcelld = Extract[{25, 40, 55, 70, 85, 100}, d]};
Rmir = 0.998; Tcell = 0.99; ρ = 1.1;

ParameterList = {
(* 1 *) "Operating Temperature [K]",
(* 2 *) "IBr Pressure [Torr]",
(* 3 *) "Gain Path Length [cm]",
(* 4 *) "Solar Concentration",
(* 5 *) "Coupler Reflectivity",
(* 6 *) "Area/ Laser Tube [\\(cm^2)]",
(* 7 *) "Pumping Path Length [cm]",
(* 8 *) "λcutoff (lower) [m]",
(* 9 *) "λcutoff (upper) [m]",
(* 10 *) "Flow Velocity [m/s]";

Parameter = ParameterList[[2]];

q = 1; Label[DataLabel]; Setq = Pcellq
; q += 1; If[(q <= series), Goto[DataLabel]];
Label[CalcMany];
Ntag = 1;

```

Hyperlink To:

[Single Data Entry](#)

[Kinetic Model #2](#)

[Approx Kinetic Model](#)

■ Compute Evolution of Laser Populations Under Continuous Solar Pumping
Kinetic Package #1: Interpolation Map Model (A)

```

If[ ((UserTag == 1) && (a3 != 2)), Goto[EndLong] ];

If[UserTag == 1, Null, tmax = 1.0 10^-2]; StartTime = SessionTime[];
ClearAll[Γ, IBr, Iod, BrStar, Br, ΔN, γ, Iod2, Br2,
  IStar, Photon, PowerOut, LLaser, FinalList, t];

If[Ntag == 1, n = 1, n = 0]; Label[Recycle];
Laser_n = .;
IBrData_n = .; IodData_n = .; BrStarData_n = .; BrData_n = .; Iod2Data_n = .;
Br2Data_n = .; IStarData_n = .; γData_n = .; PhotonData_n = .; PowerData_n = .;

Lc_n = N[ρ * Lg_n, 4]; β = (100 vFlow_n) / Lg_n;
ΔvD = 200 v_lase √((2 k T_n Log[2]) / (MassBr c^2)); gd = 2 / ΔvD √(Log[2] / π);
Aconc = 10^-4 Sc_n Atube_n Lg_n Sc_n; τrt = (2 Lc_n) / c; τp = τrt / (1 - (Tcell^4 Rmir Rcoup_n));
PumpPwr_n = (SolarIncW * Sc_n * Lg_n * Atube_n / Dp_n); IBr0 = 9.659 * 10^18 (Pcell_n / T_n);
ose = 10^4 (A21 λ_lase^2) / (8 π) gd; Asp = (c ose) / (Lg_n Atube_n);
γth = 1 / (2 Lg_n) Log[1 / (Tcell^4 Rcoup_n Rmir)]; ΔNth = γth / ose; Br20 = 0.04 IBr0;
I20 = 0.04 IBr0;

p = 0; If[n == 1, While[ (p = p + 1) <= 21,
  PList[[p, 3]] = {ΔvD, gd, Aconc, τrt, τp, IBr0, ose, Asp, γth, ΔNth, "", PumpPwr,
    Rp[IBr0, Br20, I20], φIBr, Rp2[IBr0, Br20, I20], φBr2, RpTot[IBr0, Br20, I20],
    φTot[IBr0, Br20, I20], BrStarTot[IBr0, Br20, I20],
    (1 - φTot[IBr0, Br20, I20]) RpTot[IBr0, Br20, I20],
    (100 Rp2[IBr0, Br20, I20]) / RpTot[IBr0, Br20, I20]}[[p]]];

If[ ((T_n != temp1) || (Pcell_n != press1) ||
  (Dp_n != path1) || (λcutLo_n != λ11) || (λcutHi_n != λh1)),
  PUMP1 = FunctionInterpolation[Rp[x, y, z] / Sc_n, {x, 0.3 IBr0, 1.1 IBr0},
    {y, 0.035 IBr0, 0.5 IBr0}, {z, 0.035 IBr0, 0.5 IBr0}];
  Pump1a = FunctionInterpolation[Rpa[x, y, z] / Sc_n, {x, 0.3 IBr0, 1.1 IBr0},
    {y, 0.035 IBr0, 0.5 IBr0}, {z, 0.035 IBr0, 0.5 IBr0}];
  Pump1b = FunctionInterpolation[(PUMP1[x, y, z] - Pump1a[x, y, z]),
    {x, 0.3 IBr0, 1.1 IBr0}, {y, 0.035 IBr0, 0.5 IBr0}, {z, 0.035 IBr0, 0.5 IBr0}];

  PUMP2 = FunctionInterpolation[Rp2[x, y, z] / Sc_n, {x, 0.3 IBr0, 1.1 IBr0},
    {y, 0.035 IBr0, 0.5 IBr0}, {z, 0.035 IBr0, 0.5 IBr0}];
  Pump2a = FunctionInterpolation[Rp2a[x, y, z] / Sc_n, {x, 0.3 IBr0, 1.1 IBr0},
    {y, 0.035 IBr0, 0.5 IBr0}, {z, 0.035 IBr0, 0.5 IBr0}];
  Pump2b = FunctionInterpolation[(2 PUMP2[x, y, z] - Pump2a[x, y, z]),
    {x, 0.3 IBr0, 1.1 IBr0}, {y, 0.035 IBr0, 0.5 IBr0}, {z, 0.035 IBr0, 0.5 IBr0}];

  PUMP3 = FunctionInterpolation[Rp3[x, y, z] / Sc_n, {x, 0.3 IBr0, 1.1 IBr0},
    {y, 0.035 IBr0, 0.5 IBr0}, {z, 0.035 IBr0, 0.5 IBr0}];
  Pump3a = FunctionInterpolation[Rp3a[x, y, z] / Sc_n, {x, 0.3 IBr0, 1.1 IBr0},

```

```

{y, 0.035 IBr0, 0.5 IBr0}, {z, 0.035 IBr0, 0.5 IBr0}];
Pump3b = FunctionInterpolation[(2 PUMP3[x, y, z] - Pump3a[x, y, z]),
{x, 0.3 IBr0, 1.1 IBr0}, {y, 0.035 IBr0, 0.5 IBr0}, {z, 0.035 IBr0, 0.5 IBr0}];

temp1 = Tn; press1 = Pcelln; path1 = Dpn; λ11 = λcutLo_n; λh1 = λcutHi_n];

Γ = A21 + (kq1 * IBr[t]) + (kq2 * Iod[t]) + (kq3 * Iod2[t]) +
(kq4 * Br2[t]) + (kq5 * BrStar[t]) + (kq6 * Br[t]);
ΔN = BrStar[t] - (1/2) Br[t];
ψ = IBr[t] + Br2[t] + Iod2[t] + (Iod[t] + BrStar[t] + Br[t]) / 2;

Laser_n := NDSolve[{
  IBr'[t] == - Sc_n * PUMP1[IBr[t], Br2[t], Iod2[t]] - (IBr[t] * β) + ((ψ * β) / 1.08)
    + (ke2 * Br[t] * Iod2[t]) +
    (ke3 * Iod[t] * Br2[t]) - IBr[t] ((ke1 * Br[t]) + (ke4 * Iod[t]))
    + IBr[t]
    ((kr4 * BrStar[t] * Iod[t]) + (kr3 * Br[t] * Iod[t]) + (kr5 * IStar[t] * Br[t])),
  IBr[0] == IBr0,

  Iod'[t] ==
  Sc_n * PUMP1[IBr[t], Br2[t], Iod2[t]] + Sc_n * Pump3b[IBr[t], Br2[t], Iod2[t]]
    + (ke2 * Br[t] * Iod2[t]) +
    IStar[t] (A21IStar + (kq7 * IBr[t]) + (kq8 * Iod2[t]) + (kq9 * Br2[t]))
    + (ke1 * Br[t] * IBr[t]) -
    Iod[t] ((ke3 * Br2[t]) + (ke4 * IBr[t]) + (kr4 * BrStar[t] * IBr[t])
    + (kr3 * Br[t] * IBr[t]) + (kr7 * IStar[t] * IBr[t]) + (2 kr6 * Iod[t] * IBr[t])),
  Iod[0] == 0,

  BrStar'[t] ==
  Sc_n * Pump1a[IBr[t], Br2[t], Iod2[t]] + Sc_n * Pump2a[IBr[t], Br2[t], Iod2[t]]
    - (BrStar[t] * β) - c ose (Lg_n / Lc_n) ΔN Photon[t]
    - BrStar[t] (Γ + (kr2 * Br[t] * IBr[t]) + (kr4 * BrStar[t] * IBr[t])),
  BrStar[0] == 0,

  Br'[t] ==
  Sc_n * Pump1b[IBr[t], Br2[t], Iod2[t]] + Sc_n * Pump2b[IBr[t], Br2[t], Iod2[t]]
    -
    (Br[t] * β) + c ose (Lg_n / Lc_n) ΔN Photon[t] + (Γ * BrStar[t]) + (ke3 * Iod[t] * Br2[t])
    + (ke4 * Iod[t] * IBr[t]) -
    Br[t] ((ke1 * IBr[t]) + (ke2 * Iod2[t]) + (kr2 * BrStar[t] * IBr[t])
    + (2 kr1 * Br[t] * IBr[t]) + (kr3 * Iod[t] * IBr[t]) + (kr5 * IStar[t] * IBr[t])),
  Br[0] == 0,

  Iod2'[t] ==
  - Sc_n * PUMP3[IBr[t], Br2[t], Iod2[t]] - (Iod2[t] * β) + ((0.04 ψ * β) / 1.08)
    + (ke4 * Iod[t] * IBr[t]) + (kr7 * IStar[t] * Iod[t] * IBr[t])
    + (kr6 * Iod[t] ^ 2 * IBr[t]) - (Iod2[t] * ke2 * Br[t]),
  Iod2[0] == 0.04 IBr0,

```

```

Br2'[t] == -Scn * PUMP2[IBr[t], Br2[t], Iod2[t]] - (Br2[t] * beta)
+ ((0.04 * psi * beta) / 1.08) + Br[t] ((ke1 * IBr[t]) + (kr2 * BrStar[t] * IBr[t])
+ (kr1 * Br[t] * IBr[t])) - (ke3 * Iod[t] * Br2[t]),
Br2[0] == 0.04 IBr0,

IStar'[t] == Scn * Pump3a[IBr[t], Br2[t], Iod2[t]] -
(IStar[t] * (beta + A21IStar)) - IStar[t] ((kq7 * IBr[t])
+ (kq8 * Iod2[t]) +
(kq9 * Br2[t]) + (kr7 * Iod[t] * IBr[t]) + (kr5 * Br[t] * IBr[t])),
IStar[0] == 0,

Photon'[t] ==
(Asp BrStar[t] + c ose (Lgn / Lcn) (deltaN - deltaNth) Photon[t]), Photon[0] == 0,

{IBr[t], Iod[t], BrStar[t],
Br[t], Iod2[t], Br2[t], IStar[t], Photon[t]}, {t, 0, tmax},
MaxSteps -> Infinity;

PhotonData_n = Evaluate[Photon[t] /. Laser_n]; PhotonData_n = Extract[PhotonData_n, 1];
IBrData_n = Evaluate[IBr[t] /. Laser_n]; IBrData_n = Extract[IBrData_n, 1];
BrStarData_n = Evaluate[BrStar[t] /. Laser_n]; BrStarData_n = Extract[BrStarData_n, 1];
BrData_n = Evaluate[Br[t] /. Laser_n]; BrData_n = Extract[BrData_n, 1];
IodData_n = Evaluate[Iod[t] /. Laser_n]; IodData_n = Extract[IodData_n, 1];
Br2Data_n = Evaluate[Br2[t] /. Laser_n]; Br2Data_n = Extract[Br2Data_n, 1];
Iod2Data_n = Evaluate[Iod2[t] /. Laser_n]; Iod2Data_n = Extract[Iod2Data_n, 1];
IStarData_n = Evaluate[IStar[t] /. Laser_n]; IStarData_n = Extract[IStarData_n, 1];
gammaData_n = (BrStarData_n - (1/2) BrData_n) ose;
PowerData_n = PhotonData_n * h * vlase * c * Tcell  $\frac{(1 - Rcouple_n)}{2}$ ;
n += 1; If[n <= series, Goto[Recycle]]; n = 0;
Print[
"Total Processing Time: ", N[(SessionTime[] - StartTime) / 60, 3], " minutes"];
Label[EndLong]; Play[ Sin[700 t + 25 t Sin[350 t]], {t, 0, 5} ]

Total Processing Time: 220. minutes

- Sound -

```

■ Kinetic Package #2: Interpolation Map Model (B)

Using Interpolated Representations of Solar Pumping; Integrated Quantum Yields

```

If[ ((UserTag == 1) && (a3 != 2)), Goto[EndLong] ];

If[UserTag == 1, Null, tmax = 1.0 10^-2]; StartTime = SessionTime[];
ClearAll[Γ, IBr, Iod, BrStar, Br, ΔN, γ, Iod2, Br2,
  IStar, Photon, PowerOut, LLaser, Finallist, t];

If[Ntag == 1, n = 1, n = 0];
Label[Recycle];

Laser_n =.;
IBrData_n =.; IodData_n =.; BrStarData_n =.; BrData_n =.; Iod2Data_n =.;
Br2Data_n =.; IStarData_n =.; γData_n =.; PhotonData_n =.; PowerData_n =.;

Lc_n = N[ρ * Lg_n, 4]; β = (100 vFlow_n) / (1 + 0 * Lg_n);
ΔvD = 200 vlase √((2 k T_n Log[2]) / (MassBr c^2)); gd = 2 / ΔvD √(Log[2] / π);
Aconc = 10^(-4) Sc_n Atube_n Lg_n Sc_n;
τrt = (2 Lc_n) / c; τp = τrt / (1 - (Tcell^4 Rmir Rcoup_n));
PumpPwr_n = (SolarIncW * Sc_n * Lg_n * Atube_n / Dp_n); IBr0 = 9.659 * 10^18 (Pcell_n / T_n);
ose = 10^4 (A21 λlase^2) / (8 π) gd; Asp = (c ose) / (Lg_n Atube_n);
γth = 1 / (2 Lg_n) Log[1 / (Tcell^4 Rcoup_n Rmir)]; ΔNth = γth / ose; Br20 = 0.04 IBr0;
I20 = 0.04 IBr0;

p = 0; If[n == 1, While[ (p = p + 1) <= 21,
  PList[[p, 3]] = {ΔvD, gd, Aconc, τrt, τp, IBr0, ose, Asp, γth, ΔNth, "", PumpPwr,
    Rp[IBr0, Br20, I20], φIBr, Rp2[IBr0, Br20, I20], φBr2, RpTot[IBr0, Br20, I20],
    φTot[IBr0, Br20, I20], BrStarTot[IBr0, Br20, I20],
    (1 - φTot[IBr0, Br20, I20]) RpTot[IBr0, Br20, I20],
    (100 Rp2[IBr0, Br20, I20]) / RpTot[IBr0, Br20, I20]}[[p]]];

If[ ((T_n != temp2) || (Pcell_n != press2) ||
  (Dp_n != path2) || (λcutLo_n != λl2) || (λcutHi_n != λh2)),
  Pump1 = FunctionInterpolation[Rp[x, y, z] / Sc_n, {x, 0.6 IBr0, 1.05 IBr0},
    {y, 0.035 IBr0, 0.3 IBr0}, {z, 0.035 IBr0, 0.3 IBr0}];
  Pump2 = FunctionInterpolation[Rp2[x, y, z] / Sc_n, {x, 0.6 IBr0, 1.05 IBr0},
    {y, 0.035 IBr0, 0.3 IBr0}, {z, 0.035 IBr0, 0.3 IBr0}];
  Pump3 = FunctionInterpolation[Rp3[x, y, z] / Sc_n, {x, 0.6 IBr0, 1.05 IBr0},
    {y, 0.035 IBr0, 0.3 IBr0}, {z, 0.035 IBr0, 0.3 IBr0}];
  temp2 = T_n; press2 = Pcell_n; path2 = Dp_n; λl2 = λcutLo_n; λh2 = λcutHi_n];

Γ = A21 + (kq1 * IBr[t]) + (kq2 * Iod[t]) + (kq3 * Iod2[t]) +
  (kq4 * Br2[t]) + (kq5 * BrStar[t]) + (kq6 * Br[t]);
ΔN = BrStar[t] - (1/2) Br[t];
ψ = IBr[t] + Br2[t] + Iod2[t] + (Iod[t] + BrStar[t] + Br[t]) / 2;

Laser_n := NDSolve[{

```

```

IBr'[t] == - Scn * Pump1[IBr[t], Br2[t], Iod2[t]] - (IBr[t] * β) + ((ψ * β) / 1.08)
+ (ke2 * Br[t] * Iod2[t]) +
  (ke3 * Iod[t] * Br2[t]) - IBr[t] ((ke1 * Br[t]) + (ke4 * Iod[t]))
+ IBr[t]
  ((kr4 * BrStar[t] * Iod[t]) + (kr3 * Br[t] * Iod[t]) + (kr5 * IStar[t] * Br[t])),
IBr[0] == IBr0,

Iod'[t] == Scn * Pump1[IBr[t], Br2[t], Iod2[t]] +
  (2 - φIod2) Scn * Pump3[IBr[t], Br2[t], Iod2[t]]
+ (ke2 * Br[t] * Iod2[t]) +
  IStar[t] (A21IStar + (kq7 * IBr[t]) + (kq8 * Iod2[t]) + (kq9 * Br2[t]))
+ (ke1 * Br[t] * IBr[t]) -
  Iod[t] ((ke3 * Br2[t]) + (ke4 * IBr[t]) + (kr4 * BrStar[t] * IBr[t])
  + (kr3 * Br[t] * IBr[t]) + (kr7 * IStar[t] * IBr[t]) + (2 kr6 * Iod[t] * IBr[t])),
Iod[0] == 0,

BrStar'[t] == φIBr * Scn * Pump1[IBr[t], Br2[t], Iod2[t]] +
  φBr2 * Scn * Pump2[IBr[t], Br2[t], Iod2[t]]
- (BrStar[t] * β) - c ose (Lgn / Lcn) ΔNPhoton[t]
- BrStar[t] (Γ + (kr2 * Br[t] * IBr[t]) + (kr4 * BrStar[t] * IBr[t])),
BrStar[0] == 0,

Br'[t] == (1 - φIBr) * Scn * Pump1[IBr[t], Br2[t], Iod2[t]] +
  (2 - φBr2) * Scn * Pump2[IBr[t], Br2[t], Iod2[t]]
-
  (Br[t] * β) + c ose (Lgn / Lcn) ΔNPhoton[t] + (Γ * BrStar[t]) + (ke3 * Iod[t] * Br2[t])
+ (ke4 * Iod[t] * IBr[t]) -
  Br[t] ((ke1 * IBr[t]) + (ke2 * Iod2[t]) + (kr2 * BrStar[t] * IBr[t])
  + (2 kr1 * Br[t] * IBr[t]) + (kr3 * Iod[t] * IBr[t]) + (kr5 * IStar[t] * IBr[t])),
Br[0] == 0,

Iod2'[t] ==
- Scn * Pump3[IBr[t], Br2[t], Iod2[t]] - (Iod2[t] * β) + ((0.04 ψ * β) / 1.08)
+ (ke4 * Iod[t] * IBr[t]) + (kr7 * IStar[t] * Iod[t] * IBr[t])
+ (kr6 * Iod[t] ^ 2 * IBr[t]) - (Iod2[t] * ke2 * Br[t]),
Iod2[0] == 0.04 IBr0,

Br2'[t] == - Scn * Pump2[IBr[t], Br2[t], Iod2[t]] - (Br2[t] * β)
+ ((0.04 ψ * β) / 1.08) + Br[t] ((ke1 * IBr[t]) + (kr2 * BrStar[t] * IBr[t])
+ (kr1 * Br[t] * IBr[t])) - (ke3 * Iod[t] * Br2[t]),
Br2[0] == 0.04 IBr0,

IStar'[t] == φIod2 * Scn * Pump3[IBr[t], Br2[t], Iod2[t]] -
  (IStar[t] * (β + A21IStar)) - IStar[t] ((kq7 * IBr[t])
  + (kq8 * Iod2[t]) +
  (kq9 * Br2[t]) + (kr7 * Iod[t] * IBr[t]) + (kr5 * Br[t] * IBr[t])),
IStar[0] == 0,

Photon'[t] ==

```

```

(Asp BrStar[t] + c ose (Lgn / Lcn) (ΔN - ΔNth) Photon[t]), Photon[0] == 0},

{IBr[t], Iod[t], BrStar[t],
 Br[t], Iod2[t], Br2[t], IStar[t], Photon[t]}, {t, 0, tmax},
MaxSteps -> Infinity};

PhotonDatan = Evaluate[Photon[t] /. Lasern]; PhotonDatan = Extract[PhotonDatan, 1];
IBrDatan = Evaluate[IBr[t] /. Lasern]; IBrDatan = Extract[IBrDatan, 1];
BrStarDatan = Evaluate[BrStar[t] /. Lasern]; BrStarDatan = Extract[BrStarDatan, 1];
BrDatan = Evaluate[Br[t] /. Lasern]; BrDatan = Extract[BrDatan, 1];
IodDatan = Evaluate[Iod[t] /. Lasern]; IodDatan = Extract[IodDatan, 1];
Br2Datan = Evaluate[Br2[t] /. Lasern]; Br2Datan = Extract[Br2Datan, 1];
Iod2Datan = Evaluate[Iod2[t] /. Lasern]; Iod2Datan = Extract[Iod2Datan, 1];
IStarDatan = Evaluate[IStar[t] /. Lasern]; IStarDatan = Extract[IStarDatan, 1];
γDatan = (BrStarDatan - (1/2) BrDatan) ose;
PowerDatan = PhotonDatan * h * vlase * c * Tcell (1 - Rcoupn) / 2;

n += 1; If[n <= series, Goto[Recycle]]; n = 0;
Print[
 "Total Processing Time: ", N[(SessionTime[] - StartTime) / 60, 3], " minutes";
 Label[EndLong]; Play[Sin[700 t + 25 t Sin[350 t]], {t, 0, 5}]

Total Processing Time: 115. minutes

- Sound -

```

Hyperlink To:

Generate Plots

■ Kinetic Package #3 (Rapid Processing Model C)

Using Integrated Absorption Cross Sections; Scaling Factor for Solar Attenuation

```

If[ (UserTag == 1) && (a3 != 3) , Goto[EndShort]];
If[UserTag == 1, Null, tmax = 1.0 10^-2]; StartTime = SessionTime[];
ClearAll[Γ, IBr, Iod, BrStar, Br, ΔN, γ, Iod2, Br2,
  IStar, Photon, PowerOut, LLaser, FinalList, t];

If[Ntag == 1, n = 1, n = 0];
Label[Recycle];

Laser_n =.;
IBrData_n =.; IodData_n =.; BrStarData_n =.; BrData_n =.; Iod2Data_n =.;
Br2Data_n =.; IStarData_n =.; γData_n =.; PhotonData_n =.; PowerData_n =.;

Lc_n = N[ρ * Lg_n, 4]; β = (100 vFlow_n) / Lg_n;
ΔvD = 200 vLase √((2 k T_n Log[2]) / (MassBr c^2)); gd = 2 / ΔvD √(Log[2] / π);
Aconc = 10^(-4) Sc_n Atube_n Lg_n Sc_n;
τrt = (2 Lc_n) / c; τp = τrt / (1 - (Tcell^4 Rmir Rcoup_n));
PumpPwr_n = (SolarIncW * Sc_n * Lg_n * Atube_n / Dp_n); IBr0 = 9.659 * 10^18 (Pcell_n / T_n);
ose = 10^4 (A21 λlase^2) / (8 π) gd; Asp = (c ose) / (Lg_n Atube_n);
γth = 1 / (2 Lg_n) Log[1 / (Tcell^4 Rcoup_n Rmir)]; ΔNth = γth / ose; Br20 = 0.04 IBr0;
I20 = 0.04 IBr0;

p = 0; If[n == 1, While[(p = p + 1) <= 21,
  PList[[p, 3]] = {ΔvD, gd, Aconc, τrt, τp, IBr0, ose, Asp, γth, ΔNth, "", PumpPwr,
  Rp[IBr0, Br20, I20],
    φIBr[IBr0, Br20, I20], Rp2[IBr0, Br20, I20], φBr2e[IBr0, Br20, I20],
  RpTot[IBr0, Br20, I20], φTot[IBr0, Br20, I20], BrStarTot[IBr0, Br20, I20],
  (1 - φTot[IBr0, Br20, I20]) RpTot[IBr0, Br20, I20],
  (100 Rp2[IBr0, Br20, I20]) / RpTot[IBr0, Br20, I20],
  (100 Rp3[IBr0, Br20, I20]) / RpTot[IBr0, Br20, I20]}[[p]]];

Photo = PolynomialFit[Table[{Ω,
  NIntegrate[λ (1 - Exp[-σabs[λ, T_n] Ω]), {λ, λcutLo_n, λcutHi_n}] /
  NIntegrate[λ, {λ, λcutLo_n, λcutHi_n}], {Ω, 10^17, 10^19, 10^16}], 10];

Pump[IBr_] := If[(Dp_n * IBr >= 10^19), 1,
  Photo[Dp_n * IBr]] * (Sc_n / Dp_n) NIntegrate[F[λ], {λ, λcutLo_n, λcutHi_n}];

ibrInt = NIntegrate[F[λ] * σabs[λ, T_n], {λ, λcutLo_n, λcutHi_n}];
br2Int = NIntegrate[F[λ] * σabs2[λ, T_n], {λ, λcutLo_n, λcutHi_n}];
i2Int = NIntegrate[F[λ] * σabs3[λ, T_n], {λ, λcutLo_n, λcutHi_n}];

Denom := IBr[t] * ibrInt + Br2[t] * br2Int + Iod2[t] * i2Int;

Γ := A21 + (kq1 * IBr[t]) + (kq2 * Iod[t]) + (kq3 * Iod2[t]) +
  (kq4 * Br2[t]) + (kq5 * BrStar[t]) + (kq6 * Br[t]);

```

```

ΔN := BrStar[t] - (1/2) Br[t];
ψ := IBr[t] + Br2[t] + Iod2[t] + (Iod[t] + BrStar[t] + Br[t]) / 2;

Laser_n := NDSolve[{
  IBr'[t] == - (IBr[t] * ibrInt / Denom) * Pump[IBr[t]] - (IBr[t] * β) + ((ψ * β) / 1.08)
    + (ke2 * Br[t] * Iod2[t]) +
    (ke3 * Iod[t] * Br2[t]) - IBr[t] ((ke1 * Br[t]) + (ke4 * Iod[t]))
    + IBr[t]
    ((kr4 * BrStar[t] * Iod[t]) + (kr3 * Br[t] * Iod[t]) + (kr5 * IStar[t] * Br[t])),
  IBr[0] == IBr0,

  Iod'[t] ==
    (IBr[t] * ibrInt + (2 - φIod2) Iod2[t] i2Int) / Denom * Pump[IBr[t]] - (Iod[t] * β)
    + (ke2 * Br[t] * Iod2[t]) +
    IStar[t] (A21IStar + (kq7 * IBr[t]) + (kq8 * Iod2[t]) + (kq9 * Br2[t]))
    + (ke1 * Br[t] * IBr[t]) -
    Iod[t] ((ke3 * Br2[t]) + (ke4 * IBr[t]) + (kr4 * BrStar[t] * IBr[t])
    + (kr3 * Br[t] * IBr[t]) + (kr7 * IStar[t] * IBr[t]) + (2 kr6 * Iod[t] * IBr[t])),
  Iod[0] == 0,

  BrStar'[t] ==
    ((φIBr * ibrInt * IBr[t] + φBr2 * br2Int * Br2[t]) / Denom * Pump[IBr[t]]) -
    (BrStar[t] * β)
    - c ose (Lg_n / Lc_n) ΔN Photon[t] -
    BrStar[t] (Γ + (kr2 * Br[t] * IBr[t]) + (kr4 * BrStar[t] * IBr[t])),
  BrStar[0] == 0,

  Br'[t] ==
    (((1 - φIBr) * IBr[t] ibrInt + (2 - φBr2) * Br2[t] br2Int) / Denom * Pump[IBr[t]]) -
    (Br[t] * β) + c ose (Lg_n / Lc_n) ΔN Photon[t] + (Γ * BrStar[t]) +
    (ke3 * Iod[t] * Br2[t]) + (ke4 * Iod[t] * IBr[t])
    - Br[t] ((ke1 * IBr[t]) + (ke2 * Iod2[t]) + (kr2 * BrStar[t] * IBr[t])
    + (2 kr1 * Br[t] * IBr[t]) + (kr3 * Iod[t] * IBr[t]) + (kr5 * IStar[t] * IBr[t])),
  Br[0] == 0,

  Iod2'[t] ==
    - ((i2Int * Iod2[t]) / Denom * Pump[IBr[t]]) - (Iod2[t] * β) + ((0.04 ψ * β) / 1.08)
    + (ke4 * Iod[t] * IBr[t]) + (kr7 * IStar[t] * Iod[t] * IBr[t])
    + (kr6 * Iod[t]^2 * IBr[t]) - (Iod2[t] * ke2 * Br[t]),
  Iod2[0] == 0.04 IBr0,

  Br2'[t] ==
    - ((br2Int * Br2[t]) / Denom * Pump[IBr[t]]) - (Br2[t] * β) + ((0.04 ψ * β) / 1.08)
    + Br[t] ((ke1 * IBr[t]) + (kr2 * BrStar[t] * IBr[t]) + (kr1 * Br[t] * IBr[t])) -
    (ke3 * Iod[t] * Br2[t]),
  Br2[0] == 0.04 IBr0,

  IStar'[t] ==
    ((i2Int * Iod2[t]) / Denom * φIod2 * Pump[IBr[t]]) - (IStar[t] * (β + A21IStar))

```

```

- IStar[t] ((kq7 * IBr[t]) + (kq8 * Iod2[t]) + (kq9 * Br2[t])
+ (kr7 * Iod[t] * IBr[t]) + (kr5 * Br[t] * IBr[t])),
IStar[0] == 0,

Photon'[t] ==
(Asp BrStar[t] + c ose (Lgn / Lcn) (ΔN - ΔNth) Photon[t]), Photon[0] == 0),

{IBr[t], Iod[t], BrStar[t],
Br[t], Iod2[t], Br2[t], IStar[t], Photon[t]}, {t, 0, tmax},
WorkingPrecision -> 8, MaxSteps -> Infinity};

PhotonDatan = Evaluate[Photon[t] /. Lasern]; PhotonDatan = Extract[PhotonDatan, 1];
IBrDatan = Evaluate[IBr[t] /. Lasern]; IBrDatan = Extract[IBrDatan, 1];
BrStarDatan = Evaluate[BrStar[t] /. Lasern]; BrStarDatan = Extract[BrStarDatan, 1];
BrDatan = Evaluate[Br[t] /. Lasern]; BrDatan = Extract[BrDatan, 1];
IodDatan = Evaluate[Iod[t] /. Lasern]; IodDatan = Extract[IodDatan, 1];
Br2Datan = Evaluate[Br2[t] /. Lasern]; Br2Datan = Extract[Br2Datan, 1];
Iod2Datan = Evaluate[Iod2[t] /. Lasern]; Iod2Datan = Extract[Iod2Datan, 1];
IStarDatan = Evaluate[IStar[t] /. Lasern]; IStarDatan = Extract[IStarDatan, 1];
γDatan = (BrStarDatan - (1 / 2) BrDatan) ose;
PowerDatan = PhotonDatan * h * vlase * c * Tcell (1 - Rcoupn) / 2;

n += 1; If[n <= series, Goto[Recycle]]; n = 0;
Label[EndShort];
Print["Total Processing Time: ", N[(SessionTime[] - StartTime) / 60, 3],
" minutes"]; Play[Sin[700 t + 25 t Sin[350 t]], {t, 0, 5}]

```

Total Processing Time : 26.1 minutes

Hyperlink To:

[Single Data Entry](#)

[Multiple Data Entry](#)

[Animate Plots](#)

■ Generate Graphical Plots of Laser System Parameters

```

t = .; tplot = tmax / 5; FinalList = {};
If[Ntag == 1, Goto[Family]];
  IBrList = {IBrData0};
BrStarList = {BrStarData0}; BrList = {BrData0}; IodList = {IodData0};
  Iod2List = {Iod2Data0}; Br2List = {Br2Data0}; IStarList = {IStarData0};
  PhotonList = {PhotonData0}; γList = {γData0}; PowerList = {PowerData0};
Goto[ConstructStream];

Label[Family];
  IBrList = BrStarList = BrList = IodList = Iod2List =
  Br2List = IStarList = PhotonList = γList = PowerList = {};

  z = 0; While[(z = z + 1) <= series,
{AppendTo[IBrList, IBrDataz], AppendTo[BrStarList, BrStarDataz], AppendTo
[BrList, BrDataz], AppendTo[IodList, IodDataz], AppendTo[Iod2List, Iod2Dataz],
AppendTo[Br2List, Br2Dataz], AppendTo[IStarList, IStarDataz],
AppendTo[PhotonList, PhotonDataz], AppendTo[γList, γDataz],
AppendTo[PowerList, PowerDataz]}]; z += 1;
  IBrList = Flatten[IBrList];
BrStarList = Flatten[BrStarList]; BrList = Flatten[BrList];
  IodList = Flatten[IodList];
Iod2List = Flatten[Iod2List]; Br2List = Flatten[Br2List];
  IStarList = Flatten[IStarList];
PhotonList = Flatten[PhotonList]; γList = Flatten[γList];
  PowerList = Flatten[PowerList];

Label[ConstructStream];
LLaser = {IBrList, "Population Evolution of [IBr]", "[IBr] \!\!(cm-3)",
PhotonList, "Photon Buildup with Time", "Photons/\!\!(cm3)", BrStarList,
"Population Evolution of [Br(P1/2)]",
"\!\![\!\!(Br*\)] \!\!(cm-3)", BrList,
"Population Evolution of [Br(P3/2)]", "[Br] \!\!(cm-3)", IStarList,
"Population Evolution of [I(P1/2)]", "\!\!(I*\) \!\!(cm-3)", IodList,
"Population Evolution of [I(P3/2)]", "[I] \!\!(cm-3)", Br2List,
"Population Evolution of [Br2]", "[Br2] \!\!(cm-3)", Iod2List,
"Population Evolution of [I2]", "[I2] \!\!(cm-3)", γList,
"Evolution of γ with Time",
"γ \!\!(cm-1)", PowerList, "Laser Output Power",
"Power (W/\!\!(cm2)");

If[Ntag == 1, Goto[FamilyPlot]];
x = -1; While[(x = x + 1) <= 9,
  AppendTo[FinalList, {Plot[LLaser[[{3 x} + 1]], {t, 0, tplot}, PlotLabel ->
  StyleForm[LLaser[[{3 x} + 2]], FontWeight -> "Bold", FontSize -> 10],
  PlotRange -> All, Frame -> True, FrameLabel -> {" t (s)", LLaser[[{3 x} + 3]]},
  DisplayFunction -> Identity, ImageSize -> 400}]]];

```

```

Goto[EndRoutine];

Label[FamilyPlot];
x = -1; While[ (x = x + 1) <= 9,
AppendTo[FinalList, {Plot[Evaluate[LLaser[[(3 x) + 1]]], {t, 0, tplot},
PlotLabel ->
StyleForm[LLaser[[(3 x) + 2]], FontWeight -> "Bold", FontSize -> 10],
PlotStyle -> {{GrayLevel[0]}, {Hue[0.07], Dashing[ {.01} ]},
{Hue[0.6], Dashing[ {.03, .01} ]},
{Hue[0.32], Dashing[ {.02} ]}, {GrayLevel[0.7]}},
{Hue[0.55], Dashing[ {.04, .01} ]}, {Hue[0.78], Dashing[ {0.02, 0.01} ]},
{Hue[0.12], Dashing[ {.01, .02} ]}},
PlotLegend -> {N[Set1], N[Set2], N[Set3], N[Set4], N[Set5], N[Set6]},
LegendSize -> { .4, .4},
LegendBackground -> GrayLevel[0.95], LegendPosition -> {1, 0},
LegendShadow -> {0.015, -0.015},
LegendLabel -> StyleForm[Parameter, FontSlant ->
"Italic"],
PlotRange -> All, Frame -> True, FrameLabel -> {" t (s)", LLaser[[(3 x) + 3]]},
DisplayFunction -> Identity}}];

Label[EndRoutine];
q = 0; While[ (q = q + 1) <= 10, Show[FinalList[[q]],
DisplayFunction -> $DisplayFunction, ImageSize -> {578, 334}]];

If[series == 0, d = 0, d = 1];
Print["\n\nOperating Temperature: ", Td, " K\nCell Pressure: ", Pcelld,
" Torr\nPumping Path Length: ", Dpd, " cm\nLength/Gain Cell: ", Lgd,
" cm\nCavity Length: ", Lcd, " cm\nSolar Concentration: ", Scd,
"\nOutput Coupler Reflectivity: ", Rcoupld, "\nR1T1T2: ", N[Rmir*Tcell2],
"\nArea/ Laser Tube: ", Atubed,
" \\(cm2)\nWavelength range: ", N[109λcutLod], " - ", N[109λcutHid],
" nm\nFlow Rate: ", vflowd, " m/s\n"];

TableForm[Delete[PList, {{12}, {13}, {14}, {15}, {16}}], TableSpacing -> {1, 2}]

Print[StyleForm["\n          Total Output Energy (Plotted Duration):",
FontSlant -> "Italic", FontSize -> 10]];
If[series == 0, {Print["          ", NIntegrate[PowerData0,
{t, 0, tplot}, AccuracyGoal -> 3], " Joules/\\(cm2)"],
{w = 0; While[ (w = w + 1) <= series,
EnergyOutw = NIntegrate[PowerDataw, {tt, 10-8, tplot}, MaxRecursion -> 20]];
w = 0; t = tplot;
Print[TableForm[Table[{SequenceForm[Parameter, ": ", N[Setw, 4]],
SequenceForm[N[EnergyOutw, 4], " J/\\(cm2)"],
SequenceForm[N[PowerDataw, 4],
" W/\\(cm2)"], SequenceForm[pwrw = N[Atubew PowerDataw / 2, 4], " W"],
SequenceForm["ηT=", ηw = N[100 * pwrw / PumpPwrw, 4], "%"}], {w, 1, series}],
TableSpacing -> {1, 1}]]];

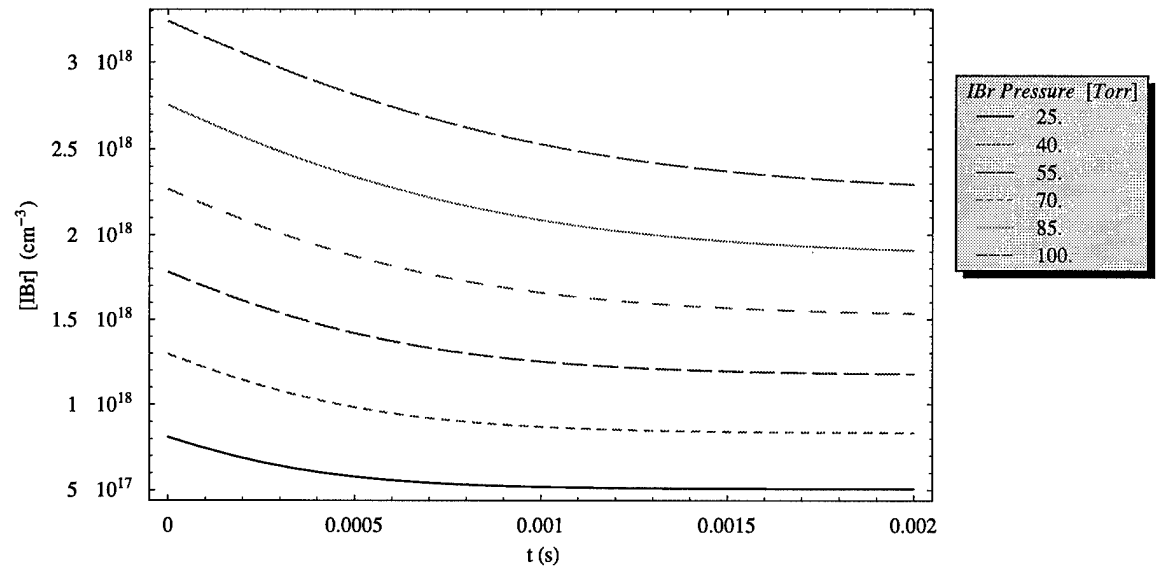
```

```

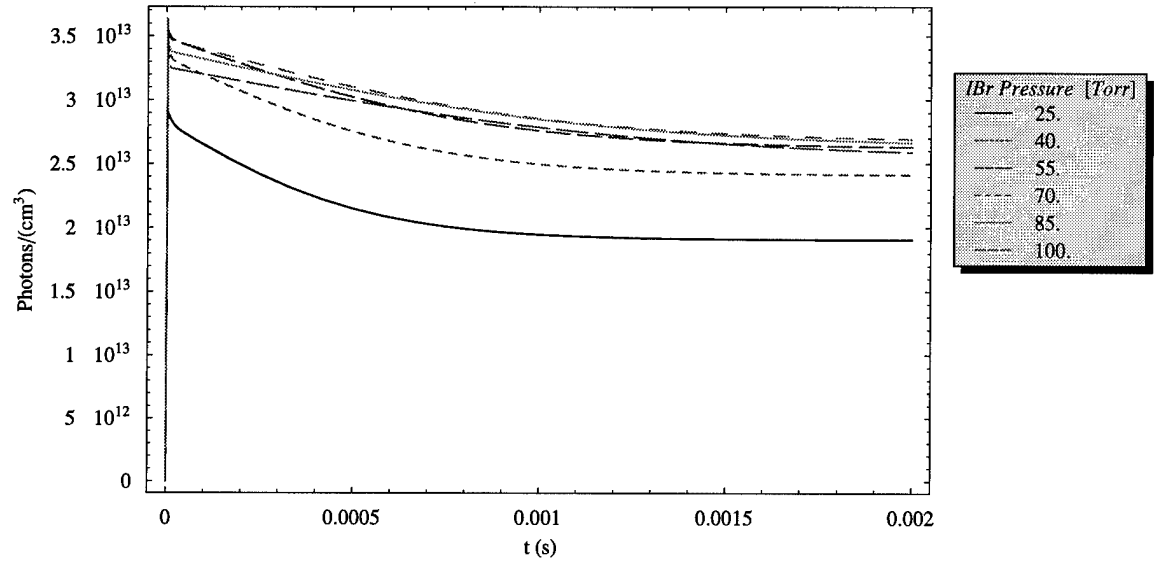
Print["\nPopulation Distribution at t = ", N[tplot], " s:"]; t = tplot;
If[series > 0, {Print["(For ", Parameter, " = ", N[Set1, 4], ")"], q = 1}, q = 0];
DistList = {{ "[IBr] : ", IBrData_q, " \\(cm^-3\\)",
  {"[Photons] : ", PhotonData_q, " \\(cm^-3\\)",
  {"[Br(P1/2)] : ", BrStarData_q, " \\(cm^-3\\)",
  {"[Br(P3/2)] : ", BrData_q, " \\(cm^-3\\)",
  {"[I(P1/2)] : ", IStarData_q, " \\(cm^-3\\)",
  {"[I(P3/2)] : ", IodData_q, " \\(cm^-3\\)",
  {"[Br2] : ", Br2Data_q, " \\(cm^-3\\)",
  {"[I2] : ", Iod2Data_q, " \\(cm^-3\\)",
  {"Powerout : ", PowerData_q, " \\(W/cm^2\\)",
  {"", pwr_q = N[Atube_q * PowerData_q / 2], " W"},
  {"ηT (CW)", η_q = N[100 * pwr_q / PumpPwr_q], "%"},
  {"\\([IBr] \\ / [IBr]0) : ", IBrData_q / ((9.659 * 10^18) / T_q Pcell_q)}}};
Print[TableForm[DistList, TableSpacing -> {1, 1}]]; t = .;

```

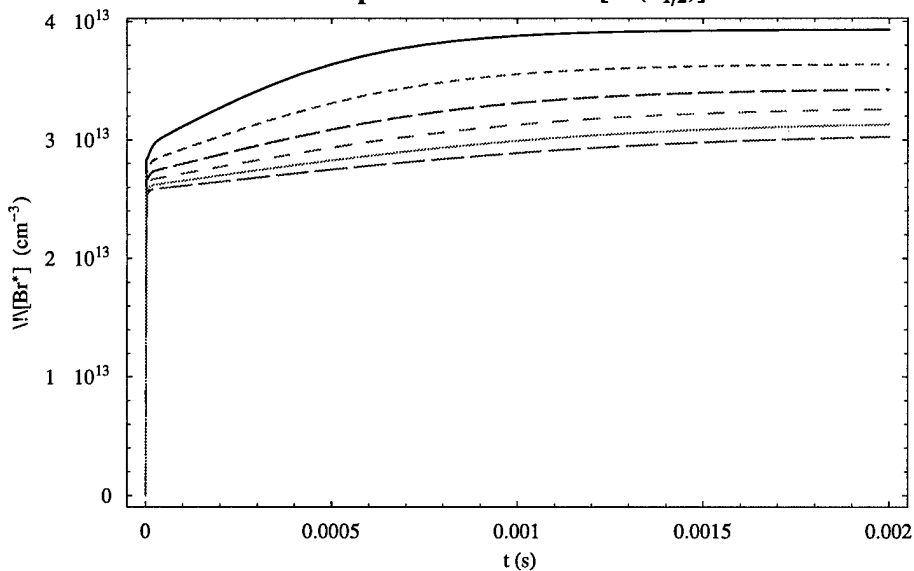
Population Evolution of [IBr]



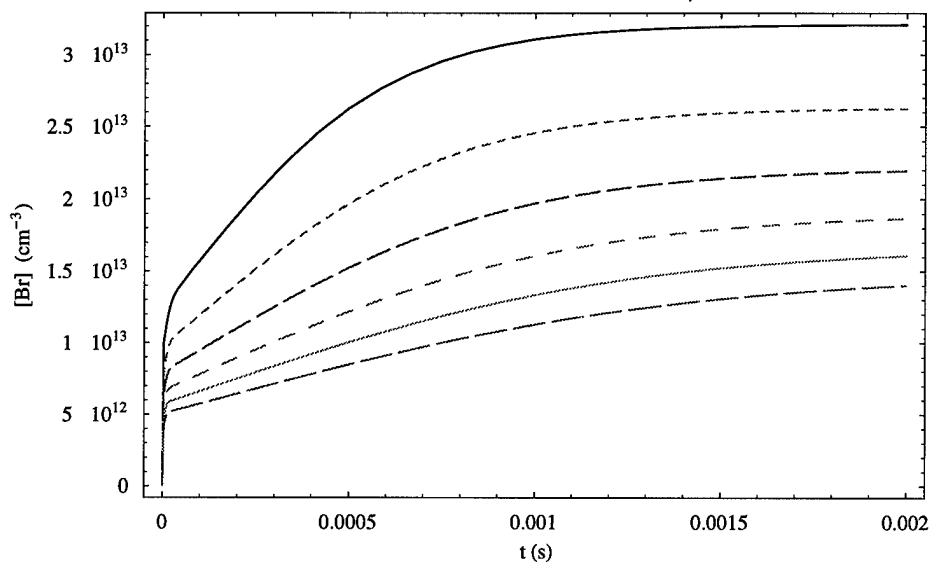
Photon Buildup with Time



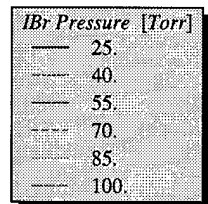
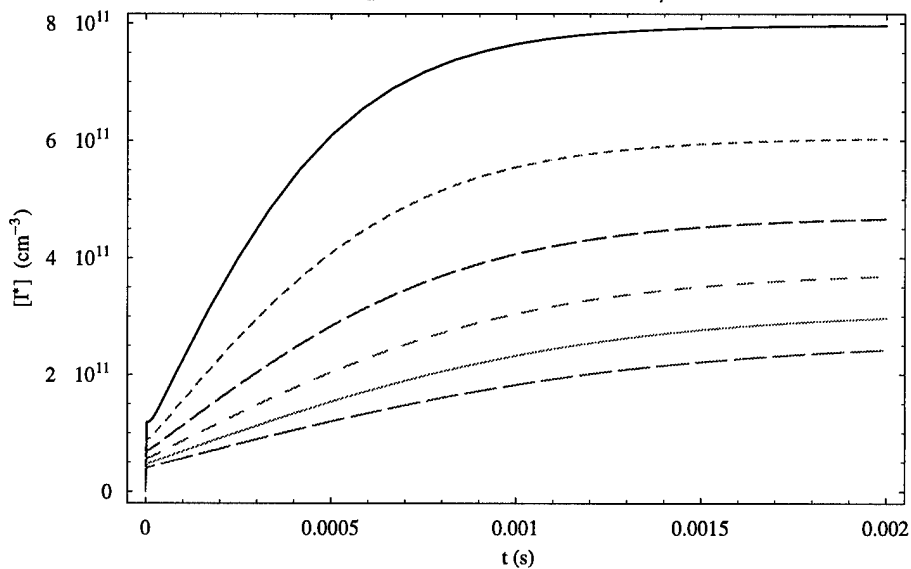
Population Evolution of [Br(P_{1/2})]



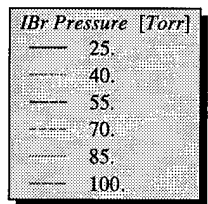
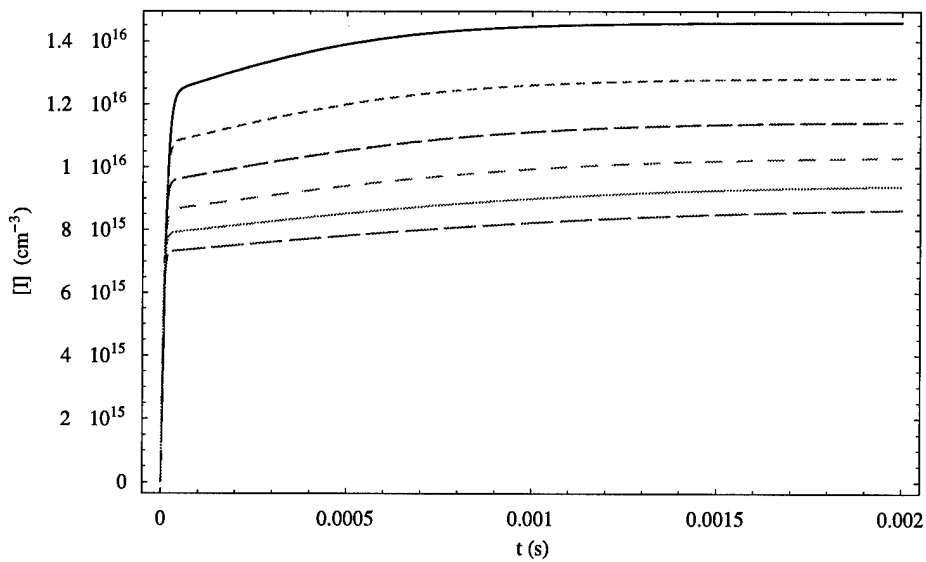
Population Evolution of [Br(P_{3/2})]



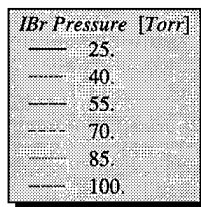
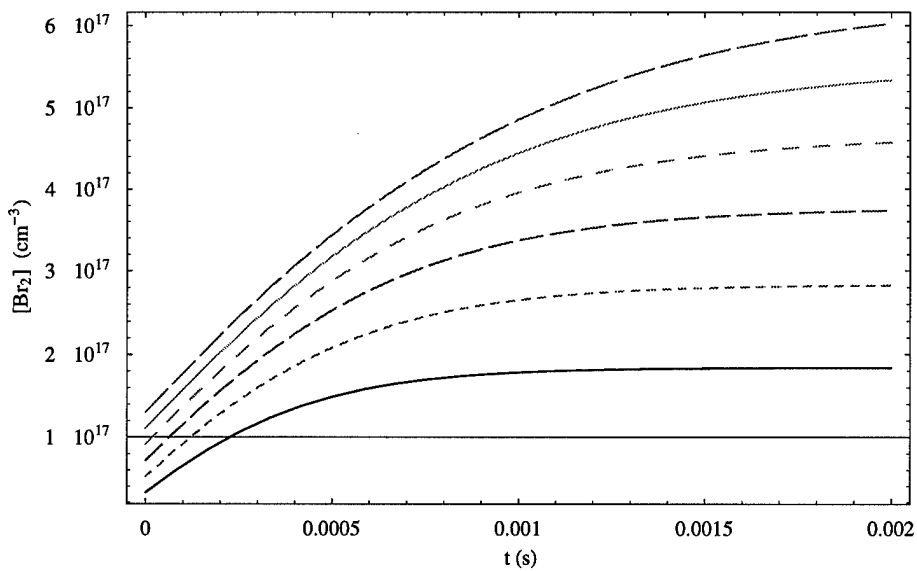
Population Evolution of $[I(P_{1/2})]$



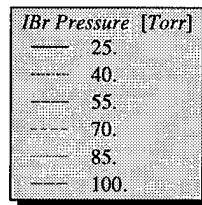
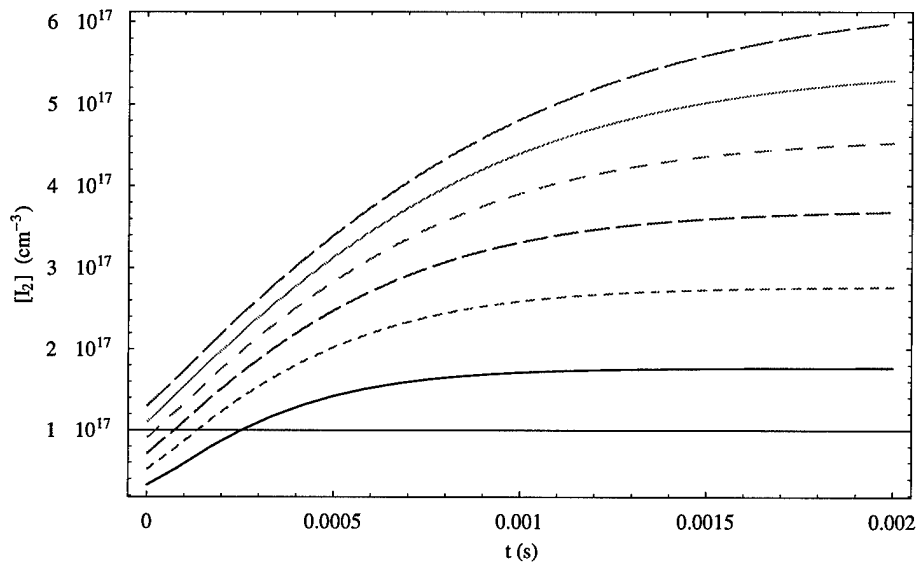
Population Evolution of $[I(P_{3/2})]$



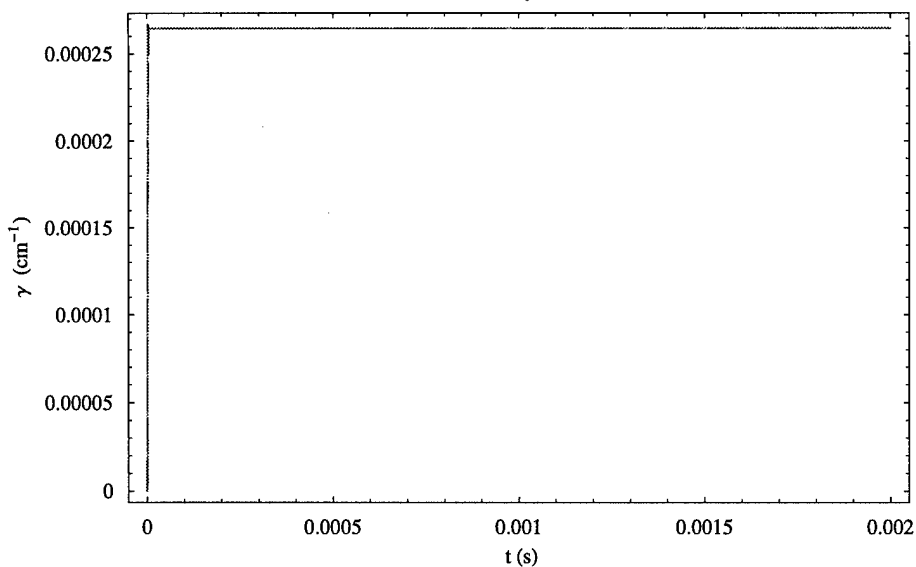
Population Evolution of [Br₂]



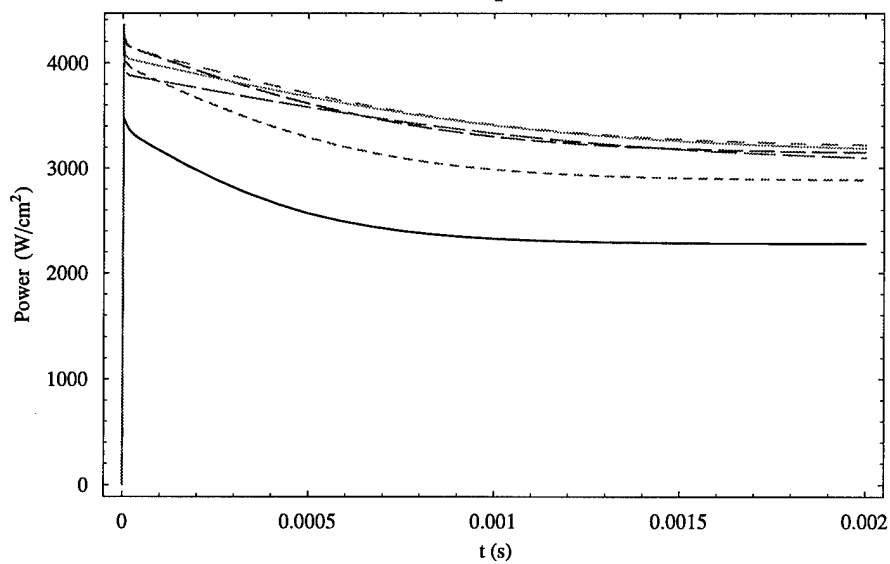
Population Evolution of [I₂]



Evolution of γ with Time



Laser Output Power



Operating Temperature: 298.2 K
 Cell Pressure: 25 Torr
 Pumping Path Length: 1.5 cm
 Length/Gain Cell: 300 cm
 Cavity Length: 330. cm
 Solar Concentration: 20000
 Output Coupler Reflectivity: 0.89
 $R_1 T_1 T_2$: 0.97814
 Area/ Laser Tube: 0.785 cm²
 Wavelength range: 457.7 - 545.3 nm
 Flow Rate: 0 m/s

Doppler-Broadened Linewidth	Δv_D :	1.52374×10^8	Hz
Peak Transition Lineshape	$g(v_0)$:	6.16536×10^{-9}	s
Exposed Area of Solar Concentrator	A_c :	9.42×10^6	m ²
Photon Round Trip	τ_{rt} :	2.2×10^{-8}	s
Photon Lifetime	τ_p :	1.49885×10^{-7}	s
Initial Concentration/ IBr	$[IBr]_0$:	8.09775×10^{17}	cm ⁻³
Stim Emission Cross-Section	σ_{st} :	1.13836×10^{-17}	cm ²
Spontaneous Emission Rate	A_{sp} :	1.45014×10^{-9}	s ⁻¹
Threshold Gain Coefficient	γ_{th} :	0.000264562	cm ⁻¹
Threshold Population Inversion	ΔN_{th} :	2.32407×10^{13}	cm ⁻³
Initial Photodissociation Rate (Total)	R_{p_T} :	3.71437×10^{20}	cm ⁻³ s ⁻¹
Br* Quantum Yield (Combined)	ϕ_T :	0.643373	
Initial Br(P _{1/2}) Pump Rate (Total)	$R_{p_{Br^*}}$:	2.3435×10^{20}	cm ⁻³ s ⁻¹
Initial Br(P _{3/2}) Pump Rate (Total)	$R_{p_{Br}}$:	1.32465×10^{20}	cm ⁻³ s ⁻¹
Initial Br ₂ Photolysis Contribution	$R_{p_{Br_2/T}}$:	1.08494	%
Initial I ₂ Photolysis Contribution	$R_{p_{I_2/T}}$:	1.92728	%

Total Output Energy (Plotted Duration):

I _{Br} Pressure [Torr]: 25.	4.558 J/cm ²	2279. W/cm ²	894.4 W	$\eta_T=0.209$ %
I _{Br} Pressure [Torr]: 40.	5.77 J/cm ²	2885. W/cm ²	1132. W	$\eta_T=0.2646$ %
I _{Br} Pressure [Torr]: 55.	6.296 J/cm ²	3148. W/cm ²	1236. W	$\eta_T=0.2888$ %
I _{Br} Pressure [Torr]: 70.	6.442 J/cm ²	3221. W/cm ²	1264. W	$\eta_T=0.2954$ %
I _{Br} Pressure [Torr]: 85.	6.377 J/cm ²	3189. W/cm ²	1251. W	$\eta_T=0.2925$ %
I _{Br} Pressure [Torr]: 100.	6.194 J/cm ²	3097. W/cm ²	1216. W	$\eta_T=0.2841$ %

Population Distribution at t = 0.002 s:

(For I_{Br} Pressure [Torr] = 25.)

[I _{Br}] :	5.06585×10^{17}	cm ⁻³
[Photons] :	1.90469×10^{13}	cm ⁻³
[Br(P _{1/2})] :	3.92852×10^{13}	cm ⁻³
[Br(P _{3/2})] :	3.20891×10^{13}	cm ⁻³
[I(P _{1/2})] :	7.95823×10^{11}	cm ⁻³
[I(P _{3/2})] :	1.4583×10^{16}	cm ⁻³
[Br ₂] :	1.83953×10^{17}	cm ⁻³
[I ₂] :	1.76694×10^{17}	cm ⁻³
Power _{out} :	2278.8	W / cm ²
	894.429	W
η_T (CW)	0.209034	%
$\frac{[I_{Br}]}{[I_{Br}]_0}$:	0.625588	

Hyperlink To:

Single Data Entry

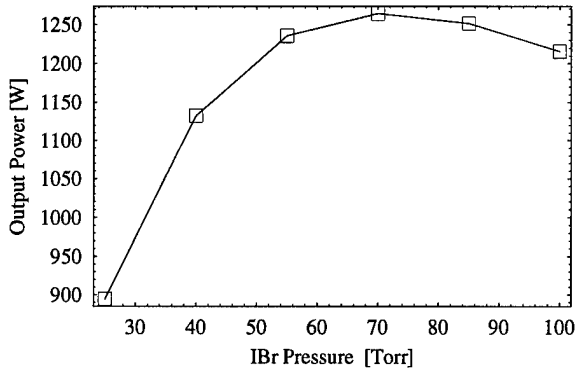
Multiple Data Entry

CW Model

```

If[series != 0, MultipleListPlot[Table[{Sets, pwrs}, {s, 1, series}],
  SymbolShape -> {PlotSymbol[Box, {Filled -> False}]}, PlotJoined -> True,
  Frame -> True, FrameLabel -> {Parameter, "Output Power [W]"}];

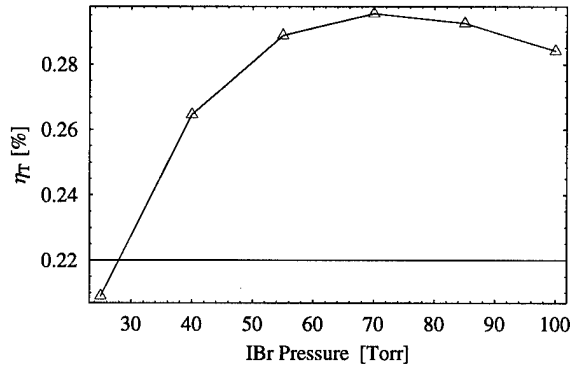
```



```

If[series != 0, MultipleListPlot[Table[{Sets, ηs}, {s, 1, series}],
  SymbolShape -> {PlotSymbol[Triangle, {Filled -> False}]}, PlotJoined -> True,
  Frame -> True, FrameLabel -> {Parameter, "ηT [%]"}];

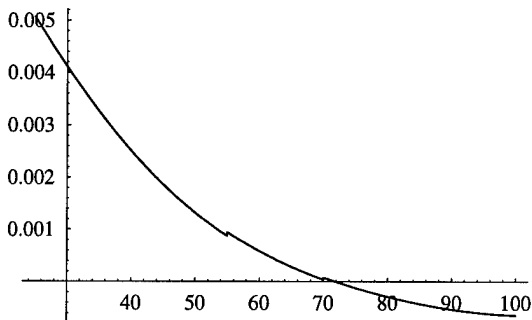
```



```

qq = Interpolation[Table[{Sets, ηs}, {s, 1, series}]]; Plot[qq'[Optimal],
  {Optimal, Set1, Setseries]]; FindRoot[0 == qq'[Optimal], {Optimal, Set3}]
Print["Max Efficiency: ", qq%[[1, 2]]]

```



```
{Optimal -> 71.8411}
```

```
Max Efficiency: 0.29552
```

■ Efficiency Analysis

```
t = tplot;
If[Ntag == 1, {a = 4, q = 4, IBr0q = ((9.659 * 1018) / Tq Pcellq)}, {a = 0, q = 0}];
```

Total Efficiency {photonic, energetic}:

```
ηt = {((Atubea PowerDataa / 2) / (SolarIncP * Sca * h * vlase * Atubea * Lga / Dpa)),
      (Atubea PowerDataa) / (2 * PumpPwra)}
{0.00869123, 0.0029545}
```

Spectral Efficiency {photonic, energetic}:

```
ηs = {NIntegrate[F[λ], {λ, λcutLoa, λcutHia}] / NIntegrate[F[λ],
      {λ, 10-7, 10-2}], NIntegrate[(10-2 h c) / λ F[λ], {λ, λcutLoa,
      λcutHia}] / NIntegrate[(h c) 10-2 / λ F[λ], {λ, 10-7, 10-2}]}}
{0.0620002, 0.114055}
```

Absorptive Efficiency {photonic, energetic}:

```
ηa = { (Rp[IBrDataa, Br2Dataa, Iod2Dataa] + Rp2[IBrDataa, Br2Dataa, Iod2Dataa]) /
      ((Sca / Dpa) NIntegrate[F[λ], {λ, λcutLoa, λcutHia}]},
      ( (Sca / Dpa) NIntegrate[ ( (h c / 100 λ) F[λ]
      (IBrDataa * σabs[λ, Ta] + Br2Dataa * σabs2[λ, Ta]) / (IBrDataa * σabs[λ, Ta]
      + Br2Dataa * σabs2[λ, Ta] + Iod2Dataa * σabs3[λ, Ta]) *
      (1 - Exp[- (IBrDataa * σabs[λ, Ta]
      + Br2Dataa * σabs2[λ, Ta] + Iod2Dataa * σabs3[λ, Ta]) Dpa]) ,
      {λ, λcutLoa, λcutHia}] ) /
      ( (Sca / Dpa) NIntegrate[ ( (h c / 100 λ) F[λ], {λ, λcutLoa, λcutHia}] ) } }
{0.821978, 0.823118}
```


■ Sensitivity Analysis of Kinetic Processes Associated with IBr Photolysis and Br ($^2P_{1/2}$) → Br ($^2P_{3/2}$) Lasing

```

quench := { (kq1 * BrStarDataq * IBrDataq), (kq2 * BrStarDataq * IodDataq),
  (kq3 * BrStarDataq * Iod2Dataq), (kq4 * BrStarDataq * Br2Dataq), (kq5 * BrStarDataq2),
  (kq6 * BrStarDataq * BrDataq), (A21 * BrStarDataq) };
Kq7 := kq7 * IStarDataq * IBrDataq;
Kq8 := kq8 * IStarDataq * Iod2Dataq;
Kq9 := kq9 * IStarDataq * Br2Dataq;
Kq10 := A21IStar * IStarDataq;
ψψ := (IBrDataq + Br2Dataq + Iod2Dataq + (IodDataq + BrStarDataq + BrDataq) / 2);
PumpA := Rpa[IBrDataq, Br2Dataq, Iod2Dataq];
PumpB := Rp2a[IBrDataq, Br2Dataq, Iod2Dataq];
PumpC := Rp3a[IBrDataq, Br2Dataq, Iod2Dataq];
PumpT := RpTot[IBrDataq, Br2Dataq, Iod2Dataq];
ratio1 = Rp2[IBrDataq, Br2Dataq, Iod2Dataq] / PumpT;
ratio2 = Rp3[IBrDataq, Br2Dataq, Iod2Dataq] / PumpT;
PumpStar := PumpA + PumpB;
PumpGround :=
  Rpb[IBrDataq, Br2Dataq, Iod2Dataq] + Rp2b[IBrDataq, Br2Dataq, Iod2Dataq];
Ke1 := ke1 * IBrDataq * BrDataq;
Ke2 := ke2 * BrDataq * Iod2Dataq;
Ke3 := ke3 * IodDataq * Br2Dataq;
Ke4 := ke4 * IBrDataq * IodDataq;
Kr1 := kr1 * IBrDataq * BrDataq2;
Kr2 := kr2 * IBrDataq * BrStarDataq * BrDataq;
Kr3 := kr3 * IBrDataq * BrDataq * IodDataq;
Kr4 := kr4 * IBrDataq * BrStarDataq * IodDataq;
Kr5 := kr5 * IBrDataq * IStarDataq * BrDataq;
Kr6 := kr6 * IodDataq2 * IBrDataq;
Kr7 := kr7 * IStarDataq * IBrDataq * IodDataq;
StimEm :=  $\frac{c \text{ use } Lq_q}{Lc_q} \left( \text{BrStarData}_q - \frac{1}{2} \text{BrData}_q \right) \text{PhotonData}_q$ ;
FlowOutIBr := β * IBrDataq;
FlowOutBr := β * BrDataq;
FlowOutBrStar := β * BrStarDataq;
FlowOutIod := β * IodDataq;
FlowOutIStar := β * IStarDataq;
FlowOutIod2 := β * Iod2Dataq;
FlowOutBr2 := β * Br2Dataq;
FlowInIBr := β * ψψ / 1.08;
FlowInBr2 := 0.04 β * ψψ / 1.08;
FlowInIod2 := 0.04 β * ψψ / 1.08;
FlowInTot := FlowInIBr + FlowInBr2 + FlowInIod2;
t = tplot; If[series > 0, Print["(For ", Parameter, " = ", Setq, ")"]];
RateTag = " \\(cm^-3\\) \\(s^-1\\)"; PopTag = " \\(cm^-3\\) ";

```

```

KList = {{ "(RP*IBr)", "hv + IBr → I + Br*", PumpA, RateTag},
  {"(RP*Br2)", "hv + Br2 → Br + Br*", PumpB, RateTag},
  {"(RP*I2)", "hv + I2 → I + I*", PumpC, RateTag},
  {"(RPTot)", "hv + XY → X + Y*, Y", PumpT, RateTag},
  {"(RPBr2/T)", "Br2 Photolysis Percentage", N[100*ratio1, 3], "percent"},
  {"(RPI2/T)", "I2 Photolysis Percentage", N[100*ratio2, 3], "percent"},
  {"(RPBr*)", "hv + XBr → X + Br*", PumpStar, RateTag},
  {"(RPBr)", "hv + XBr → X + Br", PumpGround, RateTag},
  {"(Qstim)", "hv + Br* → 2hv + Br", StimEm, RateTag},
  {"(FlowT)", "Total Molecular Inflow", FlowInTot, RateTag},
  {"(IFLOW)", "Total [I] Outflow", FlowOutIod, RateTag}, {"", "", ""},
  {"(Kq1)", "Br* + IBr → Br + IBr", quench[[1]], RateTag},
  {"(Kq2)", "Br* + I → Br + I", quench[[2]], RateTag},
  {"(Kq3)", "Br* + I2 → Br + I2", quench[[3]], RateTag},
  {"(Kq4)", "Br* + Br2 → Br + Br2", quench[[4]], RateTag},
  {"(Kq5)", "Br* + Br* → Br + Br*", quench[[5]], RateTag},
  {"(Kq6)", "Br* + Br → Br + Br", quench[[6]], RateTag},
  {"(A21Br)", "Br* → Br + hv", quench[[7]], RateTag},
  {"(Kq7)", "I* + IBr → I + IBr", Kq7, RateTag},
  {"(Kq8)", "I* + I2 → I + I2", Kq8, RateTag},
  {"(Kq9)", "I* + Br2 → I + Br2", Kq9, RateTag},
  {"(A21I)", "I* → I + hv", Kq10, RateTag},
  {"", "", ""}, {"(Ke1)", "Br + IBr → I + Br2", Ke1, RateTag},
  {"(Ke2)", "Br + I2 → IBr + I", Ke2, RateTag},
  {"(Ke3)", "I + Br2 → IBr + Br", Ke3, RateTag},
  {"(Ke4)", "I + IBr → I2 + Br", Ke4, RateTag}, {"", "", ""},
  {"(Kr1)", "Br + Br + IBr → Br2 + IBr", Kr1, RateTag},
  {"(Kr2)", "Br* + Br + IBr → Br2 + IBr", Kr2, RateTag},
  {"(Kr3)", "Br + I + IBr → 2IBr", Kr3, RateTag},
  {"(Kr4)", "Br* + I + IBr → 2IBr", Kr4, RateTag},
  {"(Kr5)", "I* + Br + IBr → 2IBr", Kr5, RateTag},
  {"(Kr6)", "I + I + IBr → I2 + IBr", Kr6, RateTag},
  {"(Kr7)", "I* + I + IBr → I2 + IBr", Kr7, RateTag}}; t = .;
Print["\nRelative Magnitudes of Kinetic Processes at t = ", N[tplot], " s:"];
Print[TableForm[KList, TableSpacing -> {1, 2}]]; t = .;

```

(For Coupler Reflectivity = 0.895)

Relative Magnitudes of Kinetic Processes at t = 0.01 s:

(RP* _{IBr})	hν + IBr → I + Br*	2.53366 × 10 ²⁰	cm ⁻³ s ⁻¹
(RP* _{Br₂})	hν + Br ₂ → Br + Br*	2.31146 × 10 ¹⁹	cm ⁻³ s ⁻¹
(RP* _{I₂})	hν + I ₂ → I + I*	4.9577 × 10 ¹⁹	cm ⁻³ s ⁻¹
(RP _{Tot})	hν + XY → X + Y*, Y	4.87414 × 10 ²⁰	cm ⁻³ s ⁻¹
(RP _{Br₂/T})	Br ₂ Photolysis Percentage	6.87	percent
(RP _{I₂/T})	I ₂ Photolysis Percentage	12.2	percent
(RP _{Br*})	hν + XBr → X + Br*	2.76481 × 10 ²⁰	cm ⁻³ s ⁻¹
(RP _{Br})	hν + XBr → X + Br	1.84949 × 10 ²⁰	cm ⁻³ s ⁻¹
(Q _{stim})	hν + Br* → 2hν + Br	1.94754 × 10 ²⁰	cm ⁻³ s ⁻¹
(Flow _T)	Total Molecular Inflow	0	cm ⁻³ s ⁻¹
(I _{Flow})	Total [I] Outflow	0	cm ⁻³ s ⁻¹
(Kq1)	Br* + IBr → Br + IBr	4.8475 × 10 ¹⁹	cm ⁻³ s ⁻¹
(Kq2)	Br* + I → Br + I	6.27917 × 10 ¹⁸	cm ⁻³ s ⁻¹
(Kq3)	Br* + I ₂ → Br + I ₂	2.73516 × 10 ¹⁹	cm ⁻³ s ⁻¹
(Kq4)	Br* + Br ₂ → Br + Br ₂	1.78445 × 10 ¹⁸	cm ⁻³ s ⁻¹
(Kq5)	Br* + Br* → Br + Br*	6.88652 × 10 ¹⁴	cm ⁻³ s ⁻¹
(Kq6)	Br* + Br → Br + Br	1.52047 × 10 ¹³	cm ⁻³ s ⁻¹
(A21 _{Br})	Br* → Br + hv	2.01228 × 10 ¹³	cm ⁻³ s ⁻¹
(Kq7)	I* + IBr → I + IBr	3.43747 × 10 ¹⁹	cm ⁻³ s ⁻¹
(Kq8)	I* + I ₂ → I + I ₂	6.08287 × 10 ¹⁸	cm ⁻³ s ⁻¹
(Kq9)	I* + Br ₂ → I + Br ₂	9.84195 × 10 ¹⁸	cm ⁻³ s ⁻¹
(A21 _I)	I* → I + hv	2.90299 × 10 ¹²	cm ⁻³ s ⁻¹
(Ke1)	Br + IBr → I + Br ₂	1.32928 × 10 ²¹	cm ⁻³ s ⁻¹
(Ke2)	Br + I ₂ → IBr + I	4.38311 × 10 ²⁰	cm ⁻³ s ⁻¹
(Ke3)	I + Br ₂ → IBr + Br	1.2958 × 10 ²¹	cm ⁻³ s ⁻¹
(Ke4)	I + IBr → I ₂ + Br	1.03739 × 10 ¹⁹	cm ⁻³ s ⁻¹
(Kr1)	Br + Br + IBr → Br ₂ + IBr	1.65071 × 10 ¹⁵	cm ⁻³ s ⁻¹
(Kr2)	Br* + Br + IBr → Br ₂ + IBr	3.69205 × 10 ¹³	cm ⁻³ s ⁻¹
(Kr3)	Br + I + IBr → 2IBr	2.98993 × 10 ¹⁵	cm ⁻³ s ⁻¹
(Kr4)	Br* + I + IBr → 2IBr	5.01554 × 10 ¹⁵	cm ⁻³ s ⁻¹
(Kr5)	I* + Br + IBr → 2IBr	3.27265 × 10 ¹¹	cm ⁻³ s ⁻¹
(Kr6)	I + I + IBr → I ₂ + IBr	4.87407 × 10 ²⁰	cm ⁻³ s ⁻¹
(Kr7)	I* + I + IBr → I ₂ + IBr	1.77832 × 10 ¹⁴	cm ⁻³ s ⁻¹

Hyperlink To:

Single Data Entry

Multiple Data Entry

CW Model

```

If[a4 == 2, Goto[EndSens1]];
CoeffList = {{Ke2, Ke3, Kr3, Kr4, Kr5, FlowInIBr}, {"IBr Population (+)"},
{"ke2", "ke3", "kr3", "kr4", "kr5", "InFlow"}, {-PumpA, -Ke1, -Ke4, -FlowOutIBr},
{"IBr Population (-)"}, {"Photolysis", "ke1", "ke4", "OutFlow"},
{φIBr * PumpA, φBr2 * PumpB}, {"Br(P1/2) Population (+)"},
{"IBr\nPhotolysis", "Br2\nPhotolysis"},
-Flatten[Prepend[{Kr2, Kr4, FlowOutBrStar}, quench]],
{"Br(P1/2) Population (-)"}, {"kq1", "kq2", "kq3", "kq4", "kq5", "kq6", "A21",
"kr2", "kr4", "OutFlow"},
Flatten[Prepend[{(1 - φIBr) * PumpA, (1 - φBr2) * PumpB, Ke3, Ke4}, quench]],
{"Br(P3/2) Population (+)"}, {"kq1", "kq2", "kq3", "kq4", "kq5", "kq6", "A21",
"IBr Photo", "Br2 Photo", "ke3", "ke4"}, {-Ke1, -Ke2, -2 Kr1, -Kr2,
-Kr3, -Kr5, -FlowOutBr}, {"Br(P3/2) Population (-)"},
{"ke1", "ke2", "kr1", "kr2", "kr3", "kr5", "OutFlow"},
{φIod2 * PumpC}, {"I(P1/2) Population (+)"}, {"I2 Photo"}, {-Kq7, -Kq8, -Kq9,
-Kq10, -Kr5, -Kr7, -FlowOutIStar}, {"I(P1/2) Population (-)"}, {"kq7", "kq8",
"kq9", "A21", "kr5", "kr7", "OutFlow"}, {PumpA, (2 - φIod2) * PumpC, Ke1, Ke2},
{"I(P3/2) Population (+)"}, {"IBr Photo", "I2 Photo", "ke1", "ke2"},
{-Ke3, -Ke4, -Kr3, -Kr4, -2 Kr6, -Kr7, -FlowOutIod},
{"I(P3/2) Population (-)"}, {"ke3", "ke4",
"kr3", "kr4", "kr6", "kr7", "OutFlow"}, {Ke1, Kr1, Kr2, FlowInBr2},
{"Br2 Population (+)"}, {"ke1", "kr1", "kr2", "InFlow"},
{-PumpB, -Ke3, -FlowOutBr2},
{"Br2 Population (-)"}, {"Br2\nPhotolysis", "ke3", "OutFlow"},
{Ke4, Kr6, Kr7, FlowInIod2}, {"I2 Population (+)"},
{"ke4", "kr6", "kr7", "InFlow"}, {-Ke2, -FlowOutIod2},
{"I2 Population (-)"}, {"ke2", "OutFlow"}];

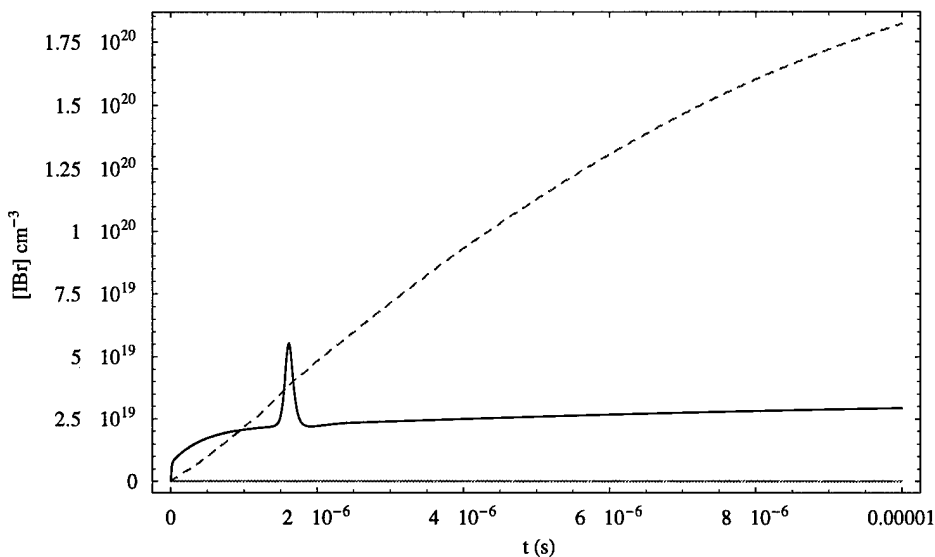
LabelList = {"[IBr] \\\(cm-3)", "\\([Br*]) \\\(cm-3)",
"[Br] \\\(cm-3)", "\\([I*]) \\\(cm-3)",
"[I] \\\(cm-3)", "[Br2] \\\(cm-3)", "[I2] \\\(cm-3)"};

CoeffPlot = {}; p = -2;
While[p = p + 3 <= 40,
AppendTo[CoeffPlot, Plot[Evaluate[CoeffList[[p]],
{t, 0, tplot/1000},
PlotLabel -> StyleForm[SequenceForm["Kinetic Contributions to ",
Extract[CoeffList[[p+1], 1]],
FontWeight -> "Bold", FontSize -> 11], PlotStyle ->
{{GrayLevel[0]}, {Hue[0.07], Dashing[ {.01} ]}, {Hue[0.6], Dashing[ {.03, .01} ]},
{Hue[0.32], Dashing[ {.02} ]},
{GrayLevel[0.7]}, {Hue[0.55], Dashing[ {.04, .01} ]},
{Hue[0.78], Dashing[ {0.02, 0.01} ]}, {Hue[0.12], Dashing[ {.01, .02} ]},
{GrayLevel[0.85]},
{Hue[0.85], Dashing[ {.03} ]}, {Hue[0.65], Dashing[ {.01, .03} ]},
{Hue[0.78], Dashing[ {0.02, 0.01} ]}], PlotLegend -> CoeffList[[p+2]],
LegendSize -> {0.4, .85},
LegendBackground -> GrayLevel[0.95], LegendPosition -> {1, -0.3},
LegendShadow -> {0.015, -0.015}, LegendLabel -> StyleForm["Kinetic Process",

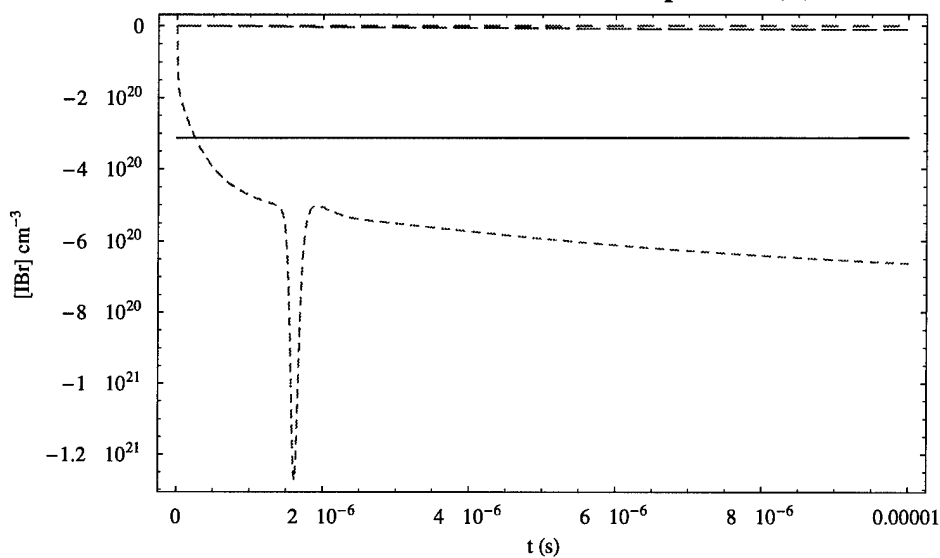
```

```
FontSlant -> "Italic"], PlotRange -> All, Frame -> True,  
DisplayFunction -> Identity,  
FrameLabel -> {" t (s)", LabelList[[Round[((p / 3) + 1) / 2]]]]];  
  
p = 0; While[(p = p + 1) <= 14,  
  Show[  
    CoeffPlot[[p]], DisplayFunction -> $DisplayFunction, ImageSize -> {572, 337}]];  
Label[EndSens1];
```

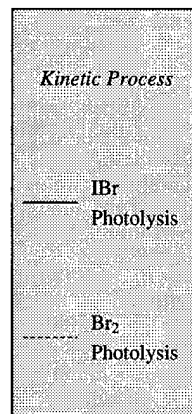
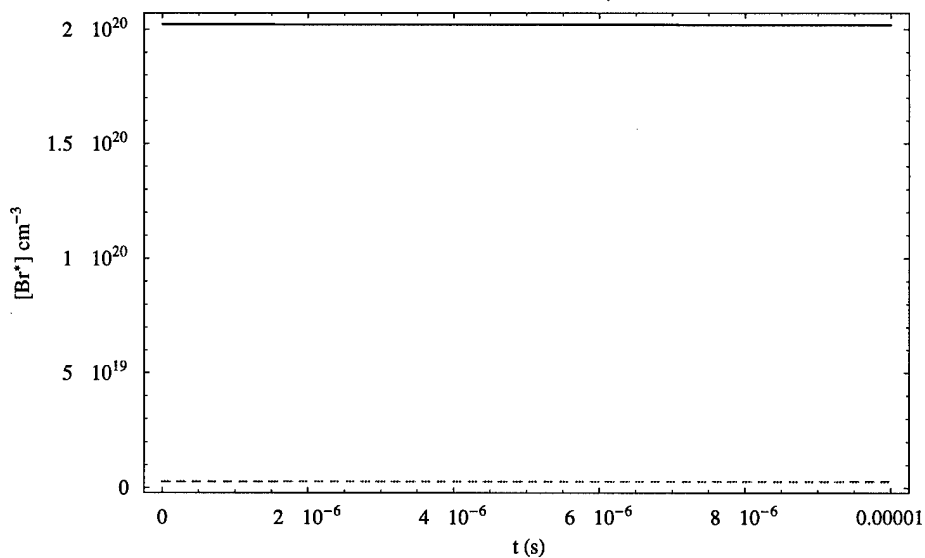
Kinetic Contributions to IBr Population (+)



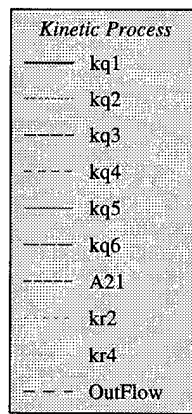
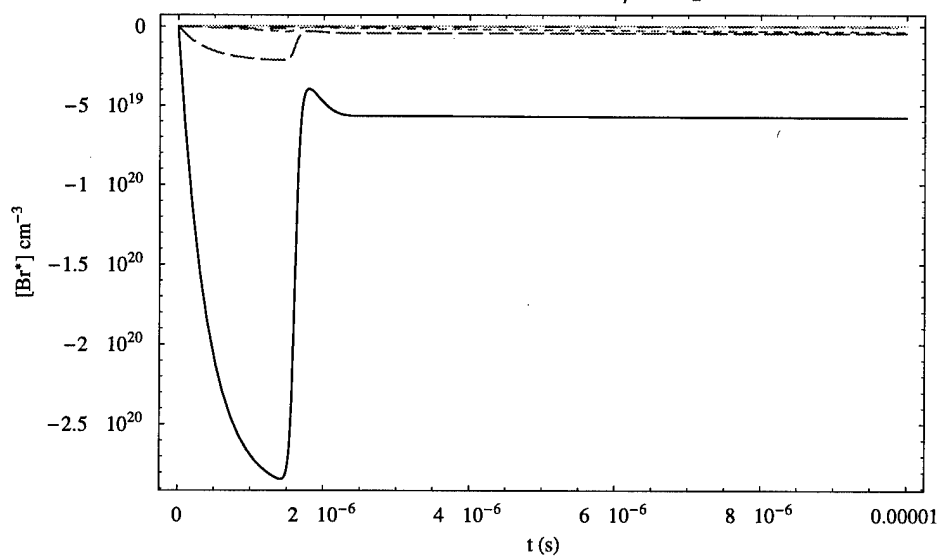
Kinetic Contributions to IBr Population (-)



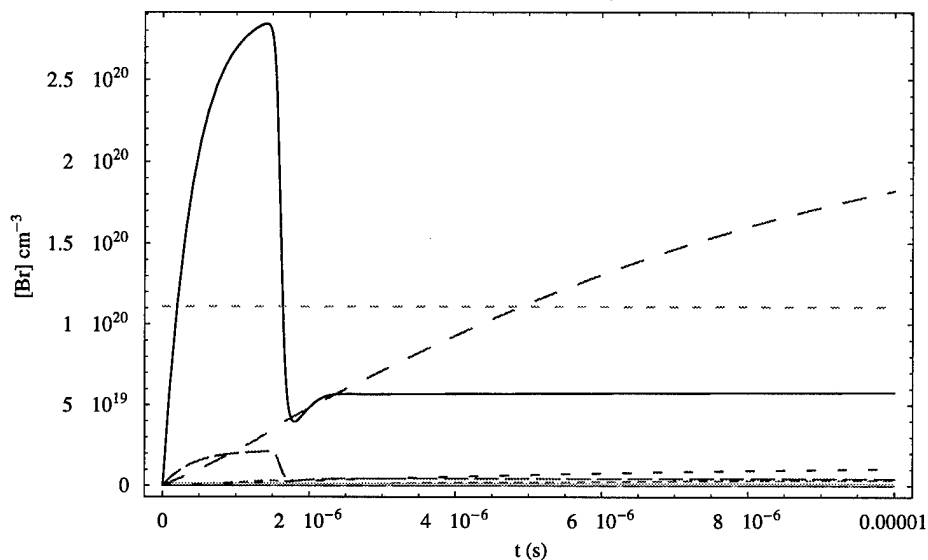
Kinetic Contributions to Br(P_{1/2}) Population (+)



Kinetic Contributions to Br(P_{1/2}) Population (-)

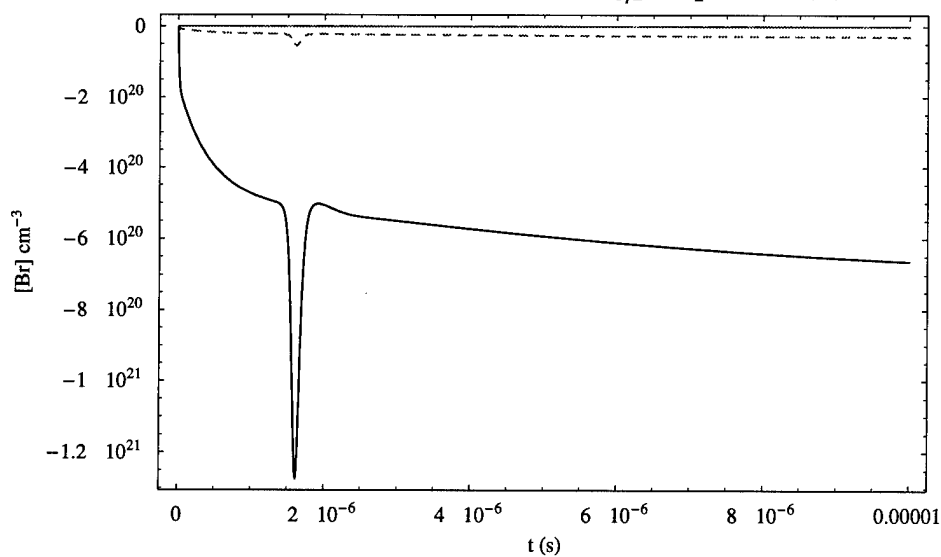


Kinetic Contributions to Br(P_{3/2}) Population (+)



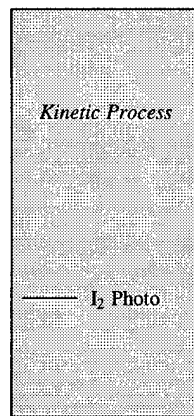
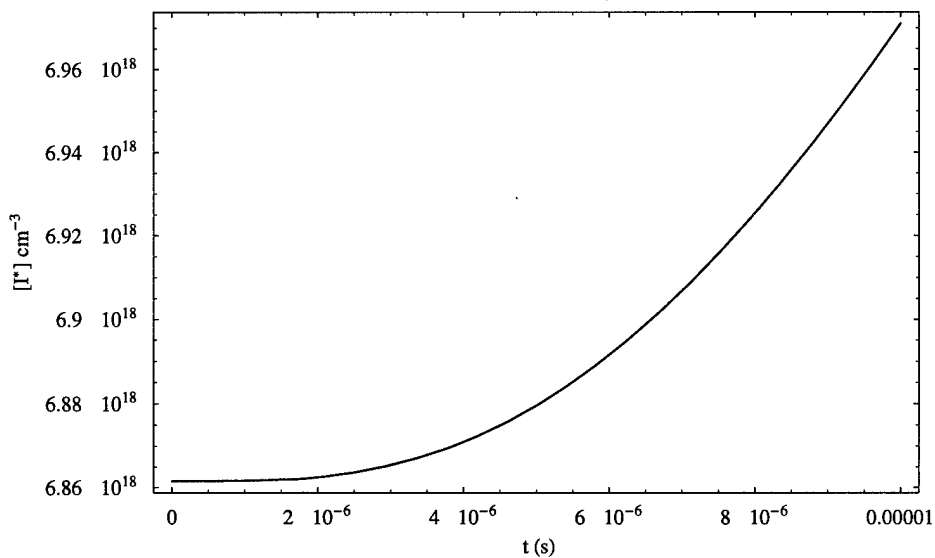
Kinetic Process	
—	kq1
---	kq2
---	kq3
---	kq4
---	kq5
---	kq6
---	A21
---	IBr Photo
---	Br ₂ Photo
---	ke3
---	ke4

Kinetic Contributions to Br(P_{3/2}) Population (-)

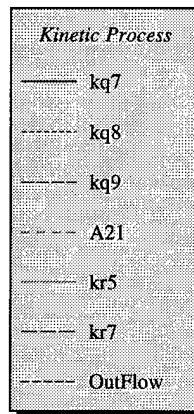
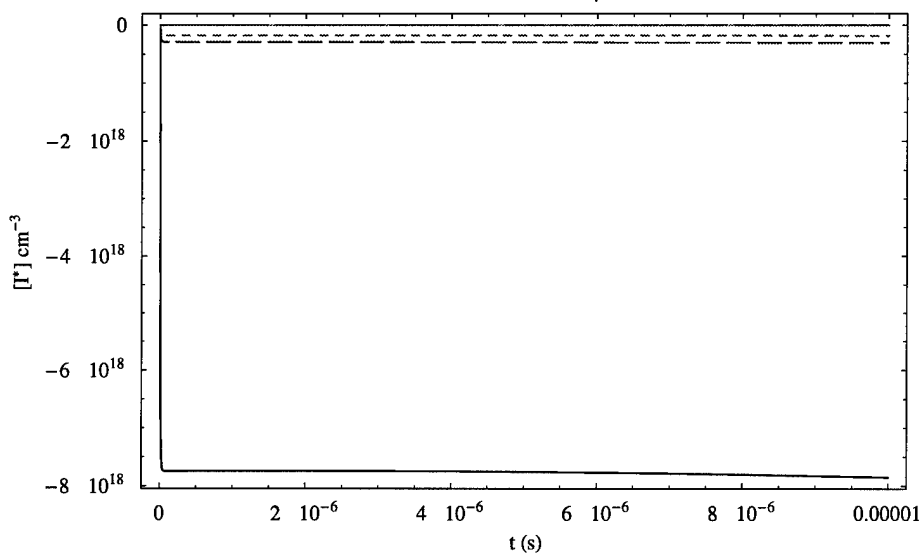


Kinetic Process	
—	ke1
---	ke2
---	kr1
---	kr2
---	kr3
---	kr5
---	OutFlow

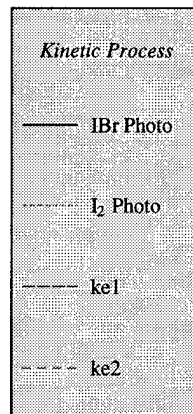
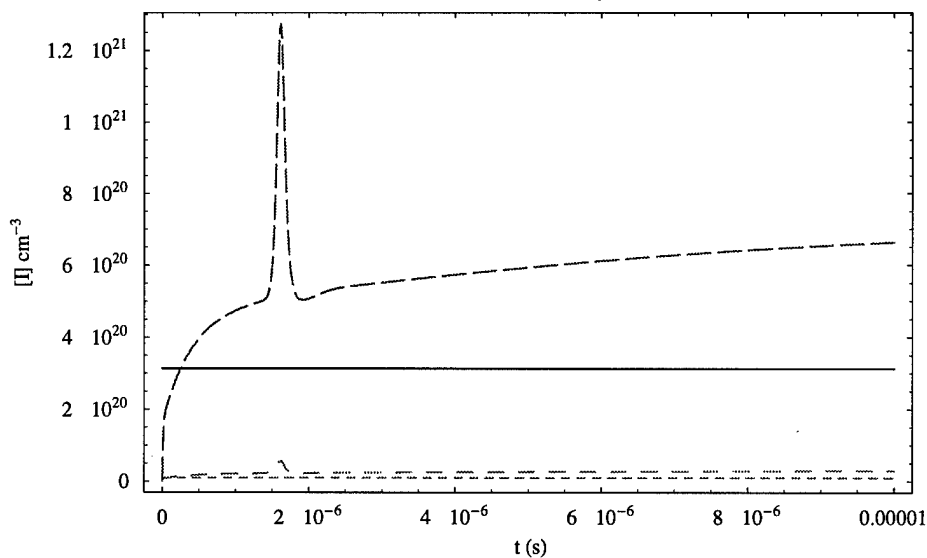
Kinetic Contributions to I(P_{1/2}) Population (+)



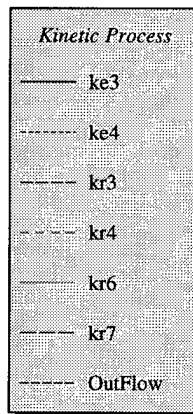
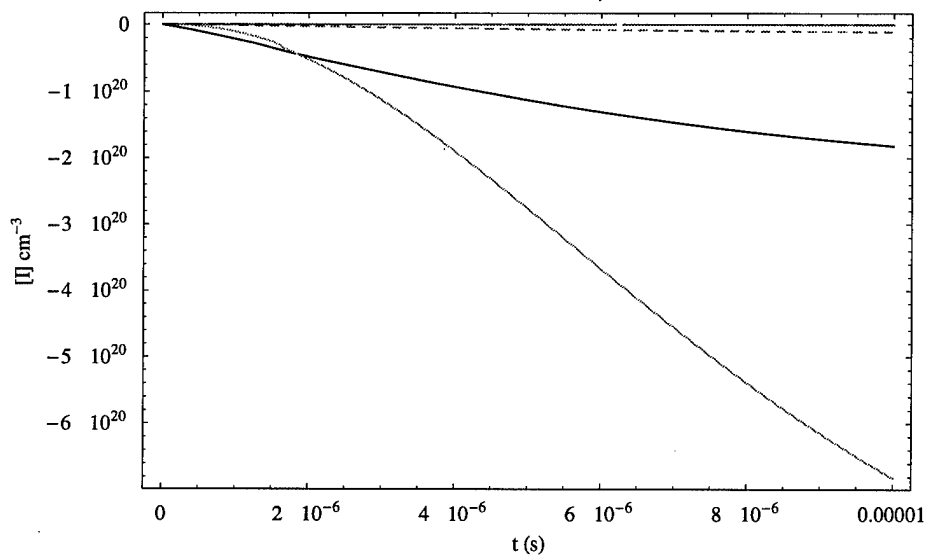
Kinetic Contributions to I(P_{1/2}) Population (-)



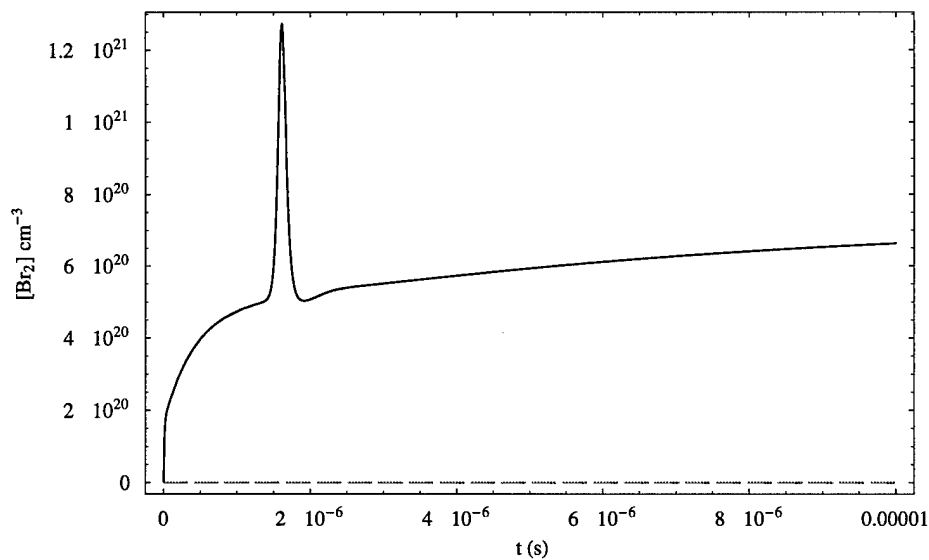
Kinetic Contributions to I(P_{3/2}) Population (+)



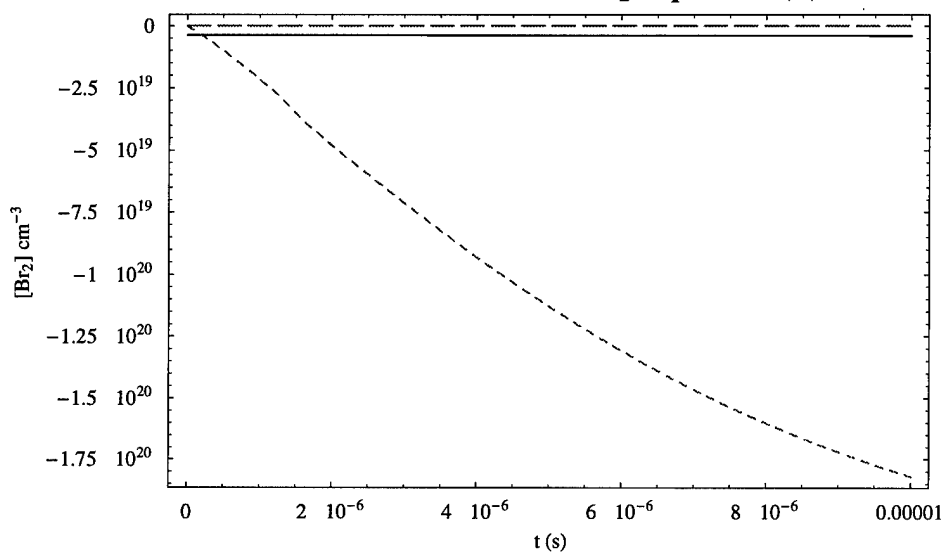
Kinetic Contributions to I(P_{3/2}) Population (-)



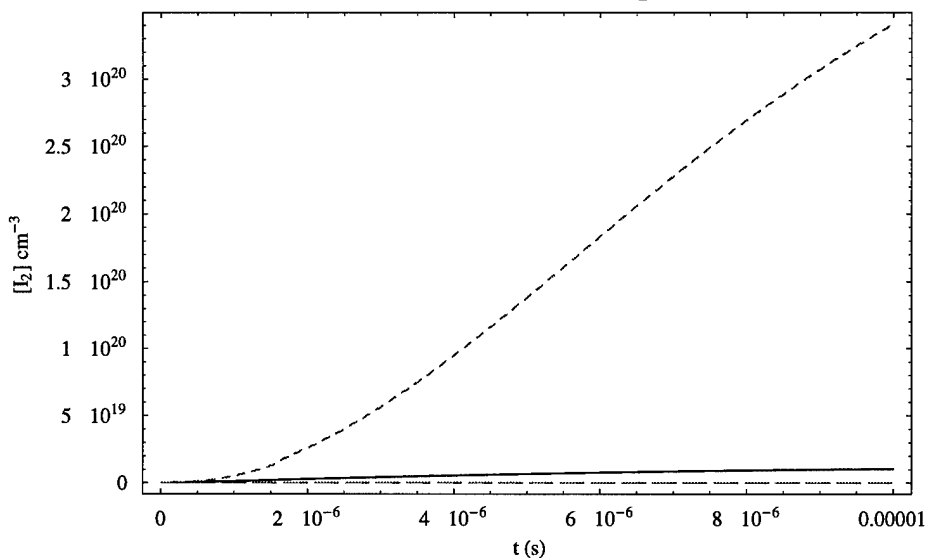
Kinetic Contributions to Br₂ Population (+)



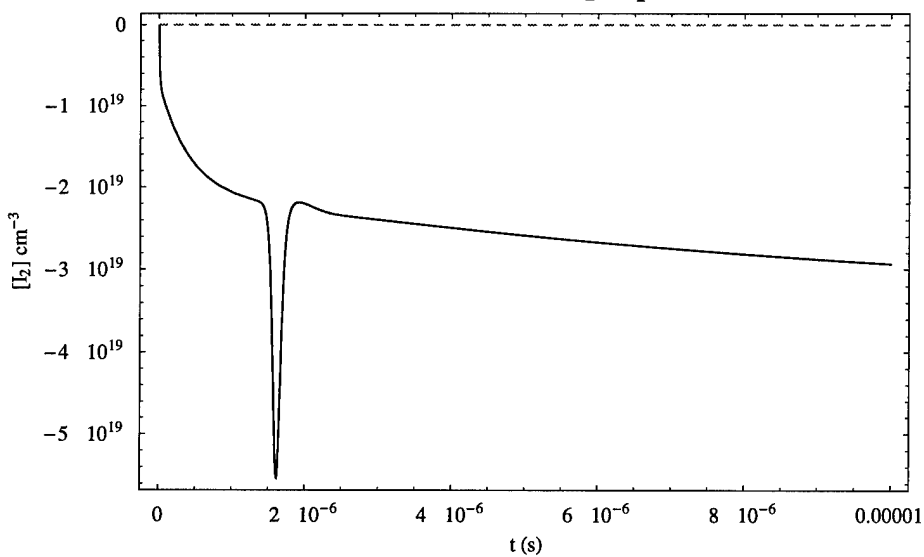
Kinetic Contributions to Br₂ Population (-)



Kinetic Contributions to I₂ Population (+)



Kinetic Contributions to I₂ Population (-)



Hyperlink To:

[Single Data Entry](#)

[Multiple Data Entry](#)

[Recombination Analysis](#)


```

If[a5 == 2, Null, t = tmax; I2frac =  $\frac{\text{Iod2Data}_q}{\text{IBrData}_q}$ ; Br2frac =  $\frac{\text{Br2Data}_q}{\text{IBrData}_q}$ ;
  IBrfrac =  $\frac{\text{IBrData}_q}{\text{IBr0}_q}$ ; t = .;
RpCW[IBrN_, Conc_] =  $\frac{\text{Conc}}{\text{Sc}_q}$  (RpTot[IBrN, Br2frac * IBrN, I2frac * IBrN]);

```

```

Assign =
  {hh -> h, v -> vlase, ost -> ose,  $\chi$  -> Br2frac,  $\kappa$  -> I2frac, kke1 -> ke1, kkr6 -> kr6,
  kke2 -> ke2, kke3 -> ke3,
  kke4 -> ke4, L -> 0.01 Lgq, kkq1 -> kq1, kkq2 -> kq2, kkq3 -> kq3,
   $\gamma$ thr ->  $\gamma$ th,  $\phi$ t ->  $\phi$ IBr, Pump -> RpCW[IBrfrac * IBr0q, Conc], IBrr -> IBrfrac * IBr0q};
IntCW[Conc_] = Evaluate[Iv /. CWlase] /. Assign;
IodCW[Conc_] = Evaluate[Iodd /. CWlase] /. Assign;
BrStarCW[Conc_] = Evaluate[BrStarr /. CWlase] /. Assign;
BrCW[Conc_] = Evaluate[Brr /. CWlase] /. Assign;]

```

```

If[a5 == 2, Null,
  {IntCW[Scq], IBrfrac * IBr0q, IodCW[Scq], BrStarCW[Scq], BrCW[Scq]}]
{73154.7, 1.51764 × 1018, 1.03467 × 1016, 3.04542 × 1013, 1.93211 × 1013}

```

Output Power [W/cm²] (Based on Mean Circulating Photon Cavity Intensity):

[Compare to full kinetic result using IBr rate package]

```

If[a5 == 2, Null, t = tmax;
  Print[pout =  $\frac{\text{IntCW}[\text{vFlow}_q, \text{Sc}_0]}{c \tau t} \rho * \text{Lg}_q (1 - \text{Rcoup}_q)$ , " ", PowerDataq]];
t = .;

```

3840.62, 3195.31

Percent deviation from result of IBr kinetic package:

```

If[a5 == 2, Null, t = tmax;
  Print[Dev = N[(pout - PowerDataq) / PowerDataq * 100, 4], "% Deviation"]; t = .;]

```

20.2% Deviation

Hyperlink To:

[Single Data Entry](#)

[Multiple Data Entry](#)

[Sensitivity Analysis](#)

■ Recombination Analysis of IBr Photofragments
(Absent Photolysis Source & Stimulated Emission Processes)

```

If[a6 == 2, Goto[EndRecom]];
ClearAll[tsweep, trec, IBrOut, IStarOut, IodOut, BrStarOut, BrOut, Iod2Out,
  Br2Out, IBr, IOD, ISTAR, BRSTAR, BR, IOD2, BR2, IBrdata, BRSTARdata, BRdata,
  IODdata, ISTARdata, IOD2data, BR2data];

tsweep = tplot; trec = 60 * 10-0;
t = tsweep; IBrOut = {IBrList[[1]]}; IStarOut = {IStarList[[1]]};
IodOut = {IodList[[1]]}; BrStarOut = {BrStarList[[1]]}; BrOut = {BrList[[1]]};
Iod2Out = {Iod2List[[1]]}; Br2Out = {Br2List[[1]]}; t = .;

Γrec = A21 + (kq1 * IBr[t]) + (kq2 * IOD[t]) + (kq3 * IOD2[t]) +
  (kq4 * BR2[t]) + (kq5 * BRSTAR[t]) + (kq6 * BR[t]);

Recombine := NDSolve[{
  IBr'[t] ==
    IBr[t] ((kr4 * BRSTAR[t] * IOD[t]) + (kr3 * BR[t] * IOD[t]) + (kr5 * ISTAR[t] * BR[t]))
    + (ke2 * BR[t] * IOD2[t]) + (ke3 * IOD[t] * BR2[t])
    - IBr[t] ((ke1 * BR[t]) + (ke4 * IOD[t])),
  IBr[0] == Extract[Flatten[IBrOut], 1],

  IOD'[t] == (ke1 * BR[t] * IBr[t]) + (ke2 * BR[t] * IOD2[t])
    - IOD[t] ((ke3 * BR2[t]) + (ke4 * IBr[t]) + (kr4 * BRSTAR[t] * IBr[t])
    + (kr3 * BR[t] * IBr[t]) + (kr7 * ISTAR[t] * IBr[t]) + (2 kr6 * IOD[t] * IBr[t])),
  IOD[0] == Extract[Flatten[IodOut], 1],

  BRSTAR'[t] == -BRSTAR[t] (Γrec + (kr2 * BR[t] * IBr[t])),
  BRSTAR[0] == Extract[Flatten[BrStarOut], 1],

  BR'[t] == (Γrec * BRSTAR[t]) + (ke3 * IOD[t] * BR2[t]) + (ke4 * IOD[t] * IBr[t])
    - BR[t] ((ke1 * IBr[t]) +
    (ke2 * IOD2[t]) + (kr2 * BRSTAR[t] * IBr[t]) + (2 kr1 * BR[t] * IBr[t])
    + (kr3 * IOD[t] * IBr[t]) + (kr5 * ISTAR[t] * IBr[t])),
  BR[0] == Extract[Flatten[BrOut], 1],

  IOD2'[t] == (ke4 * IOD[t] * IBr[t]) + (kr7 * ISTAR[t] * IOD[t] * IBr[t])
    + (kr6 * IOD[t]2 * IBr[t]) - (IOD2[t] * ke2 * BR[t]),
  IOD2[0] == Extract[Flatten[Iod2Out], 1],

  BR2'[t] == BR[t] ((ke1 * IBr[t]) + (kr2 * BRSTAR[t] * IBr[t])
    + (kr1 * BR[t] * IBr[t])) - (ke3 * IOD[t] * BR2[t]),
  BR2[0] == Extract[Flatten[Br2Out], 1],

  ISTAR'[t] == -ISTAR[t] (A21IStar + (kq3 * IBr[t]) + (kq8 * IOD2[t]) + (kq9 * BR2[t])
    + (kr7 * IOD[t] * IBr[t]) + (kr5 * BR[t] * IBr[t])),

```

```

ISTAR[0] == Extract[Flatten[IStarOut], 1]],

{IBR[t], IOD[t], BRSTAR[t], BR[t], IOD2[t], BR2[t], ISTAR[t]},
{t, 0, trec}, MaxSteps -> 4000];

IBRdata = Abs[Evaluate[IBR[t] /. Recombine]];
BRSTARdata = Abs[Evaluate[BRSTAR[t] /. Recombine]];
BRdata = Abs[Evaluate[BR[t] /. Recombine]];
IODdata = Abs[Evaluate[IOD[t] /. Recombine]];
IOD2data = Abs[Evaluate[IOD2[t] /. Recombine]];
BR2data = Abs[Evaluate[BR2[t] /. Recombine]];
ISTARdata = Abs[Evaluate[ISTAR[t] /. Recombine]];

RRecom = {IBRdata, "Recombination Evolution of [IBr]", "[IBr] (cm-3)", IODdata,
"Recombination Evolution of [I(P3/2)]", "[I] (cm-3)",
BRSTARdata, "Recombination Evolution of [Br(P1/2)]", "[Br*] (cm-3)", BRdata,
"Recombination Evolution of [Br(P3/2)]", "[Br] (cm-3)", IOD2data,
"Recombination Evolution of [I2]", "[I2] (cm-3)", BR2data,
"Recombination Evolution of [Br2]", "[Br2] (cm-3)", ISTARdata,
"Recombination Evolution of [I(P1/2)]", "[I*] (cm-3)"; RecomList = {};

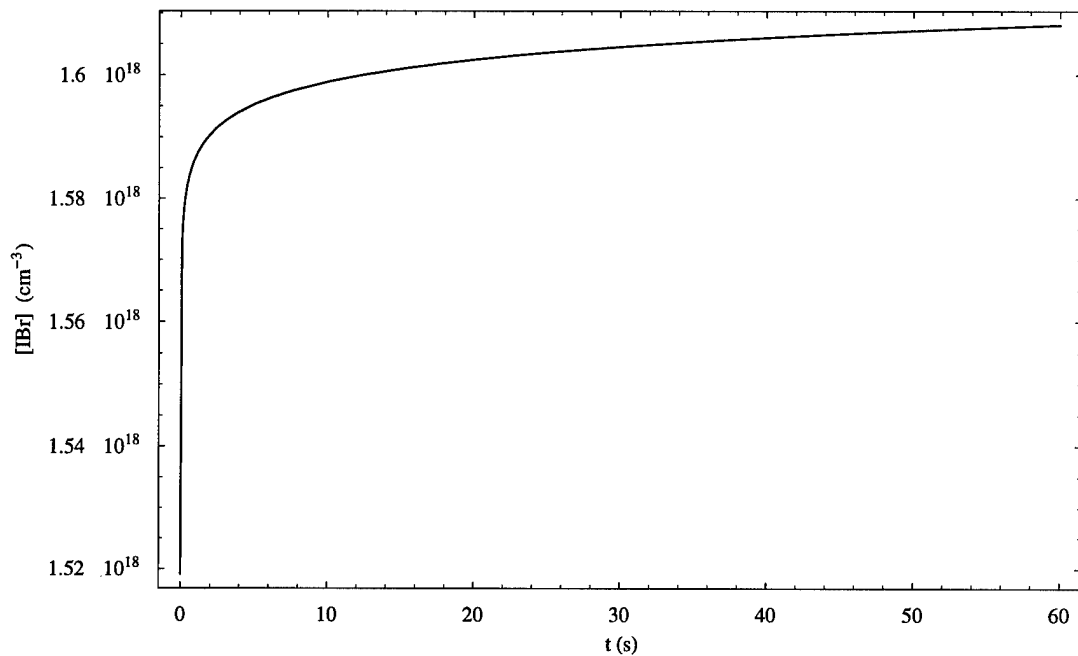
x = -1; While[(x = x + 1) <= 6,
AppendTo[RecomList, {Plot[RRecom[[ (3 x) + 1]], {t, 0, trec}, PlotLabel ->
StyleForm[RRecom[[ (3 x) + 2]], FontWeight -> "Bold", FontSize -> 11],
PlotRange -> All, Frame -> True, FrameLabel -> {" t (s)", RRecom[[ (3 x) + 3]]},
DisplayFunction -> Identity}]];

p = 0; While[(p = p + 1) <= 7,
Show[RecomList[[p]], DisplayFunction -> $DisplayFunction,
ImageSize -> {522, 386}]]; p = .; t = trec;

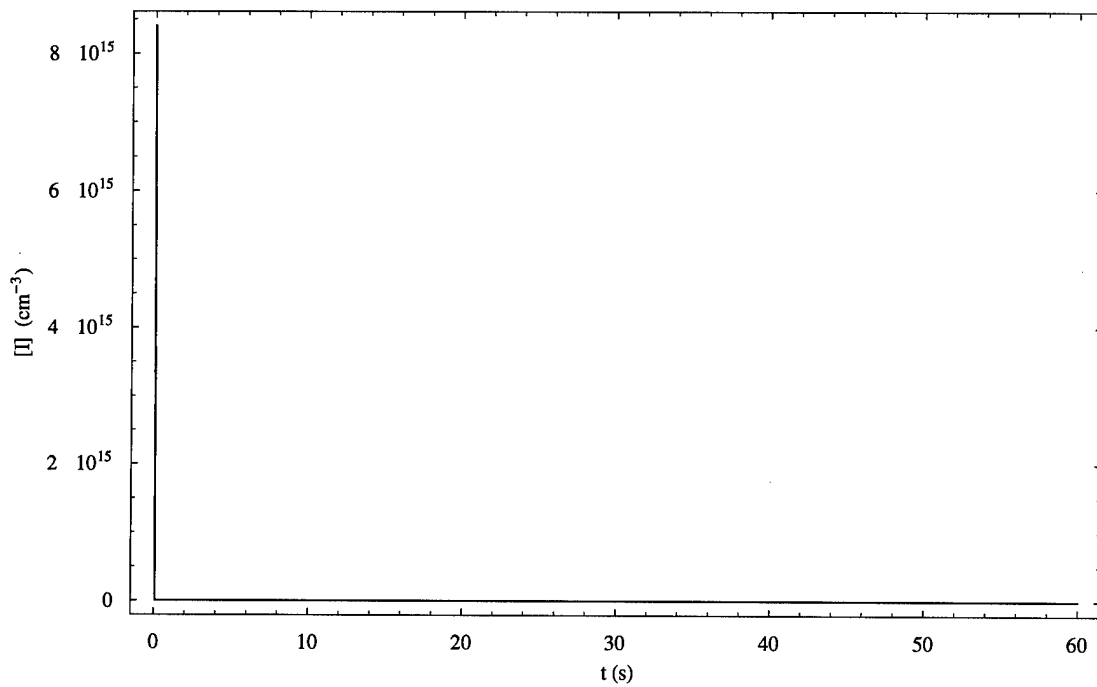
Print["\nRecombined Population Densities at t = ", N[trec], " s:"];
DistList[[1, 2]] = IBRdata[[1]];
DistList[[3, 2]] = Round[BRSTARdata[[1]]]; DistList[[4, 2]] =
BRdata[[1]];
DistList[[5, 2]] = Round[ISTARdata[[1]]]; DistList[[6, 2]] = IODdata[[1]];
DistList[[7, 2]] = BR2data[[1]]; DistList[[8, 2]] = IOD2data[[1]];
Print[TableForm[
Prepend[Take[DistList, {3, 8}], Extract[DistList, 1], TableSpacing -> {1, 1}]];
Print["Fractional Recovery of Initial IBr Precursor: ",
Extract[IBRdata, 1] / IBr0]; t = .;
Label[EndRecom];

```

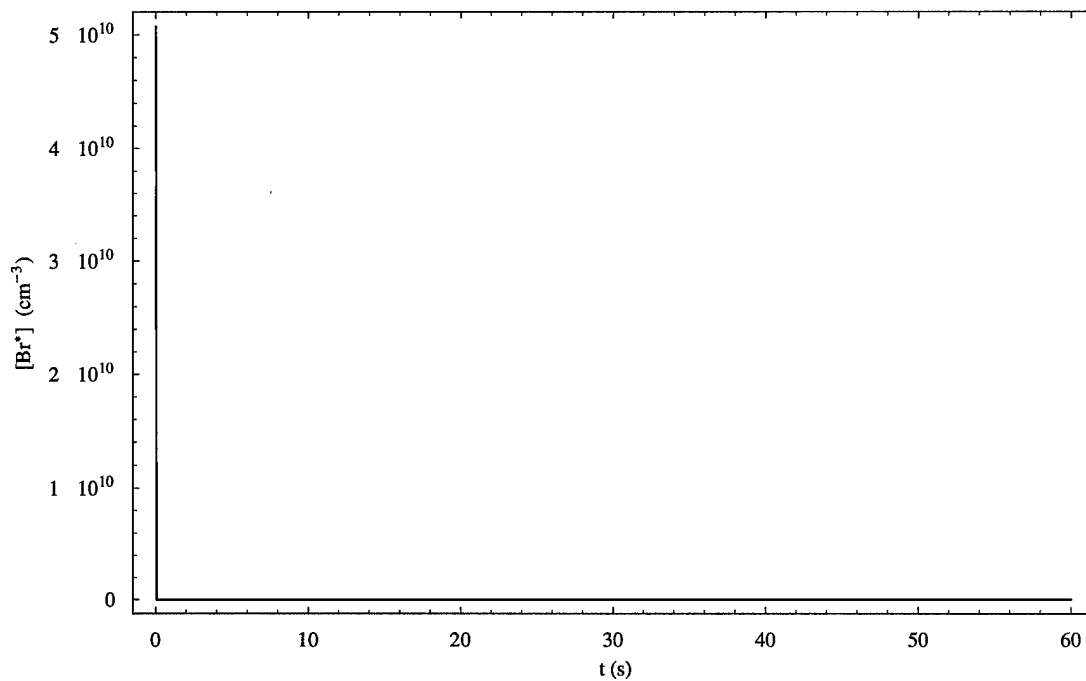
Recombination Evolution of [IBr]



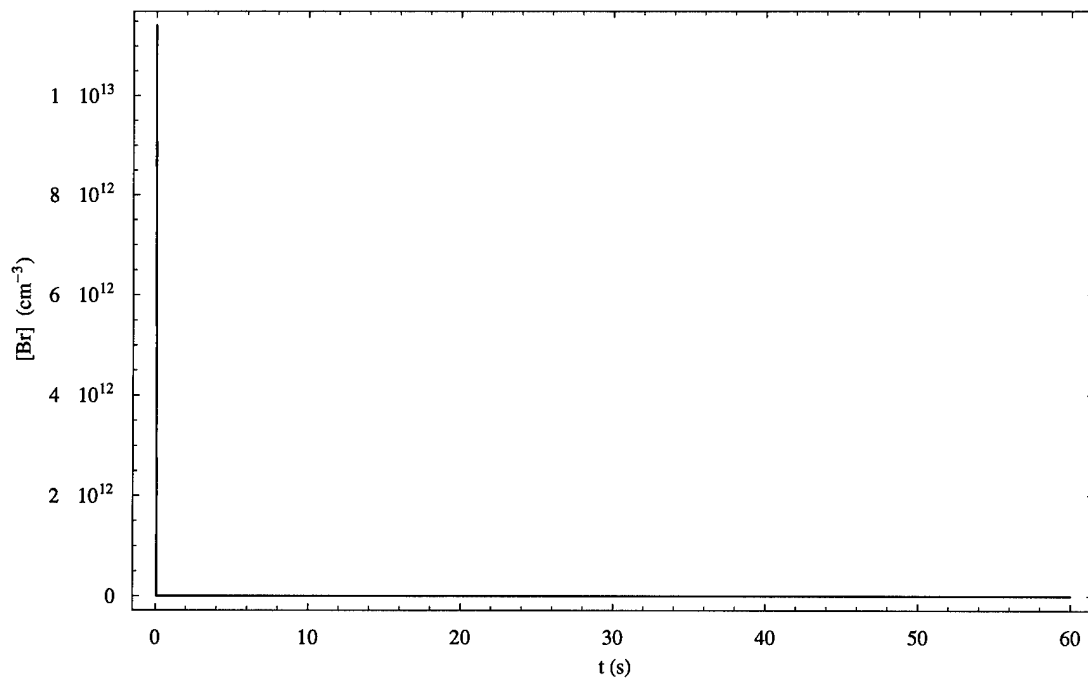
Recombination Evolution of [I(P_{3/2})]



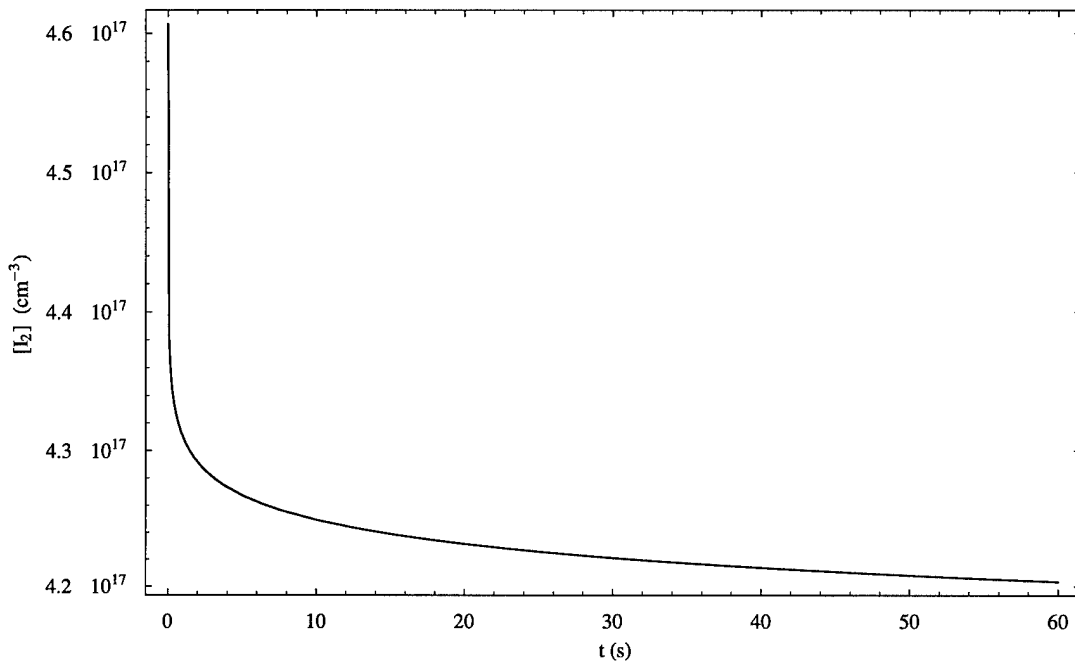
Recombination Evolution of [Br(P_{1/2})]



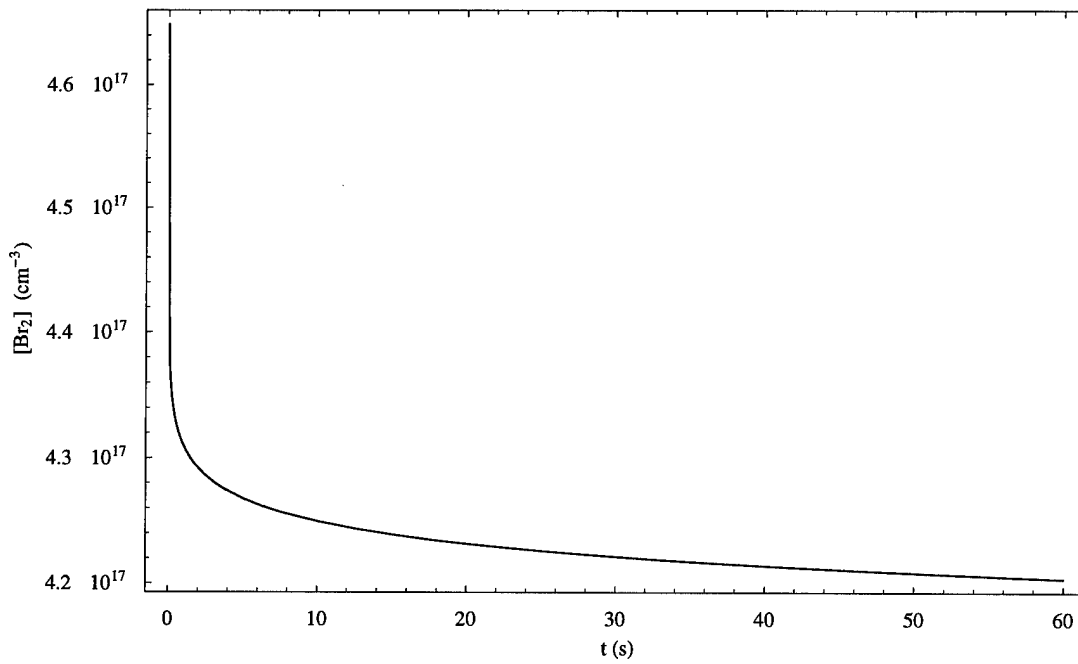
Recombination Evolution of [Br(P_{3/2})]



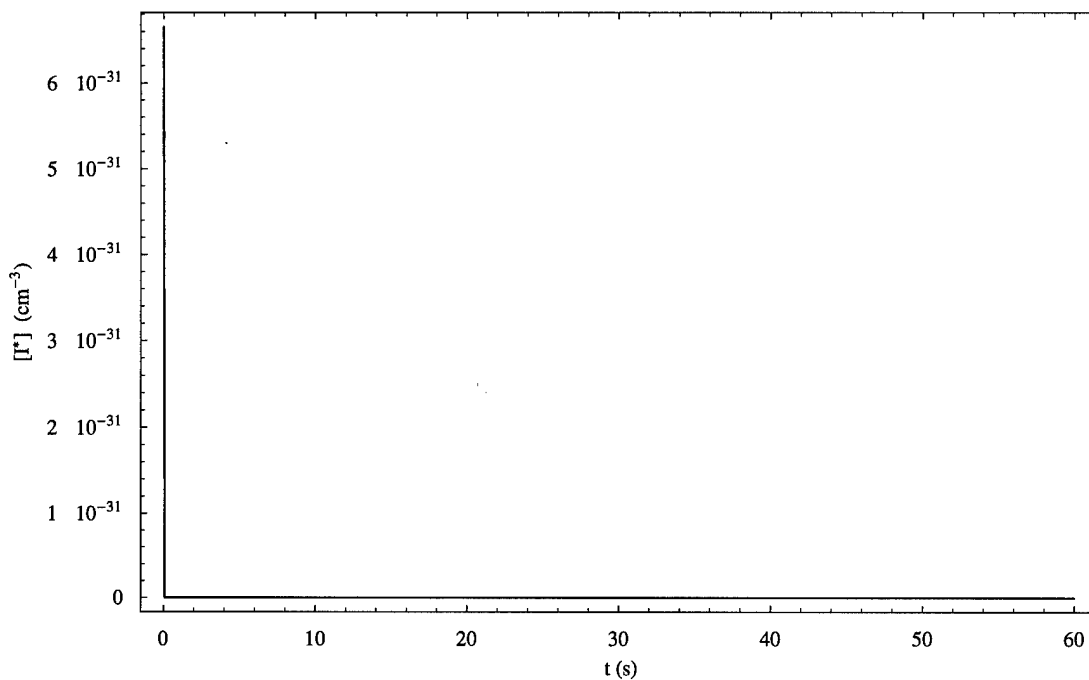
Recombination Evolution of [I₂]



Recombination Evolution of [Br₂]



Recombination Evolution of $[I(P_{1/2})]$



Recombined Population Densities at $t = 60. \text{ s}$:

$[I\text{Br}]$:	1.60807×10^{18}	cm^{-3}
$[Br(P_{1/2})]$:	0	cm^{-3}
$[Br(P_{3/2})]$:	2.08493×10^6	cm^{-3}
$[I(P_{1/2})]$:	0	cm^{-3}
$[I(P_{3/2})]$:	1.73502×10^9	cm^{-3}
$[Br_2]$:	4.20373×10^{17}	cm^{-3}
$[I_2]$:	4.20346×10^{17}	cm^{-3}

Fractional Recovery of Initial IBr Precursor: 0.709221

Vita

Captain Barry N. Behnken was born on 25 August, 1971 in Incline Village, Nevada. Upon graduating from Incline High School in 1989, he attended the U. S. Air Force Academy in Colorado Springs, Colorado, graduating with a Bachelor of Science degree in Applied Physics in June 1993. From 1993 to 1997, he was stationed at the Technical Operations Division at McClellan AFB in Sacramento, CA. While there, he served the Air Force Technical Applications Center (AFTAC) as Nuclear Materials Analyst and Chief, Gas Projects Office of the Nuclear Plant and Reactor Products Programs, respectively. Upon receipt of his M.S. in Engineering Physics from the Air Force Institute of Technology in March, 1999, he will be assigned to the Information Warfare Division of Air Intelligence Agency Headquarters at Kelly AFB, Texas.

Permanent Address: c/o Chris Behnken
694 Gary Court
Incline Village, NV 89450

Bibliography

1. De Young, R. J., G. D. Walberg, and E. J. Conway. A NASA High-Power Space-Based Laser Research and Applications Program. Washington: National Aeronautics and Space Administration, 1983.
2. Zuev, V. S., and L. D. Mikheev. Photochemical Lasers. Chur (Switzerland): Harwood Academic Publishers, 1991.
3. Peterson, Alan B., and Ian W. M. Smith. "Yields of ($4^2P_{1/2}$) As a Function of Wavelength in the Photodissociation of Br₂ and IBr," Chemical Physics, 30: 407-413 (1978).
4. Haugen, Harold K., Eric Weitz, and Stephen Leone. "Accurate Quantum Yields by Laser Gain vs. Absorption Spectroscopy: Investigation of Br/Br* Channels in Photofragmentation of Br₂ and IBr," Journal of Chemical Physics, Vol 83, No 7: 3402-3412 (1985).
5. Hwang, Heon, and Bagher M. Tabibi. "A Model for a Continuous-Wave Iodine Laser," Journal of Applied Physics, Vol 68, No 10: 4983-4989 (1990).
6. Lee, Ja H., Willard R. Weaver, and Bagher M. Tabibi. "Perfluorobutyl Iodides As Gain Media for a Solar-Pumped Laser Amplifier," Optics Communications, Vol 67, No 6: 435-439 (1988).
7. Choi, S. H., J. H. Lee, W. E. Meador, and E. J. Conway. "A 50-kW Module Power Station of Directly Solar-Pumped Iodine Laser," Journal of Solar Energy Engineering, 119: 304-311 (1997).
8. Zapata, L. E., and R. J. De Young. "Flashlamp-Pumped Iodine Monobromide Laser Characteristics," Journal of Applied Physics, Vol 54, No 4: 1686-1692 (1983).
9. Harries, W. L., and W. E. Meador. "Kinetic Modeling of an IBr Solar Pumped Laser," Space Solar Power Review, 4: 189-202 (1983).
10. Jenkins, D. "A 57 W Solar-Pumped Nd:YAG Laser." Unpublished report. University of Chicago, Chicago IL, 1996.

11. Zalesskil, V. Yu. "Iodine Laser Pumped by Solar Radiation," Soviet Journal of Quantum Electronics, Vol 13, No 6: 701-707 (1983).
12. De Young, R. J., and W. R. Weaver. "Low-Threshold Solar-Pumped Laser Using C_2F_5I ," Applied Physics Letters, Vol 49, No 7: 369-370 (1986).
13. Bony, H., M. Shapiro, and A. Yogev. "Theory and Operation of the IBr-Photodissociation Br Laser," Chemical Physics Letters, Vol 107, No 6: 603-607 (1984).
14. Lee, Ja H., and W. R. Weaver. "A Solar Simulator-Pumped Atomic Iodine Laser," Applied Physics Letters, Vol 39, No 2: 137-139 (1981).
15. Johnson, R. O., G. P. Perram, and W. B. Roh. "Dynamics of a Br ($4^2P_{1/2} \rightarrow 4^2P_{3/2}$) Pulsed Laser and a Br ($^2P_{1/2}$) - NO ($v=2 \rightarrow v=1$) Transfer Laser Driven by Photolysis of Iodine Monobromide," Applied Physics B: Lasers and Optics, 65: 5-12 (1997).
16. Giuliano, C. R., and L. D. Hess. "Reversible Photodissociative Laser System," Journal of Applied Physics, Vol 40, No 6: 2428-2430 (1969).
17. Child, M. S. "Predissociation and Photodissociation of IBr: A Case of Intermediate Coupling Strength," Molecular Physics, Vol 32, No 6: 1495-1510 (1976).
18. Pastel, Robert L., J. K. McIver, Harold C. Miller, and G. D. Hager. "Measurement of the Deactivation of Br^* by Atomic Iodine," Journal of Chemical Physics, Vol 100, No 5: 3624-3630 (1994).
19. Hofmann, Hubert, and Stephen R. Leone. "Collisional Deactivation of Laser-Excited Br^* ($^2P_{1/2}$) Atoms with Halogen and Interhalogen Molecules," Chemical Physics Letters, Vol 54, No 2: 314-319 (1978).
20. Clyne, M. A. A., and H. W. Cruse. "Atomic Resonance Fluorescence Spectrometry for the Rate Constants of Rapid Bimolecular Reactions (Part 2)," JCS Faraday II, 68: 1377-1387 (1972).
21. Johnson, Ray O., Glen P. Perram, and Won B. Roh. "Spin-Orbit Relaxation Kinetics of Br ($4^2P_{1/2}$)," Journal of Chemical Physics, Vol 104, No 18: 7052-7058 (1996).

22. Houston, Paul L. "Observation of the Reaction $I^* (^2P_{1/2}) + Br_2 \rightarrow IBr + Br^* (^2P_{1/2})$," Chemical Physics Letters, Vol 47, No 1: 137-141 (1977).
23. Gordon, E. B., A. I. Nadkhin, S. A. Sotnichenko, and I. A. Boriev. "Transformation of Spin-Orbit Excited States of Halogen Atoms in the Chemical Reactions $F + Br_2 \rightarrow BrF + Br$, $I^* + Br_2 \rightarrow IBr + Br$, and $Br + IBr \rightarrow Br_2 + I$," Chemical Physics Letters, Vol 86, No 2: 209-213 (1982).
24. Pastel, Robert L., G. D. Hager, Harold C. Miller, and Stephen R. Leone. "Efficient Br^* Laser Pumped by Frequency-Doubled Nd:YAG and Electronic-To-Vibrational Transfer-Pumped CO_2 and HCN Lasers," Chemical Physics Letters, Vol 183, No 6: 565-569 (1991).
25. Johnson, R. O., S. J. Karis, G. P. Perram, and W. B. Roh. "Characterization of a $Br (^2P_{1/2})-CO_2(10^0_1-10^0_0)$ Transfer Laser Driven by Photolysis of Iodine Monobromide," Applied Physics B: Lasers and Optics, 66: 411-415 (1998).
26. Schinke, Reinhard. Photodissociation Dynamics: Spectroscopy and Fragmentation of Small Polyatomic Molecules. Great Britain: Cambridge University Press, 1995.
27. Seery, Daniel J., and Doyle Britton. "The Continuous Absorption Spectra of Chlorine, Bromine, Bromine Chloride, Iodine Chloride, and Iodine Bromide," The Journal of Physical Chemistry, Vol 68, No 8: 2263-2266 (1964).
28. Tellinghuisen, Joel. "Transition Strengths in the Visible-Infrared Absorption Spectrum of I_2 ," Journal of Chemical Physics, Vol 76, No 10: 4736-4744 (1982).
29. Dereniak, E. L., and G. D. Boreman. Infrared Detectors and Systems. New York: John Wiley and Sons, Inc., 1996.
30. Perram, Glen P. Professor of Physics, Department of Engineering Physics, Air Force Institute of Technology. Personal communications. June 1998-March 1999.
31. Bernath, Peter F. Spectra of Atoms and Molecules. New York: Oxford University Press, Inc., 1995.
32. Rafferty, Brent D., Brian T. Anderson, Jack Glassman, Harold C. Miller, Alan I. Lampson, and Gordon D. Hager. "Experimental and Theoretical Investigation of a Coaxial Pumped Photolytic Atomic Bromine Laser," IEEE Journal of Quantum Electronics, Vol 33, No 5: 685-704 (1997).

33. Schinke, Reinhard. Photodissociation Dynamics: Spectroscopy and Fragmentation of Small Polyatomic Molecules. Great Britain: Cambridge University Press, 1995.
34. Brewer, Leo, and Joel Tellinghuisen. "Quantum Yield for Unimolecular Dissociation of I₂ in Visible Absorption," The Journal of Chemical Physics, Vol 56, No 8: 3929-3938 (1972).
35. Child, M. S., and R. B. Bernstein. "Diatomic Interhalogens: Systematics and Implications of Spectroscopic Interatomic Potentials and Curve Crossings," The Journal of Chemical Physics, Vol 59, No 11: 5916-5925 (1973).
36. Rafferty, Brent D., Brian T. Anderson, Jack Glassman, Harold C. Miller, Alan I. Lampson, and Gordon D. Hager. "Experimental and Theoretical Investigation of a Coaxial Pumped Photolytic Atomic Bromine Laser," IEEE Journal of Quantum Electronics, Vol 33, No 5: 685-704 (1997).
37. Perram, Glen P. "Approximate Analytic Solution for the Dissociation of Molecular Iodine in the Presence of Singlet Oxygen," International Journal of Chemical Kinetics, Vol 27: 817-828 (1995).
38. Haugen, Harold K., Eric Weitz, and Stephen R. Leone. "Effect of Spin-Orbit Excitation on Chemical Reactivity: Laser Transient Absorption Spectroscopy of Br (²P_{1/2}, ²P_{3/2}) + IBr Reactive Dynamics," Chemical Physics Letters, Vol 119, No 1: 75-80 (1985).
39. Baulch, D. L., J. Duxbury, S. J. Grant, and D. C. Montague. "Evaluated Kinetic Data for High Temperature Reactions," Journal of Physical Chemistry Reference Data, Vol 10, Suppl 1: 348-380, 469-475, 573 (1981).
40. Gruebele, M., I. R. Sims, E. D. Potter, and A. H. Zewail. "Femtosecond Probing of Bimolecular Reactions: The Collision Complex," Journal of Chemical Physics, Vol 95, No 10: 7763-7766 (1991).
41. Chase *et al.* Chemical Reference Data for Halogens, Journal of Physical Chemistry Chemical Reference Data, Vol 14, Suppl 1: 421, 434, 460, 1332, 1358 (1985).
42. Solomans, T. W. Graham. Organic Chemistry. New York: John Wiley and Sons, Inc., 1992.
43. Verdeyen, Joseph T. Laser Electronics. New Jersey: Prentice-Hall, Inc., 1995.

44. Efimenko, A. A., I. A. Boriev, and E. B. Gordon. "Determination of the Cross Sections of the $^2P_{1/2} - ^2P_{3/2}$ Transition in Iodine and Bromine Atoms," Soviet Journal of Quantum Electronics, Vol 15, No 8: 1127-1129 (1985).
45. Boriev, I. A., E. B. Gordon, A. I. Nadkhin, and S. A. Sotnichenko. "Determination of the Emission Cross Section for the $^2P_{1/2} - ^2P_{3/2}$ Transition of the Bromine Atom," Optical Spectroscopy (USSR), Vol 54, No 3: 233-237 (1983).
46. Milonni, Peter W. and Joseph H. Eberly. Lasers. New York: John Wiley & Sons, Inc., 1988.
47. Jenkins, D., R. Winston, J. Bliss, J. O'Gallagher, A. Lewandowski, and C. Bingham. "Solar Concentration of 50,000 Achieved with Output Power Approaching 1 kW," Journal of Solar Engineering, Vol 118: 141-145 (1996).

REPORT DOCUMENTATION PAGE

Form Approved
OMB No. 0704-0188

Public reporting burden for this collection of information is estimated to average 1 hour per response, including the time for reviewing instructions, searching existing data sources, gathering and maintaining the data needed, and completing and reviewing the collection of information. Send comments regarding this burden estimate or any other aspect of this collection of information, including suggestions for reducing this burden, to Washington Headquarters Services, Directorate for Information Operations and Reports, 1215 Jefferson Davis Highway, Suite 1204, Arlington, VA 22202-4302, and to the Office of Management and Budget, Paperwork Reduction Project (0704-0188), Washington, DC 20503.

1. AGENCY USE ONLY (Leave blank)		2. REPORT DATE March 1999	3. REPORT TYPE AND DATES COVERED Master's Thesis	
4. TITLE AND SUBTITLE KINETIC MODEL OF A SPACE-BASED, Br ($4^2P_{1/2} \rightarrow 4^2P_{3/2}$) LASER PUMPED BY SOLAR PHOTOLYSIS OF IBr			5. FUNDING NUMBERS	
6. AUTHOR(S) Barry N. Behnken, Captain, USAF				
7. PERFORMING ORGANIZATION NAME(S) AND ADDRESS(ES) Air Force Institute of Technology 2750 P. Street Wright-Patterson AFB, OH 45433-7765 (937) 255-3636			8. PERFORMING ORGANIZATION REPORT NUMBER AFIT/GAP/ENP/99M-01	
9. SPONSORING/MONITORING AGENCY NAME(S) AND ADDRESS(ES) AFRL/DEL 3550 Aberdeen Ave SE Kirtland AFB, NM 87117-5776 (505) 846-0718			10. SPONSORING/MONITORING AGENCY REPORT NUMBER	
11. SUPPLEMENTARY NOTES				
12a. DISTRIBUTION AVAILABILITY STATEMENT Approved for public release; distribution unlimited.			12b. DISTRIBUTION CODE	
13. ABSTRACT (Maximum 200 words) A kinetic model of the directly solar-pumped, atomic bromine laser—operating on the Br ($4^2P_{1/2} \rightarrow 2^2P_{3/2}$) transition under IBr photolysis—was developed, executed, and interpreted. In recognition of an evolving national interest in space-based laser development, the model presumed operation on a space station platform. Results indicate that a well-engineered IBr laser is capable of generating 1.2 kilowatts of continuous-wave (CW) power under a pumping concentration of 20,000 solar units. Such performance translates to an efficiency of roughly 0.29%, appreciably better than the 0.1% ascribed to the heretofore leading solar-pumped competitor. An extensive analysis of kinetic data suggests the unanticipated conclusion that, under proper parameter selection, sustained CW oscillation can be achieved absent any flow mechanism whatsoever. This result seems most strongly predicated upon proper bandpass discrimination: a 457-545 nm range of incidence produced optimal results. Sensitivity analysis revealed a strong degree of competition among the laser's constituent processes; two-body quenching and exchange reactions were predominant. With the significant exception of iodine recombination, three-body processes were negligible. Thermal increases, as well as rapid growth of atomic iodine, appear to pose the greatest kinetic threat to CW lasing.				
14. SUBJECT TERMS Iodine Monobromide (IBr), Bromine (Br), Laser, Solar-pumped, Space-based, Photodissociation, Computational.			15. NUMBER OF PAGES 177	
			16. PRICE CODE	
17. SECURITY CLASSIFICATION OF REPORT UNCLASSIFIED	18. SECURITY CLASSIFICATION OF THIS PAGE UNCLASSIFIED	19. SECURITY CLASSIFICATION OF ABSTRACT UNCLASSIFIED	20. LIMITATION OF ABSTRACT UL	